

AD-A035 061

TRW DEFENSE AND SPACE SYSTEMS GROUP REDONDO BEACH CALIF F/G 21/8.1
INVESTIGATION OF BEAMED ENERGY CONCEPTS FOR PROPULSION. LASER/P--ETC(U)
OCT 76 M HUBERMAN, J M SELLEN, R BENSON F04611-76-C-0003

UNCLASSIFIED

AFRPL-TR-76-66-VOL-2

NL

1 OF 2

AD
A035061



ADA035061

AFRPL-TR-76-66

INVESTIGATION OF BEAMED ENERGY CONCEPTS FOR PROPULSION

LASER/PROPELLANT COUPLING ANALYSES - VOLUME II

TRW DEFENSE AND SPACE SYSTEMS GROUP
ONE SPACE PARK
REDONDO BEACH, CALIFORNIA 90278

AUTHORS: M. HUBERMAN
J. M. SELLEN
R. BENSON
W. DAVENPORT
R. DAVIDHEISER
P. MOLMUD
L. GLATT

OCTOBER 1976

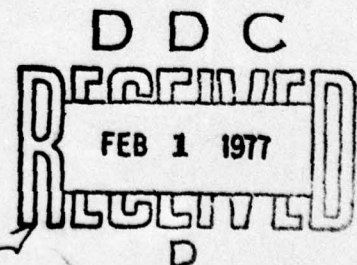
APPROVED FOR PUBLIC RELEASE;
DISTRIBUTION UNLIMITED

AIR FORCE ROCKET PROPULSION LABORATORY
DIRECTOR OF SCIENCE AND TECHNOLOGY
AIR FORCE SYSTEMS COMMAND
EDWARDS AFB, CALIFORNIA 93523

OVERLAY FOR VOLUME 2

COPY AVAILABLE TO DDC DOES NOT
PERMIT FULLY LEGIBLE PRODUCTION

Copy available to DDC does not
permit fully legible reproduction



NOTICES

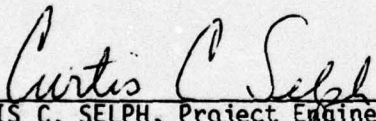
When U.S. Government drawings, specifications, or other data are used for any purpose other than a definitely related government procurement operation, the Government thereby incurs no responsibility nor any obligation whatsoever, and the fact that the Government may have formulated, furnished, or in any way supplied the said drawings, specifications or other data, is not to be regarded by implication or otherwise, or in any manner licensing the holder or any other person or corporation or conveying any rights or permission to manufacture use, or sell any patented invention that may in any way be related thereto.

FOREWORD

This document was prepared by the Applied Technology Division of TRW Defense and Space Systems Group, One Space Park, Redondo Beach, California 90278. It describes work performed under Contract F04611-76-C-0003, Job Order No. 010000PP with the Air Force Rocket Propulsion Laboratory, Edwards AFB, CA 93523. The period of performance represented by the report extended from 2 September 1975 to 1 July 1976.

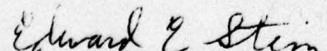
This work was sponsored and directed by the Air Force Rocket Propulsion Laboratory (AFRPL). Curtis Selph provided program management and technical guidance for the AFRPL. Program management at TRW was provided by M. N. Huberman.

This report has been reviewed by the Information Office/DOZ and is releaseable to the National Technical Information Service (NTIS). At NTIS it will be available to the general public, including foreign nations. This report is unclassified and suitable for general public release.


CURTIS C. SELPH, Project Engineer


CLARK W. HAWK, Chief
Propulsion Applications Branch

FOR THE COMMANDER


E. E. STEIN, Deputy Chief
Liquid Rocket Division

UNCLASSIFIED

SECURITY CLASSIFICATION OF THIS PAGE (When Data Entered)

19 REPORT DOCUMENTATION PAGE		READ INSTRUCTIONS BEFORE COMPLETING FORM
18 1. REPORT NUMBER AFRPL-TR-76-66-Val-21	2. GOVT ACCESSION NO.	3. RECIPIENT'S CATALOG NUMBER
4. TITLE (and Subtitle) INVESTIGATION OF BEAMED ENERGY CONCEPTS FOR PROPULSION. Laser/Propellant Coupling Analyses. Volume II.		5. TYPE OF REPORT & PERIOD COVERED FINAL <i>rest</i> , 2 Sep 1975 - 1 Jul 1976
7. AUTHOR(s) M. Huberman, J. M. Sellen, R. Benson, W. Davenport R. Davidheiser, B. Holmud, L. Blatt	8. CONTRACT OR GRANT NUMBER(s) FO 4611-76-C-0003	9. PERFORMING ORG. REPORT NUMBER
9. PERFORMING ORGANIZATION NAME AND ADDRESS TRW Defense and Space Systems Group One Space Park Redondo Beach, CA 90278		10. PROGRAM ELEMENT, PROJECT, TASK AREA & WORK UNIT NUMBERS
11. CONTROLLING OFFICE NAME AND ADDRESS Air Force Rocket Propulsion Laboratory Director of Science and Technology Air Force Systems Command Edwards AFB CA 93523		12. REPORT DATE October 1976
14. MONITORING AGENCY NAME & ADDRESS (if different from Controlling Office) (12) 132p.		13. NUMBER OF PAGES 131
16. DISTRIBUTION STATEMENT (of this Report) This report has been reviewed by the Information Office/DOZ and is releaseable to the National Technical Information Service (NTIS). At NTIS it will be available to the general public, including foreign nations. This report is unclassified and suitable for general public release.		15. SECURITY CLASS. (of this report) Unclassified
17. DISTRIBUTION STATEMENT (of the abstract entered in Block 20, if different from Report)		15a. DECLASSIFICATION/DOWNGRADING SCHEDULE
18. SUPPLEMENTARY NOTES		
19. KEY WORDS (Continue on reverse side if necessary and identify by block number) Beamed energy propulsion Spacecraft propulsion Laser propulsion		
20. ABSTRACT (Continue on reverse side if necessary and identify by block number) The objective of this program is to assess the feasibility of the beamed energy propulsion concept for Air Force missions. The work is divided into three major tasks: 1) system studies; 2) theoretical analyses of the coupling mechanisms between the beamed energy and propellant working fluid and 3) preparation of a test plan for the experimental investigation of the coupling processes for various laser/propellant combinations. The results of the study indicate that beamed energy propulsion is technically feasible. No fundamental obstacles have been identified. However considerable		

DD FORM 1473

EDITION OF 1 NOV 65 IS OBSOLETE
111

UNCLASSIFIED

SECURITY CLASSIFICATION OF THIS PAGE (When Data Entered)

409637

over
AB

UNCLASSIFIED

SECURITY CLASSIFICATION OF THIS PAGE(When Data Entered)

technical development is needed in many areas before the concept can be operationally implemented.

In order to minimize the required collector area, laser concepts are preferred over microwaves. Large diameter microwave receivers will have to be of the rectenna (rectifying antenna) type since conventional receiving reflectors cannot be fabricated to the precision required for efficient large scale collection. Thus microwaves will require electrically powered propulsion. This results in additional thousands of pounds of power conditioning equipment and radiation structure for heat rejection from the electrical subsystem.

If space based laser transmitter concepts are to be cost effective they will require the availability of megawatt level space nuclear or solar power stations. Reactant powered space based laser can not be cost effective because of the expense of transporting the reactants to orbit.

In view of the large total energy required for each mission, ground based transmitters will be most cost effective when they are operated closed cycle from central station electric power.

Laser transmitting ranges greater than several hundred nautical miles will result in excessive collector sizes. Therefore, ground based transmitters applications will be restricted to orbital functions which can be performed at low orbital altitudes. Thus, synchronous altitude functions such as circularization and repositioning in orbit will not be feasible with ground based transmitting stations, fly-by range considerations will limit thrust periods to 50 seconds (4° of orbital arc).

Three promising applications have been identified. The laser powered tug can be cost effective compared to an advanced cryogenic tug. Apsidal rotation correction and drag make-up are two other missions where significant advantages may be realized for the laser powered concept.

Extensive hardware development is required. Critical areas include the lasers, thrusters, thruster reaction chamber windows and the collection and coupling subsystems.

ACCESSION for	
NTIS	White Section <input checked="" type="checkbox"/>
DOC	Ref Section <input type="checkbox"/>
UNCLASSIFIED	<input type="checkbox"/>
JUSTIFICATION	
BY	
DISTRIBUTION/AVAILABILITY CODES	
SIC. AVAIL. and/or SPECIAL	
A	

DDC
RECEIVED
FEB 1 1977
D

TABLE OF CONTENTS

	<u>Page</u>
1. INTRODUCTION	1
2. LASER-WORKING FLUID COUPLING MECHANISMS	2
2.1 Inverse Bremsstrahlung	2
2.2 Particulate Coupling	4
2.3 Molecular Absorption	5
3. CHOICE OF WORKING FLUID FOR LASER-ASSISTED PROPULSION	7
4. COUPLING OF 4.855 μ TO METHANOL AND ITS DECOMPOSITION PRODUCTS	12
4.1 General Description of the Coupling	12
4.2 Consideration on Particulate Scattering	12
4.3 Vibrational Deactivation of CO	13
4.4 Coupling Considerations for Methanol - 4.855 μ	13
4.4.1 Thruster Requirements	13
4.4.2 Absorption by Carbon	16
4.4.3 Absorption by CO	19
4.4.4 The Role of Inverse Bremsstrahlung in Absorption	24
4.5 Conclusions	25
5. SUMMARY	27
REFERENCES	30
APPENDIX A COMBINED ONE AND TWO-DIMENSIONAL KINETIC	31
APPENDIX B PROGRAM CO FOR DETERMINATION OF CO VIBRATIONAL POPULATION DENSITY AS A FUNCTION OF TEMPERATURE AND INTENSITY AND TO PRODUCE A WEIGHTED ABSORPTION CROSS-SECTION	32
APPENDIX C LASER ABSORPTION COEFFICIENTS DUE TO INVERSE BREMSSTRAHLUNG	33
APPENDIX D THE ROLE OF VIBRATIONAL DEACTIVATION OF CO BY ELECTRONS	34
APPENDIX E SPECTRAL ABSORPTION PARAMETERS OF MOLECULAR SPECIES FOR POSSIBLE USE IN LASER-ASSISTED PROPULSION	36

LIST OF FIGURES

<u>Figure</u>		<u>Page</u>
1	Conceptual Model for Coupling Laser Energy to Working Fluid	7

LIST OF TABLES

<u>Table</u>		<u>Page</u>
1	Equilibrium Composition of Products of Decomposition of CH_3OH at 125 psia and Various Temperatures	15
2	Line Spacing ($\Delta\nu$) and f/f_{c30} versus Temperature	21
3	Weighted Absorption Cross-Section (in cm^2) for CO versus Intensity	21
4	Approximate Length Requirements for Power Absorption	22
5	Absorption Lengths for Heating to 5919°K by Temperature Intervals	23

1. INTRODUCTION

The theoretical analyses reported in this Volume 2 of the Final Report, respond to Task II of the Investigation of Beamed Energy Concepts for Propulsion program. A principal requirement of that task is the theoretical analysis of a minimum of three possible coupling processes between the incident radiation and the propulsive working fluid. These processes will be employed in the analysis of the performance of particular working fluid, methanol, in a DeLaval nozzle at a particular laser wavelength, 4.855μ .

Section 2 presents a general discussion of the coupling mechanisms, inverse bremsstrahlung, particulate absorption and molecular absorption, and their advantages for laser coupling.

Section 3 discusses the geometry of the proposed laser-fluid coupling procedure and the use of the ODE Thermodynamic Code. Three propellant candidates are discussed and a choice of one, methanol for a thorough coupling analysis is made.

Section 4 discusses the coupling of methanol and its decomposition products to CO radiation and computes the physical dimensions of the thrust chamber on those results.

Appendix E presents a compendium of spectral absorption parameters of molecular species which can be used as dopants for laser-fluid coupling.

2. LASER-WORKING FLUID COUPLING MECHANISMS

This section summarizes the characteristics and advantages and disadvantages of the three main coupling mechanisms to be considered for beamed laser propulsion; namely inverse bremsstrahlung, particulate coupling, and molecular absorption.

2.1 INVERSE BREMSSTRAHLUNG

We adopt the classical description of inverse bremsstrahlung from the theory of microwave discharges because of its simplicity and the perspective it affords us. This description is valid for most of our cases of interest (i.e., $h\nu/kT < 1$).

An electron in an electromagnetic field will alternately pick up energy from the field and then reradiate it. This reradiation will occur so long as the electron is subject to no other perturbations. However, in the event of a collision with a neutral or a charged particle, the phase relationship between the velocity of the electron and the driving field is perturbed and the electron will not reradiate all of the energy it had withdrawn from the field. The collision will essentially convert electromagnetic energy into translational energy of the electron and the colliding particle. When the colliding particle is much more massive than the electron, then the electron itself removes most of the energy. Under these circumstances the power input P to the electron varies as

$$P \sim \frac{\nu I_E}{\omega^2 + \nu^2}, \quad (1)$$

where I_E is the intensity of the electromagnetic wave, ν the electron collision frequency (generally a function of electron energy and the properties of the colliding species), and ω the angular frequency of the wave.

An energetic electron, upon colliding with a molecule, for example, can lose energy by exciting rotational, vibrational or electronic transitions, or at the very least imparting some translational energy. The electron under the influence of an electromagnetic field and as a result of collisions, will increase its translational energy until an equilibrium

is established whereby the power input via the electromagnetic wave is matched by the power losses due to the above mentioned inelastic and elastic molecular excitation.

It is this transfer of energy from the electrons to the molecules via (mainly) inelastic collisions which accomplishes the heating of a weakly ionized gas. Heating a gas via inverse bremsstrahlung suffers from a defect that is shared by some molecular absorption mechanisms, that is, the energy is imparted into internal modes of molecular excitation, and changes in translational energy must depend upon de-excitation mechanisms and relaxation to thermodynamic equilibrium distributions. Sometimes these relaxation rates are quite rapid, but sometimes, as in the case of vibrational de-excitation of CO, they can be quite slow.

An inspection of (1) shows that the power transferred to the electron, and therefore to the colliding molecular and atomic species, maximizes at $\nu = \omega$. This is of interest to us because for the present application $\omega \approx 10^{15} \text{ sec}^{-1}$ and $\nu \approx 10^{11} \text{ sec}^{-1}$; therefore the system is far off optimum with respect to power transfer.

The power transfer per unit volume varies as the electron density. As will be shown, when dealing with specific cases, electron densities of the order of $3 \times 10^{16} \text{ cm}^{-3}$ are required to produce reasonable power transfers from the wave to the electrons. Such electron densities are achieved usually by heroic means--namely, by doping the working fluid with low ionization potential elements or compounds and operating at temperatures of 5000°K or higher. Such electron densities can also be produced by localized breakdowns due to focussed laser beams or even UV or X-ray irradiation or electric arcs.

A systems factor which must be considered when planning on using inverse bremsstrahlung is the radiation augmented heat load on the walls of the thruster chamber. The working fluid will be highly absorptive at IR frequencies and, accordingly, will be highly emissive at these frequencies, radiating essentially as a blackbody, at long wavelengths, to the thruster walls. An additional radiation burden on the walls is in the visible and uv and will come from recombination radiation. This may be particularly important when ionization is maintained by laser breakdown or arcs.

2.2 PARTICULATE COUPLING

An attractive method for coupling laser energy into a working fluid is to load the fluid with particulates. The particulates will be heated by the laser and will rapidly transfer this heat energy to the fluid. The particulate heating can be non-selective in wavelength for metallic and graphitic particles.

A fairly elementary treatment of heat transfer shows that the temperature of the particle varies as the square of its radius; therefore, particles that are too large will, when irradiated, heat up to their melting and vaporization or decomposition temperatures and decrease in size. Their size will rapidly decrease until their equilibrium temperature is less than their boiling temperature, at which point they will decrease more slowly in size by evaporation.

Particle sizes may be reduced not only by boiling, but also by chemical reaction with the working fluid. Thus, carbon particles will combine with hydrogen or reduce oxygen containing molecular species and disappear at high temperatures.

Any choice of particle species for loading the working fluid must, therefore, take into account at least two factors, 1) chemical stability and 2) melting and boiling point. A third factor which might have to be considered is the absorption coefficient which varies as the conductivity for small enough particles. Tungsten, with a boiling point of 6200°K, might satisfy all of these considerations, but ceramic particles might not satisfy the third.

It is apparent that for efficient heat transfer, the particles, if they are employed, should be small. However, there is a concomitant difficulty associated with small sizes, namely, scattering of laser energy.

When the particle size is smaller than a wavelength, the particle scatters radiation in a typical dipole radiation. For our purposes, this scattering pattern is practically isotropic. When the particle is larger than the wavelength, then the scattering is mainly in the forward direction. Be that as it may, the net result of many scatterings by large particles is a fairly large broadening of a beam. For example, it is easy to show

that the mean square angular deflection $\overline{\theta^2}$ of a photon undergoing multiple scattering by large particles is given by (2),

$$\overline{\theta^2} = \left(\frac{\lambda}{D}\right)^2 2n \pi a^2 L, \quad (2)$$

where λ is the wavelength, D the diameter of the particle, n the numerical particle density, a the radius of the particle, and L the path length.

Taking $\lambda/D = .1$, $a = 10^{-3}$ cm, $n = 10^6$ cm $^{-3}$, we find $\overline{\theta^2} \approx .6$ or

$\sqrt{\overline{\theta^2}} = .8$ radian $\approx .48^\circ$. Thus, spreading and scattering of laser beams by particulates is not easy to avoid.

A further systems complication associated with particulate loading is injection. Either the particles are maintained in the working fluid as a slurry, with concomitant problems of maintaining suspension, or are injected into the working fluid in the thrust chamber.

2.3 MOLECULAR ABSORPTION

Molecular absorption offers the possibility of significant absorption at low temperatures.

The working fluid or a gaseous dopant can absorb laser energy directly by vibration-rotation molecular transitions. The component molecules can be very selective in the wavelengths that they absorb, and it may sometimes be difficult to match absorbing species with particular wavelengths. There are some species, such as NH_3 , CH_3OH and H_2O , which can absorb over a very wide spectrum of frequencies. Species which rely on excited level absorption, CO_2 at 10.6μ , can absorb appreciably only when heated above 300°K .

A candidate molecular absorber must absorb efficiently over a wide range of temperatures, or else the coupling agent must be composed of a mixture of species each one of which is effective over a limited temperature range. For example, SF_6 is a very efficient absorber of CO_2 laser radiation, but dissociates at $\sim 1700^\circ\text{K}$. The more stable CO_2 will dissociate at $\sim 2500^\circ\text{K}$. Thus, to get a temperature rise to 5000°K or more by molecular absorption, species other than CO_2 must be employed.

The molecule CO is very stable and may be heated up to 6000°K without appreciable dissociation. It, however, will absorb in only a select wavelength regime, $\sim 5\mu$, and so can practically be used only for CO lasers.

There are several potential disadvantages to the use of molecular absorption for coupling. One has been mentioned before, that of dissociation or chemical reaction leading to the removal of the absorbing species as a viable absorber. Another disadvantage is that the absorbed energy may be locked up for a rather long time in a particular vibrational state, and thus be made unavailable for augmentation of translational energy. Another possibility is bleaching at high laser intensities, effectively decreasing the population densities of absorbers. The effects of internal energy hangup and bleaching may be ameliorated by vibrational deactivating dopants or enhanced pressure and temperature.

The computation of laser energy transfer to a working fluid via molecular absorption requires a large amount of information and is a fairly detailed and involved process. The process goes as follows: The absorbing molecular species is followed in the working fluid as it is heated up and as it changes its relative density due to chemical reactions. The power absorption is computed on the basis of the population density of molecular rotational vibrational energy states near the laser line to be absorbed. These population densities are in turn controlled by the rates of stimulated emission, by absorption rates and vibrational de-excitation. The data necessary for these estimates are the absorption cross sections for each transition, the line width parameters, line densities, and the rate constants for deactivation of vibrations. The use of these data for CO for transient heating was illustrated in Reference 1, and is also illustrated in this report--but for quasi-static conditions and for conditions of changing temperature, composition, pressure and laser intensity. We have made use of data for CO only. For the convenience of other workers who may want to make similar computations for other molecular species, a compilation of similar data has been made for some select species and will be found in Appendix E.

3. CHOICE OF WORKING FLUID FOR LASER-ASSISTED PROPULSION

It is desired to transmit laser energy from a ground or other platform laser generating station to a spacecraft. The propellant carried by the spacecraft is to couple with the laser energy to produce propulsive thrust. The propellant, as a working fluid will be discharged through a DeLaval nozzle and the coupling between the working fluid and the laser energy is to occur in any reasonable region of the nozzle. Previous studies^(1,2,3) have shown that deposition of energy in supersonic gases decreases their Mach number, whereas deposition in gases of Mach number < 1 increases the Mach number. For efficiency therefore, we shall adopt the viewpoint that the laser energy couples to the working fluid in the subsonic region.

In our coupling studies we shall assume an operational configuration, adopted from Reference 2, as in Figure 1.

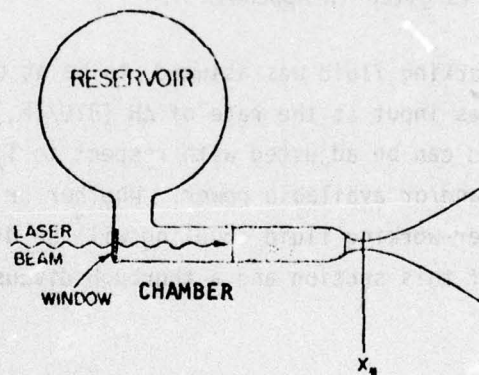


Figure 1. Conceptual Model for Coupling Laser Energy to Working Fluid.

The propellant, stored in the reservoir, in solid, liquid, or gas phase is suitably constituted so that it will absorb energy from the beam in any of its initial and subsequent phases resulting from heating, and so that little of the incident energy will escape through the throat without absorption.

The heated working fluid is to have a specific impulse of ~ 1000 sec in order to make the concept of laser assisted propulsion practicable. To this end the working fluid is to have the lowest molecule weight and the highest chamber temperature consistent with the available power supply.

We may note parenthetically that a 100% efficient conversion of 10 megawatts of power will produce a thrust of 459 lbs when the specific impulse is 1000 sec.

We investigated the propulsive efficiency of three working fluids, assuming complete conversion of the available power by the working fluid. The efficiency was determined by running the ODE-ODK-TDK thermodynamics program for each propellant or propellant mixture. A brief description of this program is given in Appendix A.

The working fluid was assumed to be at chamber pressure, P_c (psia) and energy was input at the rate of ΔH (BTU/lb.). The energy input was estimated and can be adjusted with respect to T_c (chamber temperature) limitations and/or available power. Whether or not the ΔH is consistent with the laser-working fluid coupling will be discussed briefly in a later part of this section and a thorough discussion is left for Section 4.

The available thermodynamic data, ΔH , propellant composition and nozzle geometry provide sufficient data for running the thermodynamic program. We ran the program only in the one dimension equilibrium mode. The program can also be run in the kinetic mode if so desired. The program outputs chamber temperature, density, composition (including ions and electrons), specific impulse and many other quantities at a variety of upstream or downstream area ratios.

The results contained no surprises, H_2 by far had the highest specific impulse, 1630 sec at $T_c = 4700^\circ K$ and $P_c = 125$ psia with $\epsilon = 25$. H_2 had a suspended carbon slurry. This carbon serves two purposes. The first is to provide a coupling mechanism via particle heating at low temperatures and the second is to enhance electron density at high temperatures to promote inverse bremsstrahlung coupling. This latter reason was the same motivation for testing Li-NH₃ solution as a working fluid. (According to Reference 5, 11.3 gm Li is soluble in 100 gm NH₃ at $0^\circ C$). The magnitude of the inverse bremsstrahlung coupling for these two fluids is discussed in Appendix E.

The Li-NH₃ fluid had a specific impulse of 834 sec ($T_c = 5800^\circ K$, $P_c = 750$ psia). Another propellant run was CH₃OH (methyl alcohol). This had a lower I_{sp} than the others, 775 sec at $\epsilon = 25$ and 838 sec at $\epsilon = 100$ ($T_i = 5900^\circ K$, $P_c = 125$ psia).

Let us examine these possible working fluids with the total system in mind and see what the advantages and disadvantages are for using each of them.

I. H₂

Advantage: High specific impulse at comparatively low temperatures.

Disadvantages: Low density, cryogenics, poor laser coupling.

In order to transfer energy to H₂, particulates or molecular dopants would have to be introduced either as a slurry or after injection into the combustion chamber.

II. NH₃-Li

Advantages: High density, good laser coupling at low temperatures via molecular absorption and also at high temperatures via inverse bremsstrahlung.

Disadvantages: Cryogenics, poor coupling with laser at intermediate temperatures because of the disappearance of NH₃ and insufficient electron density, laser scattering by Li in particle form when NH₃ evaporates.

III. CH₃OH

Advantages: High density, good laser coupling at all temperatures, unstable.

Disadvantages: Low I_{sp} , high T_c , possibility of laser scattering by carbon formed during dissociation.

Of the three working fluids, only one, CH₃OH, couples efficiently with laser energy (CO laser at $\sim 4.9\mu$) during all phases of its decomposition. All the others require dopants to carry the working fluid from the injection temperature to the final working temperature T_c , or in the case of NH₃-Li to a temperature where inverse bremsstrahlung can take over. It is conceivable that one could obviate the use of dopants for NH₃-Li by means of spark plugs or arcs or even breakdown caused by the laser beam in focussed operation. However, such considerations introduce systems complications which we wish to avoid for the present.

We decided to concentrate on CH_3OH as a working fluid because of its desirable laser coupling characteristics. This does not eliminate either of the other two candidates since they could be incorporated into the ensuing analysis as dopants of CH_3OH . Or, conversely, depending on systems considerations, CH_3OH could be the dopant.

4. COUPLING OF 4.855 μ TO METHANOL AND ITS DECOMPOSITION PRODUCTS

4.1 GENERAL DESCRIPTION OF THE COUPLING

The main result of this section is an analysis of the working fluid CH_3OH , coupling to $\lambda = 4.855\mu$ and leading to a tentative configuration for the thrust chamber. CH_3OH and its decomposition products will provide all the components required for effective coupling with the laser energy. Methanol (CH_3OH) will decompose after being heated to its activation energy to form solid carbon, H_2 and CO . The carbon will be an effective coupling agent until it disappears as the gas temperature increases and will be replaced by CO as the main absorber. The vibrational energy stored in the CO will be quite effectively released by impact with H_2 . The role of inverse bremsstrahlung never really becomes important in the temperature intervals of interest.

Before we discuss the procedures for determining the coupling efficiency of the methanol decomposition products with a CO laser line, we first look at laser energy loss due to particulate scattering. Then we shall consider some aspects of vibrational deactivation of CO .

4.2 CONSIDERATION ON PARTICULATE SCATTERING

Particulates will provide a convenient coupling mechanism for heat transfer from the laser beam to the working fluid. However, care must be taken so that particulate scattering of the laser beam does not add an intolerable burden of heat dissipation to the walls of the combustion chamber. This can be assured if r/λ is small enough. Here r is the radius of the particle and λ the wavelength of the scattered radiation. As an example, consider the case provided in Reference 1. A carbon particle density of $\eta = 10^{-5}/r^3 \text{ cm}^{-3}$ is provided to achieve an absorption length of 10 cm. The scattering cross section for highly conducting particles and $2\pi r/\lambda \ll 1$ is $\sigma_s = \frac{r^2}{3} \left(\frac{2\pi r}{\lambda}\right)^4$. The scattering mean free path will be $(\eta \sigma_s)^{-1}$ and the power scattered out of the beam per cm^3 of the particle suspension is $I\eta\sigma_s$, where I is the intensity of the laser beam. If $r = 3 \times 10^{-5} \text{ cm}$ and $\frac{2\pi r}{\lambda} = .1$ ($\lambda = 18.8\mu$), then $\eta\sigma_s = 1.1 \times 10^{-5} \text{ cm}^{-1}$ and insignificant scattering takes place. However, if $\frac{2\pi r}{\lambda} \approx 1$ ($\lambda = 1.88\mu$), then $\sigma_s \approx 2\pi r^2$, its maximum value. Then $\eta\sigma_s \approx 2 \text{ cm}^{-1}$ and most of the energy will be scattered out of the beam before it is absorbed (a scattering mean free path of 1/2 cm versus an absorption mean free path of 10 cm). If we are dealing with megawatts of

power in the laser beam, then this power would be scattered onto the walls of the combustion chamber which could conceivably be destroyed.

For similar reasons liquid droplets must be kept small and dense sprays or sheets of liquids must not be allowed to intercept the laser beam. The reflection of even as little as 1 percent of the laser beam could provide an intolerable heat burden for the thruster walls.

4.3 VIBRATIONAL DEACTIVATION OF CO

The molecule CO is a good candidate for the working fluid of a laser assisted propulsion method⁽¹⁾, due to its high absorption coefficient at about 4.8μ . However, at low temperatures, the absorbed energy is locked up in vibrational modes for a long time instead of contributing to the kinetic energy. For example⁽⁷⁾ at 300°K at 10 atmospheres, the vibrational relaxation time for CO is $\sim 1/10$ sec. For a CO-He mixture this time is reduced to $\sim 10^{-3}$ sec and for CO-H₂ is further reduced to $\sim 10^{-5}$ sec. Obviously the deactivation time depends on the species with which the CO molecules are interacting. For the purpose of laser-assisted propulsion, it would appear advantageous to employ a mixture of CO and H₂. When methanol decomposes, it provides not only CO but H₂ which will provide the deactivation collision. In Appendix D, we investigate the role of electrons in deactivating CO and find them, in the main, unimportant.

4.4 COUPLING CONSIDERATIONS FOR METHANOL — 4.855μ

4.4.1 Thruster Requirements

In Section 2, we demonstrated that methanol appears to be a suitable working fluid for laser-assisted propulsion, provided that it coupled efficiently with the laser energy. Now we demonstrate the coupling efficiency. When CH₃OH is run through our ODE thermodynamic code with an energy input of 2.27×10^4 BTU/lb at 125 psia, we find a chamber temperature of 5919°K and an I_{sp} of 775 sec at $\epsilon = 20$ or 838 sec at $\epsilon = 100$. The mass flow with a throat area of 7.3×10^{-4} ft² ($r^* = .183$ ") is 3.08×10^{-2} lb/sec. The power consumption is therefore 696 BTU/sec, or 7.35×10^5 watts; to be supplied by the laser beam. We envision the employment of a conventional de-Laval nozzle for this application so that the chamber diameter must be larger than the throat diameter.

The laser beam is to be absorbed by the working fluid. However, the absorption will be exponential and we should expect that some of the residual laser power will strike the shoulder of the chamber. To reduce wall heat dissipation problems, we will adjust the beam diameter so that the intensity of radiation striking the shoulder, after absorption by the gases, will be less than an arbitrary figure of 1 kW/cm^2 . We chose not to lengthen the chamber since that would be wasteful of the thermal energy input to the working gases by losses to the chamber walls. We now determine the length of the chamber by computing the absorption coefficients of the working fluid as it is being heated by the laser beam, at 125 psia.

We made a series of equilibrium runs on our ODE program, progressively changing the energy input per pound of working fluid until we reached the desired temperature of 5919°K . We obtained equilibrium temperatures and compositions at the following temperatures, all in $^\circ\text{K}$: 750, 905, 1012, 1554, 3235, 4294, and 5919. These results are given in Table 1.

We found that there was a zero energy input required to reach 750°K . This tells us that CH_3OH is inherently unstable and that once an activation energy is supplied, the substance will spontaneously decompose. Methanol itself is probably very highly absorptive to any IR radiation⁽¹⁰⁾. This absorption plus the IR radiation from the downstream products should serve to provide the above required activation energy. Upon decomposition, a fair amount of solid carbon is formed (see Table 1). [Methanol is not usually known as carbon-producing, in flames, although higher molecular weight alcohols will produce soot⁽¹¹⁾. We are, however, in this usage not mixing methanol with O_2 , but decomposing it in the absence of O_2 .] This carbon will further absorb the laser radiation until the carbon disappears at about 1500°K . Also produced, and increasing with temperature up to a maximum at about 3200°K , are CO and H_2 . This combination will be very effective in converting CO laser radiation into kinetic energy. We now make estimates of the absorption due to the carbon and CO . It will turn out that carbon plays an insignificant role in the overall energy absorption history of the methanol decomposition products.

Table 1. Equilibrium Composition of Products of Decomposition
of CH_3OH at 125 psia and Various Temperatures.

750°K	905°K	1012°K	1554°K	3235°K	4294°K	5919°K
<p>C(S) .133338 CH_4 .315652 C_2H_4 .004025 C_2H_2 .090753 H_2 .097995 H_2O .358237</p> <p>$\rho_V = 202$ $\text{NCO} = 3.3 \text{ E17}$ $\text{NH}_2 = 8.12 \text{ E18}$ $\text{N} = 8.3 \text{ E19}$ $\text{DEN} = .173 \text{ lb/ft}^3$</p>	<p>.128044 .215170 .042991 .090574 .270580 .252640</p> <p>$\rho_V = 171$ $\text{NCO} = 2.89 \text{ E18}$ $\text{NH}_2 = 1.86 \text{ E19}$ $\text{N} = 6.87319$ $\Delta H = 507 \text{ BTU/lb.}$ $\text{DEN} = .125$</p>	<p>C(S) .092676 CH_2O .000001 CH_4 .137211 C_2H_4 .126748 C_2H_2 .068171 C_2H_6 .000001 H_2 .413474 H_2O .161718</p> <p>$\rho_V = 150$ $\text{N} = 6.16 \text{ E19}$ $\text{NCO} = 7.8 \text{ E18}$ $\text{NH}_2 = 2.4 \text{ E18}$ $\Delta H = 623$ $\text{DEN} = 9.6 \text{ E-2}$</p>	<p>C(S) 0.000000 CH_2O .000001 CH_3 .000001 CH_4 .004299 C_2H_4 .331226 C_2H_2 .000658 C_2H_6 .000005 C_2H_8 .000004 H .000009 HCO .000002 H_2 .660133 H_2O .003659</p> <p>$\rho_V = 107$ $\text{NCO} = 1.32 \text{ E19}$ $\text{NH}_2 = 2.8 \text{ E19}$ $\text{N} = 4 \text{ E19}$ $\Delta H = 2120$ $\text{DEN} = 4.48 \text{ E-2}$</p>	<p>C(S) .000000 C .000002 CH .000001 CH_2 .000001 CH_3 .000001 CH_4 .000001 C_2H_2 .000016 C_2H_4 .000005 C_2H_6 .000005 C_2H_8 .319458 C_2H_{10} .000019 C_2H_{12} .000019 C_2H_{14} .000026 C_2H_{16} .000111 E .000001 H .081430 HCO .000097 H_2 .598551 H_2O .000265 O .000001 OH .000014</p> <p>$\rho_V = 70.4$ $\text{NCO} = 6.14 \text{ E18}$ $\text{NH}_2 = 1.15 \text{ E19}$ $\Delta H = 3250$ $\text{N} = 1.93 \text{ E19}$ $\text{DEN} = 2.05 \text{ E-2}$</p>	<p>C .000270 CH .000047 CH_2 .000004 CH_3 .000004 C_2H_2 .000004 C_2H_4 .255425 C_2H_6 .000015 C_2H_8 .000004 C_2H_{10} .000056 C_2H_{12} .000019 C_2H_{14} .000002 C_2H_{16} .000002 E .000002 H .463646 HCO .000128 H_2 .279911 H_2O .000148 O .000153 OH .000166</p> <p>$\rho_V = 54.6$ $\text{NCO} = 3.7 \text{ E18}$ $\text{NH}_2 = 4.06 \text{ E18}$ $\text{N} = 1.45 \text{ E19}$ $\Delta H = 6500$ $\text{DEN} = 1.24 \text{ E-2}$</p>	<p>C .012430 C^+ .000016 CH .000230 CH_2 .000001 C_2H_2 .188966 C_2H_4 .000017 C_2H_6 .000072 C_2H_8 .000021 C_2H_{10} .000008 E .000026 H .763907 H^+ .000008 HCO .000055 HCO^+ .000002 H_2 .021390 H_2O .000017 O .012195 OH .000636 O_2 .000004</p> <p>$\rho_V = 42.2$ $\text{NCO} = 1.99 \text{ E18}$ $\text{H}_2 = 2.2 \text{ E17}$ $\Delta H = 9700$ $\text{N} = 1.05 \text{ E19}$</p>

4.4.2 Absorption by Carbon

We do not know the particle size distribution of carbon in the methanol decomposition products. The particles of larger size will be suppressed by the heating by the laser beam, as has been pointed out in Reference 1. We shall assume two different distribution functions and show that the carbon absorption coefficient is independent of the particular function chosen. The scattering coefficient, however, will not be independent of the size distribution, as has been discussed earlier.

The Deirmendjian distribution^(12,13), used for description of aerosol particle size distribution, is a combination of $1/r^4$ and r^0 dependence. We shall assume each of these dependences separately for a range of particle sizes $r_0 < r < R_0$, where $r_0 \ll R_0$.

Thus: $f_1 = \frac{a}{r^4}$, where $\int_{r_0}^R \frac{a}{r^4} dr = 1$ (3)

$\therefore a = 3r_0^3$. (4)

$f_1 = \frac{3r_0^3}{r^4}$; (5)

and

$f_2 = \frac{1}{R - r_0}$. (6)

At 750°K the mole fraction of C(s) is .133. Since the total number of particles is $8.3 \times 10^{19} \text{ cm}^{-3}$, $N_{C(s)} = 1.1 \times 10^{19} \text{ cm}^{-3}$. We assume the specific gravity of the carbon particles is 2.0. Then each particle of carbon contains $\frac{4\pi}{3} r^3 \times 2 \times \frac{6.02}{12} \times 10^{23} \text{ atoms} \approx \frac{4\pi}{3} \times 10^{23} r^3$. If n is the total number of carbon particles/ cm^3 , then:

$$n \int_{r_0}^R \frac{4\pi}{3} \times 10^{23} r^3 f dr = 1.1 \times 10^{19} \text{ cm}^{-3} . \quad (7)$$

Using f_1 , we find

$$\frac{4\pi}{3} \ln\left(\frac{R_0}{r_0}\right) n_1 r_0^3 \times 10^{23} = 1.1 \times 10^{19} \text{ cm}^{-3} . \quad (8)$$

And with f_2 ,

$$\frac{4\pi}{3} \times 10^{23} n_2 \frac{R_0^3}{4} = 1.1 \times 10^{19} \text{ cm}^{-3} . \quad (9)$$

We assume the volume absorption coefficient, $\alpha = 8 \times 10^3 \text{ cm}^{-1}$ as given in Ref. 1.

The absorption cross-section for each particle is given by $\alpha V = 8 \times 10^3 \times \frac{4}{3} \pi r^3$. The absorption coefficient is then given by

$$K = n\alpha \int_{r_0}^R r^3 f dr . \quad (10)$$

Thus,

$$K_1 = n_1 \alpha \frac{4}{3\pi} \times 3r_0^3 \ln\left(\frac{R_0}{r_0}\right) ; \quad (11)$$

$$K_2 = n_2 \alpha \frac{4}{3\pi} \times \frac{R_0^3}{4} . \quad (12)$$

But from the previous determinations of n_1 and n_2 , $K_1 = K_2$, and $K_1 = K_2 = .88 \text{ cm}^{-1}$.

The scattering cross-section is $\sigma_s = \frac{1}{3}\left(\frac{2\pi}{\lambda}\right)^4 r^6$ for $\frac{2\pi}{\lambda}r \ll 1$, which we shall assume.

$$\text{Then } K_s = n \int \sigma_s f dr ; \quad (13)$$

$$K_{s1} = \frac{1}{3}\left(\frac{2\pi}{\lambda}\right)^4 n_1 r_0^3 R_0^3 = \frac{R_0^3}{4\pi} = \frac{R_0^3}{4\pi} \left(\frac{2\pi}{\lambda}\right)^4 \times 10^{-4} / \ln\left(\frac{R_0}{r_0}\right) ; \quad (14)$$

$$K_{s2} = \frac{1}{3}\left(\frac{2\pi}{\lambda}\right)^4 n_2 R_0^6 + \left(\frac{2\pi}{\lambda}\right)^4 \frac{R_0^3}{\pi} \times 10^{-4} . \quad (15)$$

If we take $\frac{2\pi R_0}{\lambda} = .1$, then $K_{s2} \approx \frac{10^{-8}}{\pi R_0}$, insignificant for particle sizes of interest. K_{s1} is of the same magnitude. The above analysis is predicated upon $\frac{2\pi R_0}{\lambda} < 1$. If this is not the case, the scattering can prove important. One of the principal tasks in the experimental coupling tests should be to determine if significant scattering takes place from the particulates.

When the working fluid is at 905°K, the mole fraction of solid carbon C(s) is .128; the absorption coefficient is then $.847 \text{ cm}^{-1}$. At 1012°K solid carbon has a mole fraction of .093, but at 1554°K is negligible. We will ignore the absorption role of solid carbon, accordingly, above 1000°K.

4.4.3 Absorption by CO

Beyond 1000°K, absorption by CO dominates. We make use of the data and analysis provided in Ref. 1 for absorption coefficients of CO. We take into account the vibrational population density of the gas by solving (in steady-state) the equation (almost equivalent to Eq. (3.4) of Ref. 1)

$$\begin{aligned} \frac{dN_v}{dt} = & I\sigma_{v-1,v}[N_{v-1}-N_v] - I\sigma_{v,v+1}[N_v-N_{v+1}] - R\left[N_v-N_{v-1}e^{-\Delta E_{v,v-1}/kT}\right] + \\ & + R\left[N_{v+1}-N_v e^{-\Delta E_{v+1,v}/kT}\right], \end{aligned} \quad (16)$$

where I is the laser intensity, in photons/cm²sec, σ the absorption cross-section for a vibrational transition, $\Delta E_{v,v-1}$ the difference in vibrational energy between levels $v, v-1$, R the rate constant for CO and H₂ deactivating the vibrational energy levels. We assume R is independent of v and is given by:⁷

$$R = [\text{MF. CO}]R_1 + [\text{MF. H}_2]R_2, \text{ and}$$

$$\frac{P}{R_1} = \exp[175(T^{-1/3} - .0290) - 18.42] \quad (17)$$

$$\frac{P}{R_2} = \exp[68(T^{-1/3} - .01723) - 18.42],$$

where P is the pressure, in atmospheres, $[\text{MF CO}]$ is mole fraction of CO and $[\text{MF. H}_2]$ is mole fraction of H₂. R_1 represents the rate of self-deexcitation and R_2 the rate due to H₂ collisions. We assume no other species are effective in the de-excitation process.

The absorption cross-sections in Ref. 1 are given for a pressure of 30 atmospheres and must be corrected for 8.5 atmospheres. The absorption cross-section data were computed with magnitudes corresponding to the line center value of the absorption coefficient of the transition nearest the wavelength of 4.855 μ . It was assumed that at 30 atmospheres the lines just overlap. At 8.5 atmospheres, we no longer can make this assumption. Instead, we shall assume that our wavelength is exactly between the two nearest lines

except for the transition $v = 3 \rightarrow 2$, $J = 8$ on which line it is centered. We shall assume a Lorentz line shape:

$$f = \frac{a}{\pi[a^2 + (v - v_0)^2]} \quad (18)$$

where a is the line width parameter, proportional to pressure and $\sim 1/\sqrt{T}$, v_0 is the line center wave number. For CO, $a = .061 P \sqrt{T_0/T} \text{ cm}^{-1}$, where P is in atmospheres and $T_0 \approx 300^\circ\text{K}$.

At the line center,

$$f_c = \frac{1}{\pi a} \quad (19)$$

and in between two lines,

$$f_{1/2} = \frac{2a}{\pi[a^2 + (\frac{\Delta v}{2})^2]} \quad (20)$$

where Δv is the line separation.

Putting in the dependence of a on pressure, we find for f_c at 30 atm,

$$f_{c30} = \frac{1}{\pi .061 \times 30} \sqrt{T/T_0} \quad (21)$$

Also,

$$f_{c8.5} = \frac{1}{\pi .061 \times 8.5} \sqrt{T/T_0} \quad (22)$$

$$\therefore \frac{f_{c8.5}}{f_{c30}} = \frac{30}{8.5} = 3.52 \quad (23)$$

Between two lines at 8.5 atm,

$$f_{1/2} = \frac{2 \times .061 \times (8.5 \sqrt{T_0/T})}{\pi \left[(.061 \times 8.5 \times \sqrt{T_0/T})^2 + (\frac{\Delta v}{2})^2 \right]} \quad (24)$$

and

$$\frac{f_{1/2}}{f_{c30}} = \frac{1.898 \frac{T_0}{T}}{[.2688 \frac{T_0}{T} + (\frac{\Delta\nu}{2})^2]} \quad (25)$$

We shall modify the absorption cross-sections of Ref. 1 by multiplying by these factors. We obtain the line spacing from Reference 14.

Table 2 gives line spacing ($\Delta\nu$), f/f_{c30} vs. temperature.

Table 2. Line Spacing ($\Delta\nu$) and f/f_{c30} vs. Temperature.

T°K	750	905	1012	1554	3235
$\Delta\nu(\text{cm}^{-1})$	3.3	2.5	2.5	1.42	.67
f/f_{c30}	.268	.381	.342	.659	1.29

Above the temperature of 3235, the line density becomes so great that we assume the lines merge into a continuum and the factor, $f/f_{c30} \approx 3.52$.

A simple computer program (entitled "CO") was constructed to solve the vibrational population density as a function of temperature and intensity and to produce a weighted absorption cross-section. Appendix B provides additional details on this computer program.

Table 3 presents the absorption cross-section as function of temperature and intensity.

Table 3. Weighted Absorption Cross-Section (in cm^2) for CO vs. Intensity.

$I \frac{\text{MW}}{\text{cm}^2}$	T°K					
	750	905	1012	1554	3235	4294
0	1.2 E^{-20}	1.90 E^{-20}	1.8 E^{-20}	4.1 E^{-20}	7.0 E^{-20}	8.3 E^{-20}
.05	2.5 E^{-20}	2.2 E^{-20}	1.94 E^{-20}	4.2 E^{-20}	7.0 E^{-20}	8.3 E^{-20}
.1	4.2 E^{-20}	2.6 E^{-20}	2.1 E^{-20}	4.3 E^{-20}	7.0 E^{-20}	8.3 E^{-20}

Using these absorption cross-sections, we can determine the physical absorption length required to absorb the 737 kW determined to raise the working fluid to 5900°K. The absorption coefficients are obtained by multiplying the cross-sections by the numerical density of CO molecules; for example, resulting in $.31 \text{ cm}^{-1}$ for 4294°K at $I = 0$. This absorption coefficient enables us to obtain a first order estimate of the physical length since most of the power is to be absorbed in the temperature range 4294 to 5919°K. Thus, if the incident laser power is P and the optical depth is τ , then

$$P(1 - e^{-\tau}) = 7.37E5 \quad (26)$$

and

$$\tau = -\ln\left(1 - \frac{7.37E5}{P}\right) \quad (27)$$

Table 4 presents optical depth and physical length for absorption of 737kW as a function of input power.

Table 4. Approximate Length Requirements for Power Absorption.

P(MW)	τ	L cm
1	1.33	4.3
.9	1.71	5.5
.8	2.55	8.23

For efficiency it is worthwhile to keep the incident laser power as low as possible. Also, the lower the incident power, the less will be the incident power on the shoulders of the chamber which could conceivably be destroyed under the added heat burden. For example, when we have an 800 kW input, 63 kW remains to be dissipated beyond 8 cm, either in the gas or on the shoulders of the chamber. If the beam cross-section is 10 cm^2 , then the intensity falling on the wall shoulder would be 6.3 kW/cm^2 , which might be intolerable unless special cooling procedures were adopted or the shoulders were highly reflective.

A beam cross-section of 63 cm^2 would produce an intensity of 1 kW/cm^2 falling on the shoulders and an initial intensity of 12.7 kW/cm^2 incident on the methanol.

We now step off the absorption lengths by progressing from 750°K to 5919°K in discrete temperature jumps using the thermodynamic data and heat input requirements generated by our ODE program. Each temperature step requires a certain energy input per unit mass. This, when combined with the mass flow, produces the power absorption requirement for the fluid on being heated through this temperature region. Table 5 presents the absorption coefficients (K), absorption length, L, and power requirements for each temperature interval, starting with an initial power of 800 kW and a low intensity (such that the cross-sections for $I = 0$ can be used).

Table 5. Absorption Lengths for Heating CH_3OH to 5919°K by Temperature Intervals

T°K	750-905	905-1012	1012-1554	1554-2235	3235-4294	4294-5919
Power (MW)	1.6 E^{-2}	2.0 E^{-2}	6.9 E^{-2}	.11	.21	.31
K(cm^{-1})	.88	.85	.14	.54	.43	.307
L (cm)	.02	.03	.67	.31	1.0	5.6

The total absorption length is 7.6 cm.

4.4.4 The Role of Inverse Bremsstrahlung in Absorption

We have computed the absorption coefficients and corresponding absorption lengths by just considering particulate absorption and molecular absorption. We will now examine the role of electron inverse bremsstrahlung and show that it is negligible.

Inverse bremsstrahlung may be analyzed on the basis of classical weak plasma theory provided $h\nu < kT$ ⁽¹⁵⁾.

Under these conditions, the absorption coefficient for a plasma with n electrons per cm^3 undergoing ν collisions/sec with the background gas constituents, in a radiation field of $\omega = 2\pi f$ is given by ⁽¹⁶⁾

$$k = \frac{1}{c} \frac{4\pi n e^2 \nu}{m(\omega^2 + \nu^2)} \quad (28)$$

The collision frequency is given essentially by $\rho Q \nu$, where ρ is the numerical particle density of the CO molecules, Q the electron-CO momentum transfer collision cross-section, and ν the random speed of the electrons. In the mixture we are dealing with, the collision frequency is dominated by molecules with permanent dipole moments such as CO and H_2O .

At $T = 4294^\circ\text{K}$, $kT = .37\text{eV}$ and for $\lambda = 4.855\mu$, $h\nu = .26\text{eV}$ so the criterion $h\nu/kT < 1$ is satisfied. Also, $\nu = 4 \times 10^7 \text{ cm/sec}$, $Q = 1.4 \times 10^{-15} \text{ cm}^2$ ⁽⁸⁾
 $[\text{CO}] = 3.7 \times 10^{18} \text{ cm}^{-3}$, $n = 2.9 \times 10^{13} \text{ cm}^{-3}$. We derive $\nu = \rho Q \nu = 2 \times 10^{11} \text{ sec}^{-1}$.
Then $k = 4.4 \times 10^{-4} \text{ cm}^{-1}$, which is completely negligible.

The absorption due to inverse bremsstrahlung will become important only at ionization levels at least two orders of magnitude greater than found at this temperature. This can be accomplished either by doping or raising the temperature.

4.5 CONCLUSIONS

The longitudinal dimensions of the "combustion" chamber are determined by the absorption coefficient of the working fluid, the incident laser power and the target energy density to be absorbed to arrive at a prescribed temperature. The length of 7.6 cm was arrived at by requiring an absorption of 7.39×10^5 watts of laser power by the working fluid (the decomposition products of CH_3OH) to achieve a chamber temperature of 5919°K at a pressure of 125 psia and an input laser power of 800 kilowatts. The laser power requirements will vary as the thrust of the engine, which, other things being equal, will vary as the throat area. The absorption coefficient of the working fluid will be laser intensity dependent at low temperatures, but will be essentially independent of intensity at the higher temperatures $\approx 3000^\circ\text{K}$. It is at these higher temperatures that most of the energy is to be absorbed. Therefore, the overall length of the chamber will be insensitive to intensity. In general, it is advantageous to work with low intensity laser beams, first to decrease the thermal dissipation load on the chamber wall shoulders, second to decrease the energy density deposited in the material of the chamber window, thus limiting its temperature rise. If we limit the laser intensity falling on the chamber shoulders to a maximum of 1 kW/cm^2 , then the cross-sectional area of the incident 800 kW beam is to be greater than $\sim 60 \text{ cm}^2$, and the chamber is of commensurate area.

Large cross-sectional areas are advantageous because the gas velocities in the chamber are kept fairly low; in the case of 60 cm^2 , $\dot{m} = 3.08 \times 10^{-2} \text{ lb/sec}$ and $T = 5919^\circ\text{K}$ where the density is $7.07 \times 10^{-3} \text{ lb/ft}^3$, the velocity is 67 ft/sec. There will be, accordingly, very little pressure drop due to this streaming energy.

The efficiency of our CH_3OH -based propulsion unit is 59%. This assumes an input laser power of 800 kW with a laser power loss of 61 kW to the chamber walls and an area ratio of 100:1. The theoretical upper bound on the efficiency of the engine, assuming complete absorption of an incident laser power of $7.39 \times 10^5 \text{ wat.}$, is 64 percent.

The methanol is to be injected into the chamber in the gas phase to prevent excessive reflection and scattering of the laser beam from the liquid

sheets and droplets. Most of the energy to gassify the liquid might be obtained by using the liquid in a regenerative cooling fashion from the thruster walls. The chamber window may have to be protected from the heat and decomposition products of the methanol. This might be accomplished by subjecting the window to a continuous wash of cool He or H₂ at 125 psia. The injection of such additional materials into the working fluid will have to be taken into account when estimating absorption coefficients and performance of the propulsion system.

5. SUMMARY

A study has been made of various coupling processes between laser radiation and a propulsion working fluid flowing through a combustion chamber of a DeLaval nozzle.

The first part of the study forecasts a general discussion of three absorption mechanisms and the various advantages and disadvantages to their employment in a working fluid. The three mechanisms are molecular absorption, in which propellant molecules absorb the incoming (laser) energy, inverse bremsstrahlung, in which the electron content of the propulsive fluid is active as a coupling agent, and particulate coupling, in which the energy absorption is by small particulate matter in the propellant.

The second part discusses a particular configuration of thrust chamber and radiation flow. An initial selection is made that the radiation flow and propellant flow be in the same direction. A consequence of this coupling configuration is that the radiation enters the thruster at the upstream end of the thrust chamber. The required window at this upstream end and the attendant problems of energy absorption at this window from both the radiation beam and the heated propellant have been discussed in Section 8.0 of Volume 1.

For the selected coupling configuration, the working fluid is introduced into the thrust chamber, irradiated by the laser beam, and the heated products ejected and expanded in the thruster nozzle. Utilizing a One Dimensional Equilibrium (ODE) thermodynamic program and a model thrust chamber and nozzle, a study of three working fluids was made for possible candidates of the coupling investigations. The ODE program was run with an option whereby quantities of energy were injected into the working fluid. The most attractive working fluid on the basis of I_{sp} is hydrogen, H_2 . The coupling of H_2 to laser wavelengths can be accomplished, however, only by doping, either with particulates, selected molecular species, or (possibly) some easily ionizable elements. The difficulties attendant with low density, cryogenically stored propellants, and the mechanics of the doping of H_2 were of sufficient magnitude for us to consider other propellant candidates, even at a loss of considerable specific impulse. Two

other candidates examined were ammonia, NH_3 , with a dissolved additive (lithium, Li) and methyl alcohol, CH_3OH . The NH_3/Li is attractive because it readily absorbs the 10.6 micron line of CO_2 lasers when cold, and after heating, continues to absorb, using inverse bremsstrahlung as a coupling mechanism. The NH_3 molecule, however, decomposes at fairly low temperatures and can not, therefore, absorb sufficient energy to reach the temperatures at which the Li additive would be sufficiently ionized. A possible solution to such a loss of coupling through decomposition would be to provide additional additives which would retain the required absorption levels in these intermediate (1500°K - 3000°K) temperature regions. Another candidate examined, methanol, exhibits none of these difficulties. Methanol absorbs at all IR wavelengths and decomposes with the release of energy to form carbon monoxide, carbon, and water. The methanol decomposition products are, therefore, ideal for coupling with radiation from a CO laser. Methanol was, accordingly, selected for the more thorough coupling study.

The methanol coupling study considers CO radiation at a wavelength of 4.855 microns. Coupling with the carbon particulate matter is examined, as are molecular absorption and inverse bremsstrahlung absorption processes. For molecular absorption, previous analyses by Physical Science Incorporated are used, after a suitable modification from that earlier study pressure requirement of 30 atmospheres (450 psi) to the 8.5 atmosphere (125 psi) pressure chosen in this present application. For the 8.5 atmosphere pressure selected and for heating to 5900°K, methanol produces an I_{sp} of 838 seconds at $c = 100$, and requires 0.75 megawatts of input energy to achieve a thrust of 26 pounds in the model thruster.

To provide the necessary design information for the thrust chamber of the thruster, the ODE program was run with the methanol propellant and for a range of temperatures below 5800°K. The absorption coefficients of the methanol decomposition products were determined at 8.5 atmospheres and at the various temperatures. From this the required thrust chamber length for the absorption of most of the laser energy was found to be approximately 8 centimeters.

In the coupling process, most of the absorption is accomplished by molecular absorption. The role of inverse bremsstrahlung was found to be negligible, and particulate absorption was found to be briefly, of importance during the onset of coupling when solid carbon is present. Beyond

approximately 1500°K, however, the carbon particles disappear and particulate coupling is eliminated. The absorption of CO radiation by the CO molecule, and the relaxation of these vibrationally excited CO in collisions with H₂ provide an effective mechanism for increasing propellant temperature and the resulting specific impulse. The study also examines the possible role of electrons in providing vibrational relaxation for the CO and concludes that this process would only become effective for concentrations of electrons several orders of magnitude in excess of those actually obtained in the working fluid.

The results of the methanol coupling study indicated that other working fluids would probably, in general, require the addition of specific, doping, molecular species to provide sufficient absorption for the incident laser radiation. The available infrared absorption data of a series of molecular species is examined. The molecular species examined included HF, DF, CO₂, CO, NO, H₂O, NH₃, and CH₃OH. The results of that data review are presented in this volume as Appendix E, Spectral Absorption Parameters of Molecular Species for Possible Use in Laser-Assisted Propulsion. The data has been reduced, in some cases, so that transition cross-sections can be obtained or deduced, including the effects of line pressure broadening with increasing temperature. Absorption cross sections and high intensity effects (bleaching) can be computed from this data provided de-excitation rates are known.

The results of the analyses here indicates a successful (efficient, high specific impulse) coupling for methanol irradiated with CO laser radiation. In addition, many of the other absorbing molecular species and laser wavelength combinations exhibit significant promise.

REFERENCES

1. Caledonia, Wu, and Pirri, "Radiant Energy Absorption Studies for Laser Propulsion," Physical Sciences, Inc., NAS3-18528 1975.
2. Buonadonna, Knight, and Herzberg, "The Laser Heater Wind Tunnel, A New Approach to Hypersonic Laboratory Simulation," AIAA Paper No. 73-211, Jan. 1973.
3. A. H. Shapiro, Compressible Fluid Flow, Vol. 1, Ronald Press, 1953, p. 190 ff.
4. TRW, "Survey of Secondary Propulsion and Passive Altitude Control Systems for Spacecraft," 15 December 1967, 100C3-6001-R000.
5. Seidell, Solubilities of Inorganic Metal Organic Compounds, 4th Edition.
6. Pack and Phelps, Phys. Rev., February 1, 1961, Vol. 2, p. 362.
7. Millikan and White, "Systematics of Vibrational Relaxation," J. Chem. Phys., 39, No. 12, 1963.
8. Kieffer, L. J., "A Compilation of Electron Collision Cross-Section Data for Modeling Gas Discharge Lasers," JILA Report 13, Sept. 30, 1973.
9. Fermi, Nuclear Physics, University of Chicago, 1950, p. 145.
10. Lee, Hunt, and Plyler, "A High Resolution Study of the OH-Stretch Fundamental of Methanol," J. Mol. Spect., 57, 138-154, 1975.
11. Gaydon and Wolfhard, Flames, MacMillan, New York, 1960.
12. P. Molmud, "Laser Heating of Air Via Aerosols," TRW, 11 October 1971.
13. Kerker, Ed., Electromagnetic Scattering, Pergamon Press, 1963.
14. Ludwig, Malkmus, Reardon, and Thomson, NASA SP-3080, Handbook of IR Radiation from Combustion Gases, 1973.
15. Phelps, A. V., "Theory of Ionization During Laser Breakdown," in Physics of Quantum Electronics, Ed. Kelley, Lax, Tannenwald, McGraw-Hill, 1966.
16. Molmud, P., "The Electrical Conductivity of Weakly Ionized Gases," STL (TRW), Sept. 1962.

Appendix A

Combined One and Two-Dimensional Kinetic

Reference Computer Program: ODK and TDK (Improved 1973 Version)

Computer

CDC 6600

Program Description

The JANNAF (formerly ICRPG) combined one-and two-dimensional kinetic nozzle analysis computer program (ODK and TDK) calculates the inviscid one and two-dimensional equilibrium frozen and nonequilibrium nozzle expansion of gaseous propellant exhaust mixtures containing the six elements carbon, hydrogen, oxygen, nitrogen, fluorine, and chlorine. The program considers 40 significant gaseous, plus one inert, species present in the exhaust mixtures of propellants containing these elements and the 150 chemical reactions (13 dissociation-recombination reactions of stratified flow (film cooled engine case). Chapman-Jouget criteria detonation calculations can be made. A perfect gas nozzle analysis option is available. Interface provision is made to TDK with the Distributed Energy Release (DER) combustion vaporization code. Provision is made to interface with BLIMP, the boundary layer code. Calculations and printout is available in English and International Standard (Metric) SI units.

Documentation and References

"Two-Dimensional Kinetic Reference Computer Program", by G. R. Nickerson, R. E. Coats, J. L. Bartz, December 1973.

Appendix B

Program CO for Determination of
CO Vibrational Population Density
as a Function of Temperature and
Intensity and to Produce a
Weighted Absorption Cross-Section.

```

PROGRAM CO (TAPE6)
DIMENSION N(6),E(5),S(5)
REALN,I,K
T=750.
C THE S=S, ARE CROSS SECTIONS FOR,01,12,23,34,45,VIBRATIONAL TRANS.
S(1)=1.1E-20
S(2)=3.48E-20
S(3)=5.98E-19
S(4)=1.02E-20
S(5)=6.7E-20
      DO 251 JK=1,11
I=1.2E25*(JK-1)/10.
N(1)=1.
CCO=.004
H2=.098
T1=EXP(175.*(T**(-1./3.)-.029)-18.46)/8.5
T2=EXP(68.*(T**(-1./3.)-.0172)-18.42)/8.5
R=CCO/T1+H2/T2
E(1)=4.26E-13
E(2)=4.21E-13
E(3)=4.15E-13
E(4)=4.10E-13
E(5)=4.01E-13
K=1.4E-16
N(2)=(S(1)*I+R*EXP(-E(1)/K/T))/(R+S(1)*I)
TN=1.+N(2)
      DO 25 J=2,5
N(J+1)=N(J)*(I*(S(J-1)+S(J))+R*(1.+EXP(-E(J)/K/T)))-
+ N(J-1)*(I*S(J-1)+R*(EXP(-E(J-1)/K/T)))
N(J+1)=N(J+1)/(R+I*S(J))
TN=TN+N(J+1)
25  CONTINUE
TABS=S(1)/TN
      DO 26 L=2,5
TABS=TABS+N(L)*S(L)/TN
26  CONTINUE
WRITE(6,27)TN,(N(J),J=1,6),TABS,I
27  FORMAT (2X,E12.5/2X,6E12.2/2X,*WTD ABS CS*,2X,E12.5/
+ 2X,*INTENSITY=*,1X,E12.2/)
251 CONTINUE
      END

```

Appendix C

Laser Absorption Coefficients Due to Inverse Bremsstrahlung

Let us take the case of H_2 with $\Delta H = 9.38 \times 10^4$ and $P_c = 125$. The thermodynamic output of the ODE program predicts $1.0 \times 10^{19} \text{ cm}^{-3}$ hydrogen atoms, $3.13 \times 10^{18} \text{ cm}^{-3}$ H_2 molecules and $5.4 \times 10^{12} \text{ cm}^{-3}$ electrons. Reference 1, page 10, Figure 2.1, predicts the hydrogen atom neutral bremsstrahlung absorption cross section for $\lambda = 5$ and $10 \mu\text{m}$ at 5000°K as $\sim 2.5 \times 10^{-37} \text{ cm}^5$ and $2 \times 10^{-36} \text{ cm}^5$, respectively. These translate to absorption coefficients of $1.35 \times 10^{-5} \text{ cm}^{-1}$ and $1.08 \times 10^{-4} \text{ cm}^{-1}$, for hydrogen atoms.

The contribution from the hydrogen molecules can be estimated in the following way: the cross-section for momentum transfer for electrons impacting H_2 is approximately $(6) 10^{-15} \text{ cm}^2$. The speed of electrons at 4700°K is $\sim 4.5 \times 10^7 \text{ cm/sec}$. The electron H_2 collision frequency is therefore $\nu \sim 1.39 \times 10^{11} \text{ sec}^{-1}$. The absorption coefficient is given by $(7) \sim \frac{n\nu}{9\omega}$ where n is electron density, ν is collision frequency and $\omega = 2\pi \times \text{wave frequency} = 3.77 \times 10^{14} \text{ sec}^{-1}$ for $\lambda = 5\mu$ and $1.88 \times 10^{14} \text{ sec}^{-1}$ for $\lambda = 10\mu$. This results in an absorption coefficient of $5.9 \times 10^{-7} \text{ cm}^{-1}$ for $\lambda = 5\mu$ and 2.4×10^{-6} for $\lambda = 10\mu$. The resulting absorption coefficients imply lengths of 10^4 cm before any appreciable laser absorption is effected. Obviously electron densities two or more orders of magnitude are required for efficient coupling.

The $\text{Li} - \text{NH}_3$ example had $4.178 \times 10^{19} \text{ cm}^{-3}$ hydrogen atoms (at 750 psia) as the major constituent and $2.9 \times 10^{17} \text{ cm}^{-3}$ electrons. The absorption cross-section for $\lambda = 5\mu$ at $\sim 6000^\circ\text{K}$ is $\sim 3 \times 10^{-37} \text{ cm}^5$. The absorption coefficient then becomes 3.6 cm^{-1} or an absorption mean free path of .275 cm. This is somewhat too small and could be adjusted by reducing the concentration of Lithium in NH_3 or reducing P_c or both.

Reference 1. Caledonia, Wu, and Pirri, "Radiant Energy Absorption Studies for Laser Propulsion," Physical Sciences, Inc., NAS3-18528 1975.

Appendix D

The Role of Vibrational Deactivation of CO by Electrons

We will first derive estimates for the deactivation time due to electron impact. The reason for choosing electrons to investigate, is that they have a fairly high vibrational excitation cross-section and therefore a high de-excitation cross-section. Furthermore, electrons have very high velocities at conventional temperatures and can therefore promote vibrational transitions (collisional deactivation) at large rates. An obvious disadvantage to electrons is that their density at $\sim 300^\circ\text{K}$ is expected to be low, usually. There can be situations, however, when electron densities can be high, such as conditions of UV illumination of X-ray or β -ray irradiation or even in simple hydrocarbon flames. We shall leave our options open for the time being.

We are interested in the process:



and its inverse. Here the asterisk means an excited state. The cross section for excitation of the first vibrational level (.26eV) from ground state is $\sim 10^{-17} \text{ cm}^2$ for electron energies from .29 eV to 1.1 eV (Ref. 8). However, Reference 1 also gives values of $\sim 6 \times 10^{-16} \text{ cm}^2$ above .48 eV. We shall use the lower figures for the cross-section.

Using a principle of statistical mechanics known as "Detailed Balancing" (Fermi)⁽²⁾, we can relate the excitation cross-section denoted by σ_+ to its inverse σ_- , the cross-section for vibrational deactivation. Thus:

$$P_1^2 g_e g_{\text{CO}} \sigma_+ = P_2^2 g_e g_{\text{CO}^*} \sigma_- \quad (2)$$

where P_1 and P_2 are the momenta of the electron before and after collision and the g 's are the statistical weights for the components, e , CO and CO^* .

The P 's are related by

$$\frac{P_1^2}{2m} = \frac{P_2^2}{2m} + .26 \text{ eV} \quad (3)$$

where m is the mass of the electron. Solving for σ_+ we obtain

$$\sigma_+(v_1) = \frac{\sigma_+(v_1) \times (v_2^2 + \frac{2}{m} \times .26 \times 1.6 \times 10^{-12})}{v_2^2} \quad (4)$$

where the ratio of the g 's is taken to be 1.

The cross-section $\sigma_+(v)$ vanishes for energies less than the excitation threshold. Then for electron energies of .04 eV (300°K) we get $\sigma_+ \approx 7.5 \times 10^{-17} \text{ cm}^2$. Now the mean speed of a .04 eV electron is $1.13 \times 10^7 \text{ cm/sec}$. The de-excitation coefficient of such an electron is given by $\sigma_+ v = 8.5 \times 10^{-9} \text{ cm}^3/\text{sec}$ and the relaxation time by $\tau = 1/n\sigma_+ v$ where n is the electron density. When $n = 2.6 \times 10^{20}$ (10 atmospheres of electrons) then $\tau = 4.53 \times 10^{-13} \text{ sec}$. This relaxation time is considerably smaller than the times previously quoted. It is, however, exceedingly difficult to get such electron densities, especially at these energies. We can conversely determine the electron density which is equivalent to 10 atmosphere of hydrogen by equating relaxation times. The result is that $1.2 \times 10^{13} \text{ electrons/cm}^3$ is equivalent to 10 atmosphere of hydrogen as far as promoting vibrational relaxation in CO. As mentioned before, such electron densities are not to be expected at 300°K unless drastic measures are taken to insure their existence. Such densities may be found in seeded plasmas at 3000°K or higher. However, at such temperatures even self-deactivated CO at 10 atmospheres has a relaxation time of 10^{-6} sec . At this temperature (.265 eV), the electron deactivation cross-section is $\sim 2 \times 10^{-17} \text{ cm}^2$ and the speed is $\sim 3 \times 10^7 \text{ cm/sec}$ so that the de-excitation coefficient is approximately the same as 300°K. Accordingly, electrons will have to be injected with sufficient quantity and at low temperatures for their role in vibrational deactivation to be important.

Reference 1. Kieffer, L. J., "A Compilation of Electron Collision Cross-Section Data for Modeling Gas Discharge Lasers," JILA Report 13, Sept. 30, 1973.

Reference 2. Fermi, Nuclear Physics, University of Chicago, 1950, p. 145.

APPENDIX E

SPECTRAL ABSORPTION PARAMETERS OF MOLECULAR SPECIES FOR POSSIBLE USE IN LASER-ASSISTED PROPULSION

TABLE OF CONTENTS

	<u>Page</u>
1. ASSIGNED TASKS AND COMMENTARY	42
1.1 Identify Useful Molecular Species for Laser Beam Energized Rocket Propulsion	42
1.2 Determine, Quantitatively if Possible, Useful Absorption Parameters for the Molecular Gases as Possible Absorbing Species Candidates	42
2. MOLECULAR SPECIES SUGGESTED FOR INVESTIGATION	48
3. ABSORPTION DATA, COLLECTED OR COMPUTED FOR VARIOUS MOLECULAR SPECIES	49
3.1 HF and DF	49
3.1.1 Meridith and Smith (November 1971) Data for DF	49
3.1.2 HF Data from Meridith and Smith (November 1971) and C. M. Randall (December 1975)	53
3.1.3 Goldman, et al. (August 1973) Data for HF and DF at 1273°K	58
3.1.4 HF High Temperature Absorption Data from <u>The Handbook of IR Radiation from Combustion Gases</u> , by Ludwig, et al. (1975)	63
3.2 CO ₂	66
3.2.1 Self-Absorption of 10.4μ Region or 9.4μ Region CO ₂ Laser Lines	66
3.2.2 CO ₂ Absorption in the 1830 to 2400 cm ⁻¹ Spectral Region of CO and DF Laser Radiation	72
3.2.3 CO ₂ Absorption in the 3100 to 3750 cm ⁻¹ Spectral Region of HF Laser Radiation	75
3.3 Self Absorption of CO Laser Radiation	75
3.3.1 Bank Model Studies	75
3.3.2 Self-Absorption by the Inverse of the CO Laser Line Transition	82
3.4 NO as an Absorber for CO Laser Radiation	89
3.5 OH as an Absorber for HF Laser Radiation	93
3.6 Band Model Absorption for Water Vapor (H ₂ O)	96
3.7 Absorption by Ammonia (NH ₃) of CO ₂ Laser Radiation	99
3.8 Absorption by Methanol (CH ₃ OH) of CO ₂ and HF Laser Radiation	115

TABLE OF CONTENTS (Continued)

	Page
4. LINE WIDTH PARAMETERS	123
5. SUMMARY	125
BIBLIOGRAPHY	126

LIST OF FIGURES

Figure		Page
1	Summary of HF Experimental Line-Width Parameter Data	54
2	Line Intensities versus Wavenumber for the HF $\Delta v = 1$ Bands at 1273 K	59
3	Absorption Coefficient for HF at Standard Temperature and Pressure	64
4	Line Density for HF	65
5a-b	Variation of Half-Width with Rotational Quantum Number for the 10-4 μ m CO ₂ Band	71
5c-d	Variation of Half-Width with Rotational Quantum Number for the 9.4 μ m CO ₂ Band	71
6	$\bar{k} = \overline{S/d}$ of C ¹² O ₂ versus Wavenumber for T = 1800, 2400 and 3000 K	73
7	Value of the Line Density Parameter $1/d_0$ for the 4.3 μ Band of C ¹² O ₂	74
8	$k = \overline{S/d}$ of C ¹² O ₂ versus Wavenumber for T = 300, 600, 1200 and 1500K	76
9	$k = \overline{S/d}$ of C ¹² O ₂ versus Wavenumber for T = 1500, 1800, 2400 and 3000K	77
10	Values of the Line Density Parameter $1/d_0$ for the 2.7 μ Band of C ¹² O ₂	78
11	Absorption Coefficient for CO at Standard Temperature and Pressure	79
12	Line Density for CO	80
13	Room Temperature, High Pressure Absorption Spectra of the V = 0 \rightarrow -, V = 1 \rightarrow 2 and V = 2 \rightarrow 3 Bands of CO	83
14	Absorption Cross-Section versus Temperatures for Five Lowest Vibrational Transitions in CO at a Wavelength of 4.855 μ m	84
15	Room Temperature, High Pressure Absorption Spectra of the V = 0 \rightarrow 1, V = 1 \rightarrow 2 Bands of NO	90
16	Absorption Coefficient for NO at Standard Temperature and Pressure	91

LIST OF FIGURES (Continued)

<u>Figure</u>		<u>Page</u>
17	Line Density for NO	92
18	Absorption Coefficient for OH at Standard Temperature and Pressure	94
19	Line Density for OH	95
20	Plot of $(1/d)$ for H ₂ O versus ω Between 1150 cm ⁻¹ and 7500 cm ⁻¹ for T = 600, 1000, 1500, 2000, 2500, and 3000K	97
21	Mean Spectral Absorption Coefficient for Water Vapor at Various Temperatures - f. 2500°K	98
22	Mean Spectral Absorption Coefficient for Water Vapor at Various Temperatures - g. 3000°K	98
23	Fine Structure of the Fundamental ν_2 of NH ₃ at 10.5	100
24	Infrared Gas Spectra of Species with Symmetric Methyl Groups, Taken at Resolutions Between 0.5 2 cm ⁻¹	116
25	OH-Stretch Fundamental of Methanol	117

LIST OF TABLES

Table		Page
1	DF Parameters Computer from Meredith and Smith Data	50
1a	DF Vibrational Level Distribution at 296°K	51
1b	Approximate DF Vibrational/Rotational Level Distribution $r_v "(296^\circ\text{K}) \cdot r_j "(296^\circ\text{K})$	51
2	Einstein $A_{u \rightarrow l}$ Coefficients and Integrated Line Strengths for some Selected HF $\Delta v = 1$ P-Branch Transitions	55
2a	Vibrational Level Distributions for HF at 290°K	56
2b	Approximate Rotational Level Population Factors for HF at 296°K	56
3	Spectral Line Parameters for the HF $\Delta v = 1$ Bands at 1273K	59
4a	$\text{C}^{12}\text{O}_2^{16}$ Parameters Calculated from Young and Chapman Data, for the $\sim 10.4\mu$ $0\#0^\circ 1 \leftarrow (1\# 0^\circ \#0, 0\# 2^\circ \#0)_1$ Band; $T_0 = 300^\circ\text{K}$	68
4b	$\text{C}^{12}\text{O}_2^{16}$ Parameters Calculated from Young and Chapman Data, for the ~ 9.4 $0\# 0^\circ 1 \leftarrow (1\# 0^\circ \#0, 0\# 2^\circ \#0)_{11}$ Band; $T_0 = 300^\circ\text{K}$	69
5	Apparent Absorption Coefficients of CO	85
6	Spectral Data for the V_2 Bands of Ammonia	102
7	V_2 Band Parameters from 1140.76 to 88.108 cm^{-1}	103
8	Infrared Spectrum of CH_3OH (Frequency in cm^{-1} , Accuracy $\pm 0.5 \text{ cm}^{-1}$)	119
9	Estimates for Relative Band Intensities from IR Spectra	121
10	Model Values for the Collision Line Width Parameters	124

1. ASSIGNED TASKS AND COMMENTARY

1.1 IDENTIFY USEFUL MOLECULAR SPECIES FOR LASER BEAM ENERGIZED ROCKET PROPULSION

The molecules of interest must be capable of strong spectral absorption of monochromatic laser line radiation from the DF laser (~ 3.6 to $\sim 3.9 \mu$ region), the HF laser (~ 2.6 to 2.9μ region), the CO laser (~ 4.9 to $\sim 5.7 \mu$ region), or the CO_2 laser (either $\sim 10.4 \mu$ or $\sim 9.4 \mu$ region). The propulsion chamber gases might initially be required to absorb at a low temperature, say $\sim 300^\circ\text{K}$, but would then rapidly be heated up to ~ 4000 to 6000°K . The chamber pressures would be expected to be at $\sim 8 \frac{1}{2}$ atmospheres or perhaps higher. So absorption profiles at high temperature and high pressure are of interest. The gas or gases selected to do the initial laser beam absorption at lower temperatures may dissociate at elevated temperatures and pressures. (It then would be convenient if some of the expected dissociation products also absorbed the energizing radiation.) On the other hand, it is possible that other species of gases also injected into the chamber could take over the task. In particular, some gaseous species whose sharp low pressure, low temperature spectral line profiles would not coincide with and efficiently absorb the impinging laser line radiation, might exhibit efficient absorption of these laser lines when their absorption profiles are smeared into quasi-continua by high pressure and enriched high temperature "hot band" absorption.

1.2 DETERMINE, QUANTITATIVELY IF POSSIBLE, USEFUL ABSORPTION PARAMETERS FOR THE MOLECULAR GASES SELECTED AS POSSIBLE ABSORBING SPECIES CANDIDATES

It would be preferable to exhibit these parameters as either spectral absorption coefficients $k(\nu)$ in terms of inverse (atmosphere-centimeters-STP), or, better yet, as the absorption cross-section $\sigma(\nu)$ in terms of cm^2 per molecule. Since, owing to radiative "bleaching" processes, the assumption

of thermal equilibrium would be at best highly questionable, and possibly completely invalid, both $k(\nu)$ and $\sigma(\nu)$ should be defined in terms of the population density N_ℓ of the lower molecular states involved in the $\ell \rightarrow u$ state molecular absorption transmissions centered on ν_0 's (in the near vicinity of ν), rather than on total species populations N . If, and only if, thermal equilibrium is a reasonably valid assumption, N_ℓ is related to N by the familiar relation:

$$N_\ell \approx \left\{ N g_\ell e^{-\frac{(hc/kT)(E_\ell)}{kT}} \right\} / Q(T) \quad , \quad (1)$$

where all symbols used have their usual connotations.

No values for the desired $k(\nu)$ or $\sigma(\nu)$ functions were found directly in the literature. Where absorption coefficients or cross-sections were given explicitly, they were given at some standard temperature and pressure for the assumption of thermal equilibrium, and in terms of the total species population density, N , rather than per lower state population density, N_ℓ . These thermal equilibrium population parameters, at a standard temperature and pressure T_0 and P_0 , will be designated here by the symbols $\hat{k}(\nu; T_0, P_0)$ and $\hat{\sigma}(\nu; T_0, P_0)$. If the pressure of interest P is equal to P_0 , then

$$N \hat{\sigma}(\nu_0) \approx N_\ell \sigma(\nu_0) \quad , \quad (2)$$

and

$$\frac{\sigma(\nu_0)}{\hat{\sigma}_{T_0}(\nu_0)} = \left\{ Q(T) e^{\frac{(hc/kT_0)(E_\ell)}{kT_0}} / g_\ell \right\} \approx \frac{k(\nu_0)}{\hat{k}_{T_0}(\nu_0)} \quad . \quad (3)$$

Quite often, particularly when the most reliable data available is computed rather than directly observed, the parameters tabulated are neither σ or k (nor, in my present notation, $\hat{\sigma}_T$ or \hat{k}_{T_0}), but line transition matrix elements $|\Sigma R_{\ell \rightarrow u}|^2$, or Einstein coefficients $A_{u \rightarrow \ell}$ or $B_{\ell \rightarrow u}$, or (hopefully) line strength parameters $S_{\ell \rightarrow u}(\nu_0)$. These parameters are all inter-related by well known and relatively simple formulae, which nevertheless still require appreciable computation time to convert columns of data from one to the other.

The easiest of these to use is the line strength parameters $S_{l \rightarrow u}(v_o)$, which, however, are usually tabulated in terms of total species population density N with the assumption of thermal equilibrium at some standard temperature T_o . Again, these quantities here will be designated by $\hat{S}_{T_o}(v_o)$, with $S(v_o)/\hat{S}_{T_o}(v_o)$, also being given by an equation similar to Eq. (2).

Depending upon whether the line strength factors are listed in units of $(\text{atmosphere-cm-STP})^{-1} \cdot \text{cm}^{-1}$ or $(\text{molecules/cm}^2) \text{cm}^{-1}$,

$$\hat{S}'_{T_o}(v_o) = \int_{-\infty}^{\infty} \hat{k}_{T_o}(v_o;v) dv \quad (4a)$$

or

$$\hat{S}_{T_o}(v_o) = \int_{-\infty}^{\infty} \hat{\sigma}_{T_o}(v_o;v) dv, \quad (4b)$$

with completely similar relations between $S(v_o)$ and either $k(v_o;v)$ or $\sigma(v_o,v)$ for absorption parameters referred to lower state rather than total population densities. If the normalized spectral line profile functions are designated by $f(v,v_o)$, then:

$$f(v_o;v) = \frac{\sigma(v_o,v)}{S(v_o)} = \frac{k(v_o,v)}{S'(v_o)} = \frac{\hat{\sigma}(v_o,v)}{\hat{S}(v_o)} = \frac{\hat{k}(v_o,v)}{\hat{S}'(v_o)}, \quad (5)$$

where

$$\int_{-\infty}^{\infty} f(v_o,v) dv = 1 \quad (6)$$

It is to be noted that the cap and prime symbolizations are for this treatment only, and that in the literature the (integrated) line intensities quantities designated as \hat{S} and \hat{S}' both appear as merely S , or $S(T)$. Similarly, $\hat{\sigma}_{T_o}(v_o;v)$ and $\hat{k}_{T_o}(v_o;v)$ and $k_{T_o}(v_o,v)$ generally are labeled as $\sigma(v_o,v)$ or $k(v_o,v)$ functions.

If P_1 represents the partial pressure of the gaseous species with an absorption line centered on ν_0 , N_ℓ represents the total number density of this species in the specific lower energy state ℓ that corresponds to the $\ell \rightarrow u$ absorption transition leading to the "line" centered on ν_0 , and δx represents an absorption path increment, then

$$N \hat{\sigma}_{T_0} \delta x = N_\ell \sigma \delta x = p_1 \hat{k}_{T_0} \delta x = p_1 (N_\ell/N) k \delta x \quad (7)$$

From Eq. (5), and canceling out the common δx and $f(\nu_0, \nu)$ factors,

$$N \hat{S}_{T_0} = N_\ell S = p_1 \hat{S}_{T_0}' = p_1 (N_\ell/N) S' \quad (8)$$

For an ideal gas at thermal equilibrium, $p_1 = N kT$, and thus

$$\frac{\hat{S}'(\nu_0)}{\hat{S}(\nu_0)} = \frac{\hat{k}(\nu_0, \nu)}{\hat{\sigma}(\nu_0, \nu)} = \left(\frac{1}{kT_0} \right) \quad (9a)$$

and

$$\frac{S'(\nu_0)}{S(\nu_0)} = \frac{k(\nu_0, \nu)}{\sigma(\nu_0, \nu)} = \left(\frac{1}{kT} \right) \quad (9b)$$

However, the primed line intensities \hat{S}' and S' , and the corresponding absorption coefficients \hat{k} and k generally are meant to be expressed in terms of atmosphere-cm of the absorbing species of gas when (conceptually) reduced to STP conditions. Now, there are $\sim 2.69 \cdot 10^{19}$ molecules cm^{-3} of a gas at STP. Thus, if T is kept at (or near) the standard T_0 value, and p_1 is expressed in atmospheres as is intended, then

$$N \approx 2.69 \cdot 10^{19} \frac{\text{molecules cm}^{-3}}{(\text{atmos-STP})} \cdot p_1$$

and Eq. (9a) can be rewritten as,

$$\frac{\hat{S}'(\nu_0)}{\hat{S}(\nu_0)} = \frac{\hat{k}(\nu_0, \nu)}{\hat{\sigma}(\nu_0, \nu)} = 2.69 \cdot 10^{19} \frac{\text{molecules cm}^{-3}}{(\text{atmos-STP})} \quad (10)$$

The integrated line strength parameters S , S' , \hat{S}_T and \hat{S}_T' are virtually independent of pressure broadening effects. \hat{S}_0 and \hat{S}_0' are, however, temperature-dependent through a relation similar to Eq. (3).

The line shape factors $f(v_0, v)$ are in general both temperature and pressure dependent. For moderate temperatures and pressures, the Lorentz, or collision broadened profile,

$$f(v_0, v) = \frac{a_c}{\pi \{a_c^2 + (v - v_0)^2\}} \quad (11)$$

is a reasonably good approximation, with the pressure-dependent half-width at half maxima, a_c , being approximated by the expression,

$$a_c \approx a_0 P \sqrt{T/T_0} \quad \begin{cases} a_c \text{ in cm}^{-1} \\ a_0 \text{ in cm}^{-1} \text{ atmos}^{-1} \\ \text{evaluated at 1 atmos} \\ \text{pressure and } T = T_0 \end{cases} \quad (12)$$

and

$$P = p_1 + \sum_{i=2}^n C_i p_i \quad \begin{cases} P \text{ and } p_i \text{ in units} \\ \text{of atmospheres} \end{cases} \quad (13)$$

Here, p_1 represents the partial pressure of the spectrally absorbing species, while the p_i and C_i (usually all $C_i < 1$) are the partial pressures and relative broadening efficiency of the other constituent gases. It is seen from Eq. (11) that at the line center, $f(v_0, v_0) = (1/\pi a_c)$. At line center for collision broadened lines, therefore, depending upon how the line strength factors are defined,

$$\sigma(v_0, v_0) = \frac{S(v_0)}{\pi a_c} \quad ; \quad (14a)$$

or

$$k(v_0, v_0) = \frac{S'(v_0)}{\pi a_c} \quad ; \quad (14b)$$

with similar expressions relating the capped (thermal equil-distribution total population values) parameters $\hat{\sigma}$ and \hat{S} or \hat{k} and \hat{S}' .

It is evident from Eqs. (11) and (12) that increases in pressure both increase the effective width of each spectral line, and decrease its effectiveness in the near vicinity of the line center.

For very low pressures (which are non-applicable here) or for very high temperatures (particularly near line centers), the Doppler line profiles predominate over collision profiles. In the latter case of both high temperatures and high pressures, the Voigt line profile, which represents a convolution of Doppler and collision perturbations, should be used. For some of the high temperatures and pressures of interest in the current problem, the exponential decay Doppler profiles may predominate near the line center, while the collision profiles still predominate one or two half-widths removed from the centers. High pressures also tend to distort the molecules and cause some slight shifts in line center positions.

Also, at high temperatures (but below those leading to dissociation), higher energy vibration-rotation (and electronic) energy levels tend to be populated. This decreases the absorption from the lower energy levels but introduces new "hot bands" which tend to fill in the spectral absorption profiles and lead to quasi-continua.

It would be most useful to be able to exhibit either $k(\nu)$ or $\sigma(\nu)$ [or even $\hat{k}(\nu)$ or $\hat{\sigma}(\nu)$] as quasi-continuous spectral functions for the full spectral and temperature-pressure regimes of interest. Unfortunately, there is in the literature a paucity of that data which is useful for high spectral resolution application. Most of the high temperature-high pressure data which does exist was designed for use with low spectral resolution devices (radiometers, etc.), and consist largely of artificial "Band Model" computations. The use of these band model computations, or of the coarse spectral resolution data with which they generally are compared, generally would be highly unreliable for application to laser beam absorption.

An exception occurs, however, when the complexity and "richness" of the molecule's spectra is such that neighboring spectral lines tend to be so close together that the mean line separation in the region of the laser emission tends to be about the same, or better, less than the effective line widths. This is particularly true when the absorption "line" profiles are broadened by pressure [see Eqs. (11) and (12)], and when the absorption spectra is enriched by significant contributions from "hot band" absorption transitions originating from relatively highly excited lower state energy levels. Under these conditions, even the cruder "band model" absorption curves become reasonably valid approximations for the absorption of laser radiation.

2. MOLECULAR SPECIES SUGGESTED FOR INVESTIGATION

It was initially suggested to examine the spectra of possible reactants, CH_4 , NH_3 , CH_3OH , H_2O , N_2 , Li_2 , and possible dissociation-reaction products thereof, such as H_2 , O , OH , H , C , CO , N , and LiH . However, both the monotomic species such as O , H , C , N , etc., and the diatomic symmetric species such as O_2 , N_2 , H_2 , and Li_2 are devoid of (electric dipole active) infrared spectra.

While CH_4 has some strong infrared absorption in fundamental vibration-rotation bands near 3.3μ and near 7.66μ , these would be inefficient for absorption of any of the laser radiation of current interest. At sufficiently high temperatures, CH_4 overtone and combination bands and absorption from excited state vibrational energy levels might be of some use, but then dissociation would soon set in. It therefore was recommended that CH_4 be abandoned as a non-promising reactant.

The strongest absorption of laser lines originating in induced transitions from excited states to the ground state, would be expected to be self-absorption by the lasing species molecules themselves. It therefore was decided to also investigate absorption by ("seeded") DF , HF , and CO .

The strong 10.4μ and 9.4μ CO_2 laser emission is from (the rotational levels of) an excited vibrational state designated as $0\ 0^\circ\ 1$ down to rotational levels of a pair of low lying Fermi-resonating levels designated as $(1\ 0^\circ\ 0, 0\ 2^\circ\ 0)_I$ and $(1\ 0^\circ\ 0, 0\ 2^\circ\ 0)_{II}$, respectively. Under thermal equilibrium conditions near room temperature, the self-absorption of CO_2 owing to the reverses of these two transmissions would be expected to be relatively quite weak, since the room temperature populations of the lower state $(1\ 0^\circ\ 0, 0\ 2^\circ\ 0)_I$ and II levels are down by a factor of $\sim 10^{-3}$ from that of the corresponding ground vibrational state, $0\ 0^\circ\ 0$, levels. However, at temperatures of $\sim 1000^\circ\text{K}$ or higher, there could be appreciable self-absorption by CO_2 . At higher temperatures and pressures, "hot band" absorption and broadened line profiles would convert the closely packed CO_2 absorption spectrum into a fairly efficient quasi-continuous absorber, not only in the CO_2 9.4μ and 10.4μ regions, but possibly also in the $4.9 - 5.7 \mu$ region of the CO laser, and in the 2.6 to 2.9μ region of the HF laser.

3. ABSORPTION DATA, COLLECTED OR COMPUTED FOR VARIOUS MOLECULAR SPECIES

3.1 HF and DF

Useful references for the HF and/or DF molecules are Meridith and Smith [Nov., 1971], C. M. Randal [Dec., 1975], Ludwig, et al. [1973], and Goldman, et al. [April, 1974].

3.1.1 Meridith and Smith [Nov., 1971] Data for DF

Meridith and Smith present a tabulation of electric dipole matrix elements and of Einstein spontaneous emission $A_{u \rightarrow \ell}$ coefficients for individual lines of both the P- and R-branches of many $v'' \rightarrow v'$ transitions for both HF and DF. The integrated line intensity parameter $S(v_o)$ {remember $\sigma(v, v_o) = S(v_o) f(v_o, v)$ }, referred to the lower state population density N_ℓ , can be computed most readily from the $A_{u \rightarrow \ell}$ coefficients. The relationship is

$$S(v_o) = \left(\frac{g_u}{g_\ell} \right) \cdot \left(\frac{A_{u \rightarrow \ell}}{8\pi c v_o^2} \right) \quad (15)$$

Here the degeneracy factors g_u and g_ℓ for the upper and lower states reduce to $g_u = 2J' + 1$ and $g_\ell = 2J'' + 1$. For respective P and R branch lines, $J' = J'' - 1$ and $J' = J'' + 1$. $A_{u \rightarrow \ell}$ is, as always, in units of sec^{-1} per molecule. Then, since c is in units of cm sec^{-1} , and v_o in units of cm^{-1} , $S(v_o)$ is given in units of cm per molecule ; or more explicitly, in units of $(\text{cm}^2 \text{ per } \ell\text{-state molecule}) \cdot (\text{cm}^{-1})$, with the last (cm^{-1}) factor representing wavenumbers. Here, the ℓ -state is electronic ground state, with v and J equal to the designated v'' and J'' values for each line. Table I gives values of v_o , $A_{u \rightarrow \ell}$, and $S(v_o)$ for selected P-branch absorption lines corresponding to some of the strongest lasing lines found in one of the TRW DF lasers. Higher powered, higher temperature lasers may concentrate power in other lines, but the data shown would appear to be typical. Absorption in the R-branch lines appears to be down by factors ranging from ~ 0.1 to ~ 0.8 of corresponding P-branch lines.

The last two columns of Table I present estimates for $\sigma(v_o, v_o)$ and $\hat{\sigma}_{296^\circ\text{K}}(v_o, v)$ [see Eqs. (3), and (14a)] under the arbitrary assumptions that the line width factor $a_o = 0.1 \text{ cm}^{-1} \text{ atmos}^{-1}$ and that $P \sim 1 \text{ atmos}$. This is

Table 1. DF Parameters Computed from
Meredith and Smith Data

v' v''	Line (P_v, J'')	ν_0 (in cm^{-1})	$\overset{A}{\nu'J' \rightarrow \nu''J''}$ (in sec^{-1})	$S(\nu_0) \cdot 10^{+17}$ (in $\text{cm}^2 \cdot$ cm^{-1} per $\nu''J''$ DF molecule)	\ast $\sim \sigma(\nu_0, \nu) \cdot 10^{+17}$ (in cm^2 per $\nu''J''$ DF molecule)	$\ast, \ast\ast$ $\hat{\sigma}_{296^\circ\text{K}}(\nu_0, \nu_0)$ (in cm^2 per DF molecule in any state)
$\overset{1}{\text{---}} \overset{0}{\text{---}}$ ↓	P_1 8	2717.8	31.817	0.5045	1.506	$3.02 \cdot 10^{-19}$
	P_1 9	2691.9	31.762	0.5205	1.657	$1.44 \cdot 10^{-19}$
	P_1 10	2665.5	31.719	0.5361	1.706	$5.69 \cdot 10^{-20}$
	P_1 11	2638.7	31.672	0.5513	1.755	$2.01 \cdot 10^{-20}$
	P_1 12	$\lambda \sim 3.829\mu$ 2611.5	31.615	0.5661	1.802	$5.51 \cdot 10^{-21}$
$\overset{2}{\text{---}} \overset{1}{\text{---}}$ ↓	P_2 8	2631.5	57.181	0.9671	3.078	$4.53 \cdot 10^{-25}$
	P_2 9	2606.3	57.105	0.9984	3.178	$2.02 \cdot 10^{-25}$
	P_2 10	2580.6	57.046	1.0287	3.274	$8.01 \cdot 10^{-26}$
	P_2 11	2554.5	56.978	1.0582	3.368	$2.83 \cdot 10^{-26}$
	P_2 12	$\lambda \sim 3.956\mu$ 2528.0	56.888	1.0857	3.456	$7.74 \cdot 10^{-27}$
$\overset{3}{\text{---}} \overset{2}{\text{---}}$ ↓	P_3 7	2571.6	76.748	1.3350	4.249	$1.47 \cdot 10^{-30}$
	P_3 8	2547.4	76.613	1.3826	4.401	$7.40 \cdot 10^{-31}$
	P_3 9	2522.9	76.546	1.4282	4.546	$3.30 \cdot 10^{-31}$
	P_3 10	2497.9	76.495	1.4723	4.686	$1.30 \cdot 10^{-31}$
	P_3 11	2472.5	76.429	1.5151	4.823	$4.63 \cdot 10^{-32}$
	P_3 12	$\lambda \sim 4.087\mu$ 2446.6	76.329	1.5571	4.956	$1.17 \cdot 10^{-32}$
$\overset{4}{\text{---}} \overset{3}{\text{---}}$	P_4 8	2465.2	90.614	1.7462	5.558	$1.65 \cdot 10^{-35}$

\ast a_c Arbitrarily assumed to be 0.1 cm^{-1} .

$\ast\ast$ A thermal equilibrium population, at
 $T = 296^\circ\text{K}$, assumed.

Table 1a. DF Vibrational Level Distribution at 296°K

v''	$G_o(v'')$ (in cm^{-1})	$r_{v''}(296^\circ\text{K}) \equiv e^{-4.85963 \cdot 10^{-3} \text{ cm } G_o(v'')}$
0	0	0
1	2906.83	$7.330 \cdot 10^{-7}$
2	5722.24	$8.378 \cdot 10^{-13}$
3	8446.23	$1.493 \cdot 10^{-18}$

1b. Approximate DF Vibrational Rotational Level Distribution $r_{v''}(296^\circ\text{K})$ $r_{j''}(296^\circ\text{K})$

j''	$v'' = 0$ $\{r_{j''}(296^\circ\text{K})\}$	$v'' = 1$	$v'' = 2$	$v'' = 3$
7	$4.121 \cdot 10^{-2}$	$3.021 \cdot 10^{-8}$	$3.453 \cdot 10^{-14}$	$2.996 \cdot 10^{-20}$
8	$2.007 \cdot 10^{-2}$	$1.471 \cdot 10^{-8}$	$1.681 \cdot 10^{-14}$	
9	$8.677 \cdot 10^{-3}$	$6.360 \cdot 10^{-9}$	$7.270 \cdot 10^{-15}$	
10	$3.338 \cdot 10^{-3}$	$2.447 \cdot 10^{-9}$	$2.797 \cdot 10^{-15}$	
11	$1.145 \cdot 10^{-3}$	$8.393 \cdot 10^{-10}$	$9.593 \cdot 10^{-16}$	
12	$3.056 \cdot 10^{-4}$	$2.240 \cdot 10^{-10}$	$2.560 \cdot 10^{-16}$	

a reasonably good estimate (probably accurate within 30 or 40%) for DF-DF broadening. For DF-CO₂ broadening, and for DF-N₂ broadening, however, the a_0 values should be, respectively, of the order of ~ 0.02 and ~ 0.01 cm⁻¹ atmos⁻¹. The corresponding $\sigma(\nu_0, \nu)$ line center values consequently would be ~ 5 and ~ 10 times as large as those listed.

The ratios between the last two columns of Table I were computed by a separable anharmonic oscillator - rigid rotor approximation from the assumed thermal equilibrium relation,

$$\begin{aligned} (\hat{\sigma}_{T_0}/\sigma) &= (N_{v''j''}/N) \\ &\approx \frac{(2j''+1) e^{-\frac{hc}{kT_0} \{G_0(v'') + F_v''(j'')\}}}{Q(T_0)} \\ &\approx \left\{ \frac{e^{-\left(\frac{hc}{kT_0}\right) G_0(v'')}}{Q_v(T_0)} \right\} \cdot \left\{ \frac{(2j''+1) e^{-\left(\frac{hcB_0}{kT_0}\right) j''(j''+1)}}{Q_R(T_0)} \right\} \equiv r_{v''}(T_0) \cdot r_{j''}(T_0) . \end{aligned} \quad (16)$$

For DF, $Q_v(296^\circ\text{K}) \approx 1$, and $\{Q_R(T_0)\}^{-1} \approx \{kT_0/hcB_0\}^{-1} \approx 5.278 \cdot 10^{-2}$.

Also, $(hc/k \cdot 296^\circ\text{K}) \approx 4.75963 \cdot 10^{-3}$ cm.

Thus, the last (and least accurate) form of Eq. (16) reduces to the form

$$\left\{ \hat{\sigma}_{T_0}/\sigma \right\} \approx r_{v''}(296^\circ\text{K}) \cdot r_{j''}(296^\circ\text{K}) . \quad (17)$$

Herzberg's somewhat ancient, but still sufficiently accurate (for current purpose), molecular constants for DF, were used, giving $G_0(v) \approx 2952.54$ cm⁻¹ v - 45.71 cm⁻¹ v² and $B_0 \approx 10.860$ cm⁻¹ as well as the previously listed value of $\{Q_R(T_0)\}^{-1} \approx 5.278 \cdot 10^{-2}$. Table Ia and Ib present some values of $r_{v''}$ and of $(r_{v''})(r_{j''})$ that might be of value for future use.

3.1.2 HF Data from Meridith and Smith [November, 1971] and
C. M. Randall [4 December, 1975]

Meridith and Smith tabulate $A_{v'T' \rightarrow v''J''}$ data for HF as well as for DF. Table 11 lists these Einstein coefficients and the $S(v_o)$ integrated line intensities calculated therefrom for selected $v''J'' \rightarrow v'T'$ transitions. It also lists corresponding $\hat{S}_T(v_o)$ values, related to total rather than $v'T'$ state HF number densities. These $\hat{S}_T(v_o)$ values were copied directly from C. M. Randall [4 December, 1975] and correspond to a thermal equilibrium population distribution of HF at a temperature $T_o = 296^\circ\text{K}$. The v_o line frequency values in wave number units and the a_o line width parameters, in $\text{cm}^{-1} \text{atmos.}^{-1}$ (at 273°K) for HF-HF broadening also was taken from Randall, who claims an approximately 20% accuracy for low J-values. Figure 1 (Randall's Figure 17) gives a summary of experimental HF line width data. Here $|m| = J''$ for P branch lines and $J''+1$ for R-branch lines. The values of $a_o \approx 0.1$ for $|m| \gtrsim 0.9$ appear to be arbitrary. Randall gives no data for the ratio of foreign gas to self-broadening for HF, but his Table 5 gives such ratios for HCl for P1 through P8 lines and for CO_2 , CO, N_2 and O_2 . The average values of these ratios were 0.46, 0.39, 0.30, and 0.19, respectively. Goldman, et al. [April, 1974] suggest average ratios of 0.2 and 0.1 for the respective ratios of CO_2 and N_2 broadening as compared to self-broadening for either HF or DF.

To compute $\sigma(v_o, v_o)$ or $\hat{\sigma}_T(v_o, v_o)$ values for self-broadened HF lines, a first computation is the appropriate (collision broadened) half-widths, from the relation,

$$a_c \approx a_o P \sqrt{T_o/T} \quad (\text{Here, } T_o = 273^\circ\text{K}) \quad (12)$$

Then divide the selected $S(v_o)$ or $\hat{S}(v_o, 296^\circ\text{K})$ by $(a\pi)$. For broadening by foreign gases, the p_i partial pressures of the various gases and their relative broadening efficiencies C_i must be known or approximated, and an effective P given by Eq. (13) must be used in Eq. (12).

For HF, $B_o \approx 20.555 \text{ cm}^{-1}$, and the vibrational levels separation from the $v = 0$ ground state is given by the relation, $G_o(v) \approx 4049.186v - 88.60v^2 + 0.980v^3$. Also, at the $T_o = 296^\circ\text{K}$ assumed by Randall, $(hc/kT_o) = 4.85963 \cdot 10^{-3} \text{ cm}$, $Q_v(T_o) \approx 1$, and $\{Q_R(T_o)\}^{-1} \approx \{hcB_o/kT_o\} = 9.9890 \cdot 10^{-2}$. Tables 2a and 2b give $r_{v''}(296^\circ\text{K})$ and $r_{J''}(296^\circ\text{K})$ (see Eq. (16) for the HF molecule.

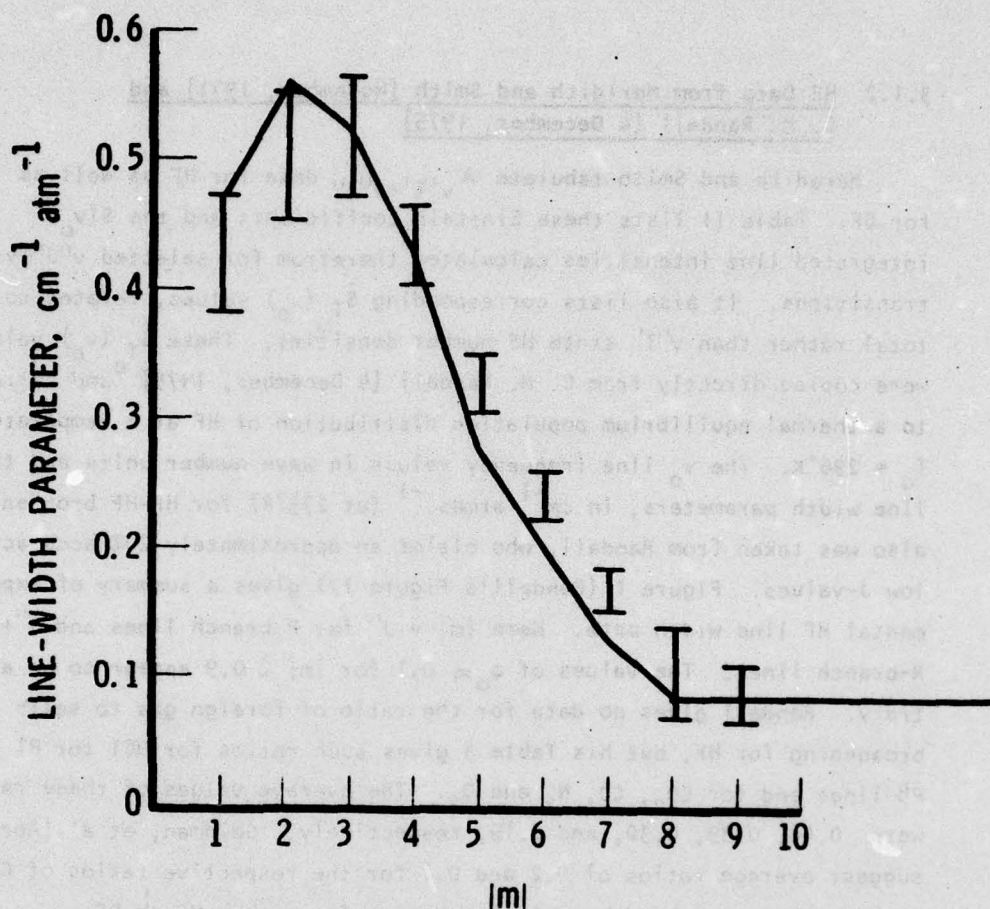


Figure 1. Summary of HF Experimental Line-Width Parameter Data. The vertical bars indicate the range of the values observed by various investigators and listed in Table 7. The values used in the present study are connected by straight line segments. $|M| = J'$ for P-branch lines and $|M| = J' + 1$ for R-branch lines.

Table 2. Einstein $A_{u \rightarrow l}$ Coefficients and Integrated Line Strengths for Some Selected HF $\Delta v = 1$ P-Branch Transitions




$v'' \quad v'$	Line ($P_v J'' J'$)	ν_0 (in cm^{-1})	$A_{u \rightarrow l}$ $v' J' \rightarrow v'' J''$ (in sec^{-1})	$s(\nu_0) \cdot 10^{18}$ [in $(\text{cm}^2 \cdot \text{cm}^{-1})$ per $v'' J''$ state molecule]	$\hat{S}(\nu_0, 296^\circ\text{K})$ [in $(\text{cm}^2 \cdot \text{cm}^{-1})$ for all HF molecules]	a_0 [in $(\text{cm} \cdot \text{atmos})^{-1}$]
$\underbrace{0 \quad 1}$ 	$P_1 \quad 4$	3788.372	116.23	8.36	$9.687 \cdot 10^{-19}$	0.50
	$P_1 \quad 5$	3741.593	114.35	8.87	$4.542 \cdot 10^{-19}$	0.33
	$P_1 \quad 6$	3693.560	113.35	9.33	$1.753 \cdot 10^{-19}$	0.24
	$P_1 \quad 7$	3644.259	112.71	9.76	$5.291 \cdot 10^{-20}$	0.15
	$P_1 \quad 8$	3593.812	112.19	10.16	$1.288 \cdot 10^{-20}$	0.1
	$P_1 \quad 9$	3542.254	111.67	10.57	$2.547 \cdot 10^{-21}$	0.1
	$P_1 \quad 10$	3489.644	111.07	10.95	$4.113 \cdot 10^{-22}$	0.1
	$P_1 \quad 11$	3436.038	110.35	11.41	$5.450 \cdot 10^{-23}$	0.1
	$P_1 \quad 12$	3381.496	109.49	11.69	$5.952 \cdot 10^{-24}$	0.1
	$P_1 \quad 13$	3326.075	108.46	12.05	$5.379 \cdot 10^{-25}$	0.1
$\underbrace{1 \quad 2}$ 	$P_2 \quad 4$	3622.617	199.27	15.68	$8.603 \cdot 10^{-27}$	0.50
	$P_2 \quad 5$	3577.538	196.26		$4.274 \cdot 10^{-27}$	0.33
	$P_2 \quad 6$	3531.212	194.71	17.54	$1.636 \cdot 10^{-27}$	0.24
	$P_2 \quad 7$	3483.694	193.75		$5.354 \cdot 10^{-28}$	0.15
	$P_2 \quad 8$	3435.037	192.97	19.15	$1.382 \cdot 10^{-28}$	0.1
	$P_2 \quad 9$	3385.299	192.15		$2.198 \cdot 10^{-29}$	0.1
	$P_2 \quad 10$	3334.533	191.18	20.65	$5.069 \cdot 10^{-30}$	0.1
	$P_2 \quad 11$	3282.797	189.98		$7.275 \cdot 10^{-31}$	0.1
	$P_2 \quad 12$	3230.145	188.51	22.06	$8.669 \cdot 10^{-32}$	0.1
$\underbrace{2 \quad 3}$ 	$P_3 \quad 4$	3461.433	252.65	21.77	$1.336 \cdot 10^{-34}$	0.50
	$P_3 \quad 5$	3417.993	249.14		$6.892 \cdot 10^{-35}$	0.33
	$P_3 \quad 6$	3373.336	247.44	24.42	$2.843 \cdot 10^{-35}$	0.24
	$P_3 \quad 7$	3327.514	246.43		$9.511 \cdot 10^{-36}$	0.15
	$P_3 \quad 8$	3280.581	245.62	26.73	$2.604 \cdot 10^{-36}$	0.1
	$P_3 \quad 9$	3232.589	244.72		$5.874 \cdot 10^{-37}$	0.1
	$P_3 \quad 10$	3183.593	243.58	28.86	$1.098 \cdot 10^{-37}$	0.1
	$P_3 \quad 11$	3133.647	242.11		$1.707 \cdot 10^{-38}$	0.1
	$P_3 \quad 12$	3082.803	240.26	30.09	$2.218 \cdot 10^{-39}$	0.1

Table 2. Einstein $A_{u \rightarrow l}$ Coefficients and Integrated Line Strengths
for Some Selected HF $\Delta v = 1$ P-Branch Transitions (cont'd)



$v'' \quad v'$	Line ($P_v J'' J'$)	ν_0 (in cm^{-1})	$A_{u \rightarrow l}$ $v' J' \rightarrow v'' J''$ (in sec^{-1})	$S(\nu_0) \cdot 10^{18}$ [in (cm^2) \cdot cm^{-1}] per $v'' J''$ state molecule)	$\hat{S}(\nu_0, 296^\circ\text{K})$ [in (cm^2) cm^{-1}] for all HF molecules)	a_0 (in (cm atmos) $^{-1}$)
$\underbrace{3 \quad 4}$ 	$P_4 4$	3304.316	280.09	26.48	$3.992 \cdot 10^{-42}$	0.50
	$P_4 5$	3262.451	276.61	28.22	$2.117 \cdot 10^{-42}$	0.33
	$P_4 6$	3219.414	275.09	29.81	$9.042 \cdot 10^{-43}$	0.24
	$P_4 7$	3175.227	274.28		$3.153 \cdot 10^{-43}$	0.15
	$P_4 8$	3129.950	273.61	33.17	$9.064 \cdot 10^{-44}$	0.10
	$P_4 9$	3083.636	272.79		$2.161 \cdot 10^{-44}$	0.1
	$P_4 10$	3036.336	271.66	35.39	$4.299 \cdot 10^{-45}$	0.1
	$P_4 11$	2988.102	270.11		$7.166 \cdot 10^{-46}$	0.1
	$P_4 12$	2938.986	268.08	37.90	$1.005 \cdot 10^{-46}$	0.1
$\underbrace{4 \quad 5}$ 	$P_5 4$	3149.2	285.31	29.70		0.50
	$P_5 5$	3108.8	282.31	31.72		0.33
	$P_5 6$	3067.3	281.20	33.57		0.24
	$P_5 7$	3024.7	280.76	35.30		0.15
	$P_5 8$	2981.0	280.40	36.95		0.10
	$P_5 9$	2936.2	279.81	38.54		0.1
	$P_5 10$	2890.5	278.83	40.08		0.1
	$P_5 11$	2843.9	277.36	41.56		0.1
	$P_5 12$	2796.5	275.34	42.99		0.1

Table 2a. Vibrational Level Distributions for HF at 290°K ^{hs}

v	G ₀ (v'')	r _{v''} (296°K)
0	0	1
1	3961.566	4.350 · 10 ⁻⁹
2	7752.792	4.455 · 10 ⁻¹⁷
3	11,377.598	9.715 · 10 ⁻²⁵
4	14,842.844	4.721 · 10 ⁻³²

2b. Approximate Rotational Level Population Factors for HF at 296°K.

J''	r _{J''} (296°K)
4	1.219 · 10 ⁻¹
5	4.489 · 10 ⁻²
6	2.257 · 10 ⁻²
7	6.318 · 10 ⁻³
8	1.428 · 10 ⁻³
9	2.366 · 10 ⁻⁴
10	3.546 · 10 ⁻⁵
11	4.314 · 10 ⁻⁶
12	4.265 · 10 ⁻⁷

3.1.3 Goldman, et al. [August, 1973] Data for HF and DF at 1273°K

Table 3 and Figure 2 and the accompanying explanation are extracted directly from Goldman, Schmidt, Riter, and Blunt. It is to be noted that the integrated line intensity parameters they presented there are in units of $(\text{cm-atmos STP})^{-1} \cdot \text{cm}^{-1}$, and thus correspond to the $\hat{S}'(\nu_0, 1273^\circ\text{K})$ for the HF values (their isotope #1 designation for $T_0 = 1273^\circ\text{K}$ used here. The tabulated line intensity parameters for DF (their isotope #2 designation) are further reduced by the naturally occurring D to H abundance ratio, and thus represent $\sim 1.56 \cdot 10^{-2} \hat{S}'(\nu_0, 1273^\circ\text{K})$. These tabulated line intensity parameters can be reduced to corresponding $\hat{S}'(\nu_0)$ values in $(\text{atmos cm})^{-1} \text{cm}^{-1}$, referred to the density of $v''J''$ -state HF or DF molecules, by multiplying by

$$\left\{ \frac{(2J'' + 1) e^{-\left\{ \frac{hc}{k \cdot 1273^\circ\text{K}} \right\} E_{v''J''}}}{Q(1273^\circ\text{K})} \right\}^{-1}$$

The $E_{v''J''}$ lower state energies in wave number units, and the J'' values are also tabulated (by Goldman, et al.) in Table 3. The Partition function for HF at 1273°K is $Q(1273^\circ\text{K}) = Q_{v''}(1273^\circ\text{K}) Q_{J''}(1273^\circ\text{K}) \approx 1.01153 \cdot 43.05 \approx 43.55$.

Goldman, et al.'s explanatory paragraphs and Figure 1 and Table 2 (re-labeled as Fig. 2 and Table 3) are given here.

The line intensities S , at temperature T , were derived from the electric dipole matrix elements $\langle v'J' | \mu | vJ \rangle$ as computed recently by MEREDITH and SMITH, according to.

$$S(T) = \frac{8\pi^3 \nu}{3hc} \frac{N_0(T)}{pQ(T)} \exp[-E(v, J)hc/kT] \times L_J |\langle v'J' | \mu | vJ \rangle|^2 (1 - \exp[-\nu hc/kT]).$$

Here S is in $\text{cm}^{-1}/(\text{atm cm})$; T in K; ν , the transition wavenumber given by $(E(v', J') - E(v, J))$ is in cm^{-1} ; $Q(T)$ is the partition function; L_J is $J + 1$ for R-branch lines and J for P-branch lines; p is the pressure in atm; k is the Boltzmann constant; h is the Planck constant; c is the velocity of light; and $N_0(T)$, the number density, is obtained using the ideal gas law. A computer program, similar to that described by KUNDE for calculating CO line parameters at elevated temperatures, was used to compute the transition wavenumber, ν , and the line intensity $S(T)$. Intensities computed at 390 K and 373 K for the (1-0) band generally agreed to within 15 per cent with the line intensities measured by KUIPERS and by SHAW and LOVELL. The resulting integrated band intensity at 390 K obtained here is $311.4 (\text{cm}^{-2} \text{atm}^{-1})$. The resulting line intensities of the HF and DF $\Delta v = 1$ bands in the ratio of their natural isotopic abundances at 1273 K, including all lines whose

Infrared spectral radiance of hot HF and DF in the $\Delta v = 1$ bands region

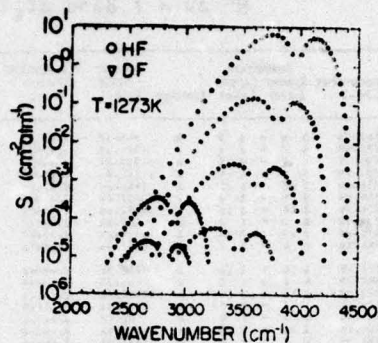


Figure 2. Line Intensities vs Wavenumber for the HF $\Delta v = 1$ Bands at 1273 K.

intensities are within a factor of 10^{-6} of the maximum line intensity are presented versus line positions in Table 1 and Fig. 1. Similar tabulations are available for temperatures up to 4000 K.

Spectral line halfwidths for pure HF, HF-CO₂, HF-He and HF-Ar mixtures have been measured and computed.^(25-28,38-42) Broadening efficiencies for five lines and 20 different foreign gases have been reported by SMITH.⁽⁴³⁾ The broadening efficiencies of CO₂ and N₂ at 373 K are of the order of 0.2 and 0.1 respectively.^(32,43) Here the results of HERGET *et al.*⁽²⁷⁾ and SHAW and LOVELL⁽³²⁾ have been adopted with a temperature dependence of $1/\sqrt{T}$. The pure HF and HF-CO₂ halfwidths for each spectral line used in the radiance calculations at 1273 K are listed in Table I.

Table 3. Spectral Line Parameters for the HF $\Delta v = 1$ bands at 1273 K

Wavenumber CM-1	Transition Lower Upper Level Level Isotope	Lower State CM-1	Wavelength Micron (μ m)	Halfwidth HF-HF HF-CO ₂ CM-1*ATM-1	Intensity CM-2* ATM-1
2316.53	6 22 - 1 21 2	5346.05	4.31190	.023	.613
2349.16	6 21 - 1 20 2	4899.22	4.79506	.035	.613
2373.53	6 23 - 1 19 2	4662.23	4.23136	.036	.613
2409.62	6 19 - 1 16 2	4444.00	4.41839	.020	.613
2439.42	6 18 - 1 17 2	4477.37	4.40821	.043	.613
2465.48	1 19 - 2 19 2	4439.58	4.40820	.045	.614
2486.91	6 17 - 1 16 2	4266.48	4.34466	.041	.613
2473.13	1 19 - 2 13 2	5104.29	4.60640	.040	.614
2469.46	6 27 - 1 26 1	4339.43	4.40158	.029	.612
2496.47	6 16 - 1 15 2	2911.21	4.31190	.043	.614
2582.49	1 13 - 2 12 2	4611.71	3.91813	.040	.614
2526.09	6 15 - 1 14 2	2973.43	3.99895	.040	.614
2527.00	1 12 - 2 11 2	4941.22	3.99506	.040	.614
2509.97	1 24 - 2 23 1	19124.59	3.94503	.040	.613
2550.30	6 26 - 1 25 1	4344.00	4.41839	.027	.612
2594.03	1 11 - 2 10 2	4281.43	4.41431	.051	.614
2599.25	6 14 - 1 13 2	4429.20	4.51229	.046	.614
2588.19	1 13 - 2 9 2	4462.82	3.87443	.053	.614
2563.43	6 13 - 1 12 2	4497.43	4.40717	.040	.614
2595.44	1 8 - 2 0 2	3692.23	3.82630	.050	.615
2636.86	1 23 - 2 22 1	1424.16	3.83616	.032	.613
2633.12	6 12 - 1 11 2	4682.23	3.82630	.040	.614
2632.09	6 25 - 1 24 1	12314.86	3.82630	.040	.612
2631.17	1 6 - 2 7 2	3800.91	3.79999	.073	.615
2638.46	6 11 - 1 10 2	4624.62	3.78365	.054	.614
2699.97	1 7 - 2 6 2	3699.00	3.76187	.052	.614
2669.22	1 22 - 2 21 1	4346.47	3.75122	.033	.613
2669.25	6 10 - 1 9 2	4167.76	3.75497	.053	.614
2676.41	6 24 - 1 23 1	4166.49	3.74627	.040	.613
2680.30	1 6 - 2 5 2	3449.62	3.77961	.038	.613
2694.66	6 9 - 1 8 2	4974.86	3.71417	.054	.615
2736.12	1 5 - 2 4 2	4224.24	3.66749	.036	.614
2736.21	2 10 - 3 10 1	14734.40	3.66749	.036	.614
2717.00	6 8 - 1 7 2	4776.00	3.67971	.073	.615
2726.03	1 21 - 2 20 1	4267.03	3.67233	.045	.615
2727.00	1 4 - 2 1 2	4117.00	3.66946	.049	.615
2735.71	6 23 - 1 22 1	19724.80	3.66946	.042	.613
2743.00	6 7 - 1 6 2	4000.00	3.66946	.052	.616
2756.23	1 3 - 2 2 2	3811.91	3.66947	.027	.612
2761.00	2 10 - 3 10 1	1424.16	3.66946	.046	.615

Table 3. Spectral Line Parameters for the HF $\Delta v = 1$ Band at 1273 K (Continued)

Wavelength CM-1	Transition Lower Upper Level Level		Isotope	Lower State CM-1	Wavelength Micron (Air)	Halfwidth HF-HF HF-HF CM-1*ATM-1	Intensity CM-2* ATM-1		
2760.3b	0	0	1	0	295.17	2.01615	.130	.023	9.59E-06
2774.0a	1	2	2	1	297.10	4.00990	.202	.002	1.10E-05
2782.7f	1	2	2	1	1319.97	2.55299	.036	.013	1.10E-06
2796.9a	0	0	1	0	319.79	1.57979	.110	.026	1.30E-06
2800.0a	0	22	1	21	1.57979	1.57979	.033	.012	1.20E-04
2816.90	0	0	1	0	2.97.95	1.57990	.035	.010	1.20E-04
2819.9a	2	27	3	16	1.633.91	1.59089	.091	.013	0.62E-05
2839.92	0	2	1	2	550.20	3.92327	.257	.002	2.3E-05
2840.9a	0	1	1	1	1.633.91	1.59089	.035	.013	0.62E-05
2859.80	0	1	2	2	2927.90	4.00670	.232	.002	1.30E-06
2957.00	6	21	1	1	1961.92	3.00982	.032	.013	2.95E-04
2967.10	0	2	1	1	3.011.95	3.01195	.002	.002	1.95E-05
2971.50	2	10	3	1	127.92.72	1.27927	.037	.010	7.7E-05
2975.1b	1	2	2	1	297.10	4.00715	.207	.002	1.10E-05
2985.10	0	1	1	0	21.72	4.00519	.210	.004	0.94E-05
2989.9a	0	1	1	0	140.90	3.00519	.060	.013	0.81E-05
2991.05	1	1	2	2	24.64.51	2.46451	.035	.010	1.10E-05
2996.91	1	10	2	17	1.630.91	3.00670	.030	.004	0.90E-06
2911.9b	1	1	2	1	311.60	3.01221	.090	.026	1.90E-05
2916.90	0	20	1	1	2.97.92	3.00597	.036	.013	0.92E-05
2925.00	2	15	0	3	122.95.03	2.41764	.035	.010	1.20E-06
2927.9a	0	0	1	0	3.011.95	3.01195	.030	.010	0.14E-05
2932.00	1	9	1	8	32.9.20	3.01195	.132	.023	0.40E-05
2948.90	3	12	1	11	101.9.10	3.01195	.030	.010	0.90E-06
2949.10	1	0	2	7	32.9.52	3.01313	.037	.010	1.90E-05
2949.9b	0	1	1	0	21.72	3.01000	.062	.002	1.30E-06
2961.03	1	17	2	16	1.630.91	3.00670	.032	.002	1.70E-05
2961.27	0	0	1	0	3.006.90	3.00719	.037	.010	1.30E-05
2966.90	0	2	1	0	30.9.15	3.00719	.037	.002	2.10E-06
2977.70	1	0	2	0	20.9.15	3.00719	.030	.010	1.00E-05
2978.10	6	10	1	1	75.10.35	4.00690	.110	.011	1.10E-02
2978.62	2	10	1	1	1.001.82	3.00910	.030	.010	0.20E-05
2979.62	0	0	1	0	1.00.20	4.00690	.209	.020	2.50E-06
2980.10	0	1	1	0	1.07.90	4.00690	.031	.010	0.30E-05
2982.03	1	9	1	8	20.9.20	3.01195	.030	.010	1.00E-05
2986.23	0	0	1	0	21.7.2	3.02552	.100	.020	2.70E-06
3006.7f	1	10	2	1	2.02.02	1.42525	.031	.010	1.30E-05
3008.10	0	2	1	0	01.90.10	3.01195	.030	.010	1.20E-05
3011.70	1	11	2	12	02.9.20	3.01195	.030	.010	1.20E-05
3021.10	0	5	1	0	32.9.30	3.00597	.110	.023	2.30E-06
3021.10	2	13	0	1	111.90.03	3.02023	.060	.010	3.7E-05
3032.0a	1	10	2	1	0.99.02	3.00690	.030	.010	7.6E-06
3036.10	0	1	1	0	1.02.02	3.02023	.030	.010	7.6E-06
3040.10	0	1	1	0	1.02.02	3.02023	.030	.010	7.6E-06
3044.0f	0	0	1	0	0.99.02	3.00690	.030	.010	7.6E-06
3048.0f	0	0	1	0	0.99.02	3.00690	.030	.010	7.6E-06
3052.0f	0	0	1	0	0.99.02	3.00690	.030	.010	7.6E-06
3056.0f	0	0	1	0	0.99.02	3.00690	.030	.010	7.6E-06
3060.0f	0	0	1	0	0.99.02	3.00690	.030	.010	7.6E-06
3064.0f	0	0	1	0	0.99.02	3.00690	.030	.010	7.6E-06
3068.0f	0	0	1	0	0.99.02	3.00690	.030	.010	7.6E-06
3072.0f	0	0	1	0	0.99.02	3.00690	.030	.010	7.6E-06
3076.0f	0	0	1	0	0.99.02	3.00690	.030	.010	7.6E-06
3080.0f	0	0	1	0	0.99.02	3.00690	.030	.010	7.6E-06
3084.0f	0	0	1	0	0.99.02	3.00690	.030	.010	7.6E-06
3088.0f	0	0	1	0	0.99.02	3.00690	.030	.010	7.6E-06
3092.0f	0	0	1	0	0.99.02	3.00690	.030	.010	7.6E-06
3096.0f	0	0	1	0	0.99.02	3.00690	.030	.010	7.6E-06
3100.0f	0	0	1	0	0.99.02	3.00690	.030	.010	7.6E-06
3104.0f	0	0	1	0	0.99.02	3.00690	.030	.010	7.6E-06
3108.0f	0	0	1	0	0.99.02	3.00690	.030	.010	7.6E-06
3112.0f	0	0	1	0	0.99.02	3.00690	.030	.010	7.6E-06
3116.0f	0	0	1	0	0.99.02	3.00690	.030	.010	7.6E-06
3120.0f	0	0	1	0	0.99.02	3.00690	.030	.010	7.6E-06
3124.0f	0	0	1	0	0.99.02	3.00690	.030	.010	7.6E-06
3128.0f	0	0	1	0	0.99.02	3.00690	.030	.010	7.6E-06
3132.0f	0	0	1	0	0.99.02	3.00690	.030	.010	7.6E-06
3136.0f	0	0	1	0	0.99.02	3.00690	.030	.010	7.6E-06
3140.0f	0	0	1	0	0.99.02	3.00690	.030	.010	7.6E-06
3144.0f	0	0	1	0	0.99.02	3.00690	.030	.010	7.6E-06
3148.0f	0	0	1	0	0.99.02	3.00690	.030	.010	7.6E-06
3152.0f	0	0	1	0	0.99.02	3.00690	.030	.010	7.6E-06
3156.0f	0	0	1	0	0.99.02	3.00690	.030	.010	7.6E-06
3160.0f	0	0	1	0	0.99.02	3.00690	.030	.010	7.6E-06
3164.0f	0	0	1	0	0.99.02	3.00690	.030	.010	7.6E-06
3168.0f	0	0	1	0	0.99.02	3.00690	.030	.010	7.6E-06
3172.0f	0	0	1	0	0.99.02	3.00690	.030	.010	7.6E-06
3176.0f	0	0	1	0	0.99.02	3.00690	.030	.010	7.6E-06
3180.0f	0	0	1	0	0.99.02	3.00690	.030	.010	7.6E-06
3184.0f	0	0	1	0	0.99.02	3.00690	.030	.010	7.6E-06
3188.0f	0	0	1	0	0.99.02	3.00690	.030	.010	7.6E-06
3192.0f	0	0	1	0	0.99.02	3.00690	.030	.010	7.6E-06
3196.0f	0	0	1	0	0.99.02	3.00690	.030	.010	7.6E-06
3200.0f	0	0	1	0	0.99.02	3.00690	.030	.010	7.6E-06
3204.0f	0	0	1	0	0.99.02	3.00690	.030	.010	7.6E-06
3208.0f	0	0	1	0	0.99.02	3.00690	.030	.010	7.6E-06
3212.0f	0	0	1	0	0.99.02	3.00690	.030	.010	7.6E-06
3216.0f	0	0	1	0	0.99.02	3.00690	.030	.010	7.6E-06
3220.0f	0	0	1	0	0.99.02	3.00690	.030	.010	7.6E-06
3224.0f	0	0	1	0	0.99.02	3.00690	.030	.010	7.6E-06
3228.0f	0	0	1	0	0.99.02	3.00690	.030	.010	7.6E-06
3232.0f	0	0	1	0	0.99.02	3.00690	.030	.010	7.6E-06
3236.0f	0	0	1	0	0.99.02	3.00690	.030	.010	7.6E-06
3240.0f	0	0	1	0	0.99.02	3.00690	.030	.010	7.6E-06
3244.0f	0	0	1	0	0.99.02	3.00690	.030	.010	7.6E-06
3248.0f	0	0	1	0	0.99.02	3.00690	.030	.010	7.6E-06
3252.0f	0	0	1	0	0.99.02	3.00690	.030	.010	7.6E-06
3256.0f	0	0	1	0	0.99.02	3.00690	.030	.010	7.6E-06
3260.0f	0	0	1	0	0.99.02	3.00690	.030	.010	7.6E-06
3264.0f	0	0	1	0	0.99.02	3.00690	.030	.010	7.6E-06
3268.0f	0	0	1	0	0.99.02	3.00690	.030	.010	7.6E-06
3272.0f	0	0	1	0	0.99.02	3.00690	.030	.010	7.6E-06
3276.0f	0	0	1	0	0.99.02	3.00690	.030	.010	7.6E-06
3280.0f	0	0	1	0	0.99.02	3.00690	.030	.010	7.6E-06
3284.0f	0	0	1	0	0.99.02	3.00690	.030	.010	7.6E-06
3288.0f	0	0	1	0	0.99.02	3.00690	.030	.010	7.6E-06
3292.0f	0	0	1	0	0.99.02	3.00690	.030	.010	7.6E-06
3296.0f	0	0	1	0	0.99.02	3.00690	.030	.010	7.6E-06
3300.0f	0	0	1	0	0.99.02	3.00690	.030	.010	7.6E-06
3304.0f	0	0	1	0	0.99.02	3.00690	.030	.010	7.6E-06
3308.0f	0	0	1	0	0.99.02	3.00690	.030	.010	7.6E-06
3312.0f	0	0	1	0	0.99.02	3.00690	.030	.010	7.6E-06
3316.0f	0	0	1	0	0.99.02	3.00690	.030	.010	7.6E-06
3320.0f	0	0	1	0	0.99.02	3.00690	.030	.010	7.6E-06
3324.0f	0	0	1	0	0.99.02	3.00690	.030	.010	7.6E-06
3328.0f	0	0	1	0	0.99.02	3.00690	.030	.010	7.6E-06
3332.0f	0	0	1	0	0.99.02	3.00690	.030	.010	7.6E-06
3336.0f	0	0	1	0	0.99.02	3.00690	.030	.010	7.6E-06
3340.0f	0	0	1	0	0.99.02	3.00690	.030	.010	7.6E-06
3344.0f	0	0	1	0	0.99.02	3.00690	.030	.010	7.6E-06
3348.0f	0	0	1	0	0.99.02	3.00690	.030	.010	7.6E-06
3352.0f	0	0	1	0	0.99.02	3.00690	.030	.010	7.6E-06
3356.0f	0	0	1	0	0.99.02	3.00690	.030	.010	7.6E-06
3360.0f	0	0	1	0	0.99.02	3.00690	.030	.010	7.6E-06
3364.0f	0	0	1	0	0.99.02	3.00690	.030	.010	7.6E-06
3368.0f	0	0	1	0	0.99.02	3.00690	.030	.010	7.6E-06
3372.0f	0	0	1	0	0.99.02	3.00690	.030	.010	7.6E-06
3376.0f	0	0	1	0	0.99.02	3.00690	.030	.010	7.6E-06
3380.0f	0	0	1	0	0.99.02	3.00690	.030	.010	7.6E-06
3384.0f	0	0	1	0	0.99.02	3.00690	.030	.010	7.6E-06
3388.0f	0	0	1	0	0.99.02	3.00690	.030	.010	7.6E-06
3392.0f	0	0	1	0	0.99.02	3.00690	.030	.010	7.6E-06
3396.0f	0	0	1	0	0.99.02	3.00690</			

Table 3. Spectral Line Parameters for the
HF $\Delta v = 1$ Band at 1273 K (Continued)

Wavenumber CM-1	Transition Lower Level Upper Level	Isotope	Lower State CM-1	Wavelength Micron (Air)	Halfwidth HF-HF HF-CO2 CM-1*ATM-1	Intensity CM-2 ATM-1
1111.12	1 10 - 2 9	1	0113.43	2.99811	.055	5.623E-02
1111.14	2 8 - 3 7	1	0113.42	2.99870	.287	4.553E-05
1113.14	2 6 - 3 5	1	0106.92	2.96362	.150	2.017E-03
1113.15	0 12 - 1 11	1	0110.47	2.95051	.009	1.370E-00
1114.25	1 2 - 2 1	1	0102.73	2.95080	.202	3.203E-05
1115.14	1 1 - 2 0	1	0102.80	2.95115	.090	7.001E-02
1117.70	2 5 - 3 4	1	0102.25	2.96200	.100	2.737E-01
1118.23	1 1 - 2 0	1	0102.99	2.95127	.230	1.713E-05
1119.12	1 0 - 2 1	1	0103.03	2.95139	.073	9.757E-02
1119.15	0 11 - 1 10	1	0107.03	2.96957	.351	1.007E-00
1119.17	2 4 - 3 3	1	0112.03	2.99819	.249	2.613E-01
1119.19	1 7 - 2 6	1	0103.23	2.96974	.092	1.170E-01
1119.22	0 10 - 1 9	1	0103.22	2.96980	.055	2.390E-00
1119.30	1 4 - 2 1	1	0103.29	2.96912	.030	1.007E-05
1119.60	2 3 - 3 2	1	0103.12	2.96943	.207	2.232E-01
1119.66	1 1 - 2 0	1	0103.90	2.95396	.202	2.400E-05
1119.71	1 6 - 2 5	1	0103.02	2.95312	.130	1.300E-01
1119.74	0 9 - 1 8	1	0103.10	2.96221	.150	2.100E-03
1119.80	2 2 - 3 1	1	0103.15	2.96250	.202	1.023E-01
1119.81	2 2 - 3 1	1	0103.15	2.96257	.207	1.015E-05
1119.84	1 5 - 2 4	1	0103.15	2.96260	.100	1.395E-01
1119.90	2 1 - 3 0	1	0103.00	2.96947	.200	9.000E-00
1119.90	1 3 - 2 2	1	0103.12	2.96949	.200	2.200E-05
1119.90	0 8 - 1 7	1	0103.00	2.96951	.073	0.300E-00
1119.97	1 4 - 2 1	1	0103.23	2.96916	.100	2.200E-05
1119.97	1 4 - 2 1	1	0103.23	2.96916	.050	1.300E-01
1119.97	0 7 - 1 6	1	0103.77	2.97430	.092	2.500E-00
1119.98	1 3 - 2 2	1	0103.25	2.96917	.130	3.000E-05
1119.99	2 0 - 2 9	1	0103.09	2.97329	.230	0.000E-00
1119.99	1 1 - 2 0	1	0103.73	2.97273	.207	1.100E-01
1119.99	0 6 - 1 5	1	0103.10	2.97230	.092	3.200E-05
1119.99	0 6 - 1 5	1	0103.10	2.97230	.130	0.000E-01
1119.99	2 1 - 3 0	1	0103.00	2.96947	.092	1.000E-01
1119.99	1 3 - 2 2	1	0103.12	2.96949	.073	2.000E-05
1119.99	0 8 - 1 7	1	0103.00	2.96951	.092	0.000E-01
1119.99	1 4 - 2 1	1	0103.23	2.96916	.092	1.300E-01
1119.99	1 4 - 2 1	1	0103.23	2.96916	.092	1.300E-01
1119.99	0 7 - 1 6	1	0103.77	2.97430	.092	1.300E-01
1119.99	1 3 - 2 2	1	0103.25	2.96917	.130	3.000E-05
1119.99	2 0 - 2 9	1	0103.09	2.97329	.230	0.000E-00
1119.99	1 1 - 2 0	1	0103.73	2.97273	.207	1.100E-01
1119.99	0 6 - 1 5	1	0103.10	2.97230	.092	3.200E-05
1119.99	0 6 - 1 5	1	0103.10	2.97230	.130	0.000E-01
1119.99	2 1 - 3 0	1	0103.00	2.96947	.092	1.000E-01
1119.99	1 3 - 2 2	1	0103.12	2.96949	.073	2.000E-05
1119.99	0 8 - 1 7	1	0103.00	2.96951	.092	0.000E-01
1119.99	1 4 - 2 1	1	0103.23	2.96916	.092	1.300E-01
1119.99	1 4 - 2 1	1	0103.23	2.96916	.092	1.300E-01
1119.99	0 7 - 1 6	1	0103.77	2.97430	.092	1.300E-01
1119.99	1 3 - 2 2	1	0103.25	2.96917	.130	3.000E-05
1119.99	2 0 - 2 9	1	0103.09	2.97329	.230	0.000E-00
1119.99	1 1 - 2 0	1	0103.73	2.97273	.207	1.100E-01
1119.99	0 6 - 1 5	1	0103.10	2.97230	.092	3.200E-05
1119.99	0 6 - 1 5	1	0103.10	2.97230	.130	0.000E-01
1119.99	2 1 - 3 0	1	0103.00	2.96947	.092	1.000E-01
1119.99	1 3 - 2 2	1	0103.12	2.96949	.073	2.000E-05
1119.99	0 8 - 1 7	1	0103.00	2.96951	.092	0.000E-01
1119.99	1 4 - 2 1	1	0103.23	2.96916	.092	1.300E-01
1119.99	1 4 - 2 1	1	0103.23	2.96916	.092	1.300E-01
1119.99	0 7 - 1 6	1	0103.77	2.97430	.092	1.300E-01
1119.99	1 3 - 2 2	1	0103.25	2.96917	.130	3.000E-05
1119.99	2 0 - 2 9	1	0103.09	2.97329	.230	0.000E-00
1119.99	1 1 - 2 0	1	0103.73	2.97273	.207	1.100E-01
1119.99	0 6 - 1 5	1	0103.10	2.97230	.092	3.200E-05
1119.99	0 6 - 1 5	1	0103.10	2.97230	.130	0.000E-01
1119.99	2 1 - 3 0	1	0103.00	2.96947	.092	1.000E-01
1119.99	1 3 - 2 2	1	0103.12	2.96949	.073	2.000E-05
1119.99	0 8 - 1 7	1	0103.00	2.96951	.092	0.000E-01
1119.99	1 4 - 2 1	1	0103.23	2.96916	.092	1.300E-01
1119.99	1 4 - 2 1	1	0103.23	2.96916	.092	1.300E-01
1119.99	0 7 - 1 6	1	0103.77	2.97430	.092	1.300E-01
1119.99	1 3 - 2 2	1	0103.25	2.96917	.130	3.000E-05
1119.99	2 0 - 2 9	1	0103.09	2.97329	.230	0.000E-00
1119.99	1 1 - 2 0	1	0103.73	2.97273	.207	1.100E-01
1119.99	0 6 - 1 5	1	0103.10	2.97230	.092	3.200E-05
1119.99	0 6 - 1 5	1	0103.10	2.97230	.130	0.000E-01
1119.99	2 1 - 3 0	1	0103.00	2.96947	.092	1.000E-01
1119.99	1 3 - 2 2	1	0103.12	2.96949	.073	2.000E-05
1119.99	0 8 - 1 7	1	0103.00	2.96951	.092	0.000E-01
1119.99	1 4 - 2 1	1	0103.23	2.96916	.092	1.300E-01
1119.99	1 4 - 2 1	1	0103.23	2.96916	.092	1.300E-01
1119.99	0 7 - 1 6	1	0103.77	2.97430	.092	1.300E-01
1119.99	1 3 - 2 2	1	0103.25	2.96917	.130	3.000E-05
1119.99	2 0 - 2 9	1	0103.09	2.97329	.230	0.000E-00
1119.99	1 1 - 2 0	1	0103.73	2.97273	.207	1.100E-01
1119.99	0 6 - 1 5	1	0103.10	2.97230	.092	3.200E-05
1119.99	0 6 - 1 5	1	0103.10	2.97230	.130	0.000E-01
1119.99	2 1 - 3 0	1	0103.00	2.96947	.092	1.000E-01
1119.99	1 3 - 2 2	1	0103.12	2.96949	.073	2.000E-05
1119.99	0 8 - 1 7	1	0103.00	2.96951	.092	0.000E-01
1119.99	1 4 - 2 1	1	0103.23	2.96916	.092	1.300E-01
1119.99	1 4 - 2 1	1	0103.23	2.96916	.092	1.300E-01
1119.99	0 7 - 1 6	1	0103.77	2.97430	.092	1.300E-01
1119.99	1 3 - 2 2	1	0103.25	2.96917	.130	3.000E-05
1119.99	2 0 - 2 9	1	0103.09	2.97329	.230	0.000E-00
1119.99	1 1 - 2 0	1	0103.73	2.97273	.207	1.100E-01
1119.99	0 6 - 1 5	1	0103.10	2.97230	.092	3.200E-05
1119.99	0 6 - 1 5	1	0103.10	2.97230	.130	0.000E-01
1119.99	2 1 - 3 0	1	0103.00	2.96947	.092	1.000E-01
1119.99	1 3 - 2 2	1	0103.12	2.96949	.073	2.000E-05
1119.99	0 8 - 1 7	1	0103.00	2.96951	.092	0.000E-01
1119.99	1 4 - 2 1	1	0103.23	2.96916	.092	1.300E-01
1119.99	1 4 - 2 1	1	0103.23	2.96916	.092	1.300E-01
1119.99	0 7 - 1 6	1	0103.77	2.97430	.092	1.300E-01
1119.99	1 3 - 2 2	1	0103.25	2.96917	.130	3.000E-05
1119.99	2 0 - 2 9	1	0103.09	2.97329	.230	0.000E-00
1119.99	1 1 - 2 0	1	0103.73	2.97273	.207	1.100E-01
1119.99	0 6 - 1 5	1	0103.10	2.97230	.092	3.200E-05
1119.99	0 6 - 1 5	1	0103.10	2.97230	.130	0.000E-01
1119.99	2 1 - 3 0	1	0103.00	2.96947	.092	1.000E-01
1119.99	1 3 - 2 2	1	0103.12	2.96949	.073	2.000E-05
1119.99	0 8 - 1 7	1	0103.00	2.96951	.092	0.000E-01
1119.99	1 4 - 2 1	1	0103.23	2.96916	.092	1.300E-01
1119.99	1 4 - 2 1	1	0103.23	2.96916	.092	1.300E-01
1119.99	0 7 - 1 6	1	0103.77	2.97430	.092	1.300E-01
1119.99	1 3 - 2 2	1	0103.25	2.96917	.130	3.000E-05
1119.99	2 0 - 2 9	1	0103.09	2.97329	.230	0.000E-00
1119.99	1 1 - 2 0	1	0103.73	2.97273	.207	1.100E-01
1119.99	0 6 - 1 5	1	0103.10	2.97230	.092	3.200E-05
1119.99	0 6 - 1 5	1	0103.10	2.97230	.130	0.000E-01
1119.99	2 1 - 3 0	1	0103.00	2.96947	.092	1.000E-01
1119.99	1 3 - 2 2	1	0103.12	2.96949	.073	2.000E-05
1119.99	0 8 - 1 7	1	0103.00	2.96951	.092	0.000E-01
1119.99	1 4 - 2 1	1	0103.23	2.96916	.092	1.300E-01
1119.99	1 4 - 2 1	1	0103.23	2.96916	.092	1.300E-01
1119.99	0 7 - 1 6	1	0103.77	2.97430	.092	1.300E-01
1119.99	1 3 - 2 2	1	0103.25	2.96917	.130	3.000E-05
1119.99	2 0 - 2 9	1	0103.09	2.97329	.230	0.000E-00
1119.99	1 1 - 2 0	1	0103.73	2.97273	.207	1.100E-01
1119.99	0 6 - 1 5	1	0103.10	2.97230	.092	3.200E-05
1119.99	0 6 - 1 5	1	0103.10	2.97230	.130	0.000E-01
1119.99	2 1 - 3 0	1	0103.00	2.96947	.092	1.000E-01
1119.99	1 3 - 2 2	1	0103.12	2.96949	.073	2.000E-05
1119.99	0 8 - 1 7	1	0103.00	2.96951	.092	0.000E-01
1119.99	1 4 - 2 1	1	0103.23	2.96916	.092	1.300E-01
1119.99	1 4 - 2 1	1	0103.23	2.96916	.092	1.300E-01
1119.99	0 7 - 1 6	1	0103.77	2.97430	.092	1.300E-01
1119.99	1 3 - 2 2	1	0103.25	2.96917	.130	3.000E-05
1119.99	2 0 - 2 9	1	0103.09	2.97329	.230	0.000E-00
1119.99	1 1 - 2 0	1	0103.73	2.97273	.207	1.100E-01
1119.99	0 6 - 1 5	1	0103.10	2.97230	.092	3.200E-05
1119.99	0 6 - 1 5	1	0103.10	2.97230	.130	0.000E-01
1119.99	2 1 - 3 0	1	0103.00	2.96947	.092	1.000E-01
1119.99	1 3 - 2 2	1	0103.12	2.96949	.073	2.000E-05
1119.99	0 8 - 1 7	1	0103.00	2.96951	.092	0.000E-01
1119.99	1 4 - 2 1	1	0103.23	2.96916	.092	1.300E-01
1119.99	1 4 - 2 1	1	0103.23	2.96916	.092	1.300E-01
1119.99	0 7 - 1 6	1	0103.77	2.97430	.092	1.300E-01
1119.99	1 3 - 2 2					

Table 3. Spectral Line Parameters for the
HF $\Delta v = 1$ Band at 1273 K (Continued)

Wavenumber CM-1	Transition			Lower State CM-1	Wavelength Micron (Air)	Halfwidth			Intensity CM-2 ^a ATM-1
	Lower Level	Upper Level	Isotope			HF-HF	HF-CO ₂	CM-1*ATM-1	
4196.69	1 15	- 2 16	1	8541.84	2.34662	.043	.014	1.317E-03	
4197.46	1 16	- 2 17	1	9134.16	2.36173	.044	.013	8.418E-04	
4201.91	0 6	- 1 7	1	8944.01	2.37837	.036	.016	1.941E-04	
4205.90	1 17	- 2 18	1	9027.71	2.37805	.040	.013	2.301E-04	
4206.48	1 18	- 2 19	1	10044.65	2.37599	.048	.013	1.541E-04	
4206.99	1 21	- 2 22	1	12077.86	2.47522	.043	.013	8.622E-05	
4210.71	1 19	- 2 20	1	11191.21	2.37425	.040	.013	5.578E-05	
4218.91	1 20	- 2 21	1	11919.57	2.37413	.039	.013	2.247E-05	
4230.00	0 7	- 1 8	1	1444.77	2.46246	.073	.015	3.204E-04	
4250.61	0 8	- 1 9	1	1409.44	2.46676	.050	.015	2.293E-04	
4268.64	0 9	- 1 10	1	1431.44	2.45579	.055	.014	1.701E-04	
4301.09	0 10	- 1 11	1	2231.22	2.32401	.051	.014	1.413E-04	
4321.25	0 11	- 1 12	1	2077.43	2.51346	.049	.014	8.294E-05	
4330.60	0 12	- 1 13	1	3150.47	2.30435	.048	.014	3.087E-05	
4350.09	0 13	- 1 14	1	3672.77	2.23580	.046	.014	2.451E-05	
4360.12	0 14	- 1 15	1	4225.71	2.44009	.045	.014	1.804E-05	
4379.59	0 15	- 1 16	1	4814.00	2.28272	.043	.014	5.444E-06	
4380.89	0 20	- 1 25	1	11036.49	2.27933	.029	.012	1.317E-05	
4400.07	0 16	- 1 17	1	5046.80	2.27767	.041	.013	2.044E-05	
4431.99	0 21	- 1 24	1	10728.50	2.27522	.038	.013	9.814E-06	
4440.30	0 17	- 1 18	1	6847.93	2.27416	.040	.013	1.194E-05	
4459.75	0 22	- 1 23	1	10011.89	2.27224	.032	.013	1.160E-06	
4461.12	0 18	- 1 19	1	6734.89	2.27151	.036	.013	5.197E-06	
4481.39	0 21	- 1 22	1	4401.32	2.27058	.033	.013	3.230E-06	
4486.02	0 19	- 1 20	1	7515.99	2.27043	.036	.013	2.154E-06	
4494.77	0 20	- 1 21	1	6273.12	2.26965	.035	.013	8.558E-06	

3.1.4 HF High Temperature Absorption Data* (from The Handbook of IR Radiation from Combustion Gases, by Ludwig, et al. [1975].)

Figures 3 and 4 are reproduced from pages 186 and 187 of Ludwig, et al. [1973]. Figure 3 (their Figure 5-12) presents spectrally-smeared-out "band model" approximations of HF absorption coefficients $k(\nu)$ [in the notation here, $\hat{k}_T(\nu)$] for temperatures T_0 of 300°K, 600°K, 1200°K, 1800°K, 2400°K, and 3000°K. They represent an approximation of the psuedo-continuous absorption curves, in units of (atmos cm at STP)⁻¹, as viewed by a low resolution spectrograph whose effective slit width was equal to at least 3 or 4 times the mean separation \bar{d} between spectral lines. However, as is seen from Figure 4 (their Figure 5-13), \bar{d} is generally greater than 10 cm⁻¹, and is ≈ 13 cm⁻¹ in most of the spectral interval between 3000 and 4100 cm⁻¹, even at $T_0 = 3000^\circ\text{K}$. At 3000°K and 8.5 atmospheres, the effective line widths, using their suggested HF line width at STP of 0.05 cm⁻¹ atmos⁻¹, is ≈ 0.13 cm⁻¹. Thus, even at 3000°K and 8.5 atmos pressure, HF will not even come close to acting as a spectrally continuous absorber of HF laser radiation. The relatively large line spacing also can be perceived in Table III of the preceding sub-section. The line spacing in any specific (v'', v') band of a diatomic molecule is approximately equal to $2B_{v''}$ (or $2B_{v'}$) for low J'' , although higher order terms occur as J'' increases. Thus, closer line spacing requires the presence of two or more overlapping (v'', v') bands in the same spectral region. B_0 equals ~ 20.55 cm⁻¹ for HF (and ~ 10.85 cm⁻¹ for DF). Relatively large B values are characteristic of HX or DX type molecules, since the B's are inversely proportional to the molecule's moment of inertia.

Thus, except for possible accidental near-coincidences, within ~ 0.1 cm⁻¹, of the positions of absorption lines from other $v''J'' \rightarrow v'J'$ transitions, it appears that HF or DF "seeding" would be useful only for the initial, "pre-bleaching," self-absorption by the inverse of the lasing transitions.

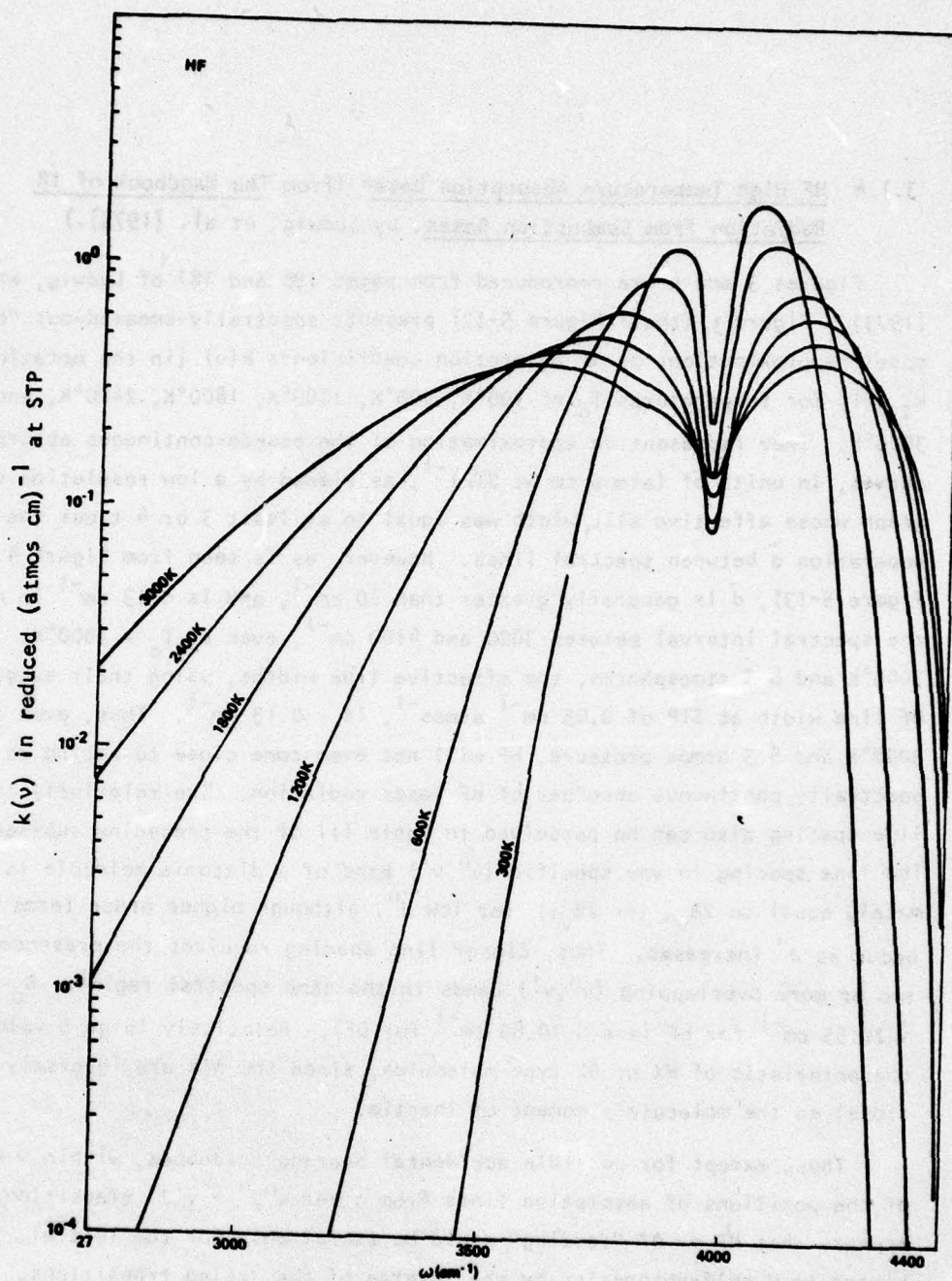


Figure 3. Absorption coefficient for HF at standard temperature and pressure.

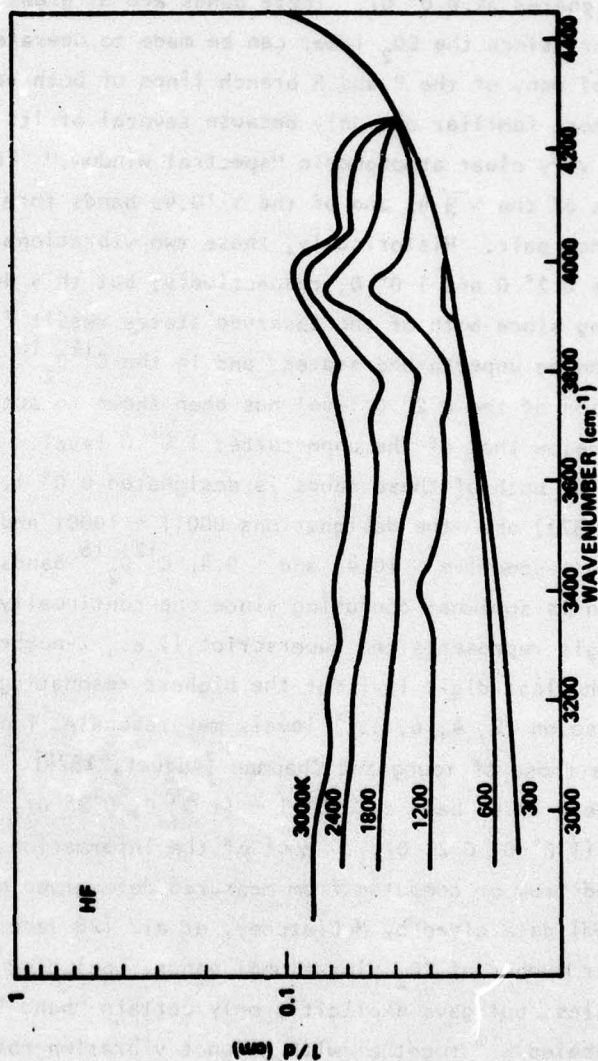


Figure 4. Line density for HF.

3.2 CO₂

3.2.1 Self-Absorption of 10.4 μ Region or 9.4 μ Region CO₂ Laser Lines

At low temperatures the ~ 9.4 micron and ~ 10.4 micron CO₂ bands exhibit relatively weak absorption [low $\hat{S}_T(v_0)$ or $\hat{S}_T^I(v_0)$ for the individual lines] because their lower state vibrational levels are respectively 1285.412 cm⁻¹ and 1388.187 cm⁻¹ above the ground vibrational state (usually designated as 0 0° 0). These bands are of great practical importance, however, since the CO₂ laser can be made to operate efficiently at the frequencies of many of the P and R branch lines of both bands. The 10.4 μ band is the more familiar one only because several of its laser lines lie in a relatively very clear atmospheric "spectral window." The lower state vibrational levels of the $\sim 9.4\mu$ and of the $\sim 10.4\mu$ bands form what is known as a Fermi Resonance pair. Historically, these two vibrational states have been designated as 0 2° 0 and 1 0° 0, respectively; but this designation is actually wrong since both of the observed states result from a mixing of the two corresponding unperturbed states, and in the C¹²O₂¹⁶ isotope, the unperturbed position of the 0 2° 0 level has been shown to actually lie above rather than below that of the unperturbed 1 0° 0 level. The upper vibrational state shared by both of these bands is designated 0 0° 1. McClatchey, et al. [26 January 1973] use the designations 00011 + 10001 and 00011 + 10002 to designate the respective $\sim 10.4\mu$ and $\sim 9.4\mu$ C¹²O₂¹⁶ bands. While compact, this notation is somewhat confusing since one continually has to recall that the third digit represents the superscript (i.e., ℓ -number) on the second (v_2) digit, and the last digit is 1 for the highest resonating level, 2 for the second, and so on (2, 4, 6, ...) levels may resonate. The notations used here, however, are those of Young and Chapman [August, 1974]. These later authors designate the $\sim 10.4\mu$ band as 0 0° 1 + (1 0° 0, 0 2° 0)₁, and the $\sim 9.4\mu$ band as 0 0° 1 + (1 0° 0, 0 2° 0)₁₁. Most of the information presented here also was extracted from or computed from measured data given by Young and Chapman. The (computed) data given by McClatchey, et al. [26 January, 1973] covered a much larger number of CO₂ vibrational bands, including bands from several isotope species, but gave explicitly only certain "band intensity" parameters that they labeled S_v^0 together with adjunct vibration-rotation interaction parameters ζ and the band center wave number positions which they call ν_0 .

but which should be labeled as ν_{00} to distinguish from the individual line positions ν_0 . The integrated line intensities that have been designated as $\hat{S}_T(\nu_0)$, in units of $\text{cm}^2 (\text{cm}^{-1})$ per CO_2 molecule (in any $V''J''$ state) can be calculated from the McClatchey, et al., data (for $T_0 = 296^\circ\text{K}$) by using the relation,

$$\hat{S}_{T_0}(\nu_0) = \left(\frac{\nu_0}{\nu_{00}} \right) \left\{ \frac{1}{2(J'+J''+1)} \right\} \left(\frac{hcB_0''}{1/2kT_0} \right) (1-\zeta)^2 S_V^0 \exp \left[- \left(\frac{hcB_0''}{kT_0} \right) J''(J''+1) \right]. \quad (18)^\dagger$$

The McClatchey relationships were used for several calculations before the discovery of Chapman. The data presented by this latter paper is not only much more closely tied to direct measurements, but also is presented in a form that is much easier to use.

Young and Chapman tabulate a parameter they labeled as (S_J/α^0) , in units of cm^{-1} at 300°K , for selected P and R-branch lines of both the $\sim 10.4\mu$ and $\sim 9.4\mu$ $\text{C}^{12}\text{O}_2^{16}$ bands. Upon inspection, this parameter turns out to be equal, in the notation adopted here, to $\left\{ \hat{S}'_{300^\circ\text{K}}(\nu_0)/a_0 \right\}$. It will be recalled that the symbol $\hat{S}'_T(\nu_0)$ designates the integrated line intensity in units of $(\text{atmos} \cdot \text{cm} \cdot \text{STP})^{-1} \text{cm}^{-1}$ referred to the total population of absorbing species molecules at partial pressure p_1 . At line center, ν_0 , with a Lorentz profile, the spectral transmission at T_0 is given by $\exp[-\hat{S}'_T(\nu_0) P \delta x (a_0 p_1 \pi)^{-1}]$. It can be seen that for a pure gas, such that $P = p_1$, the spectral transmission at line center is independent of pressure. The quantity $(\hat{S}'_T(\nu_0)/a_0)$, or in their notation (S_J/α_L^0) , thus could be determined at pressures above 50 Torr, where the Lorentz line profile is valid, and then applied to compute their S_J at very high resolution measurements at very low pressures where the Doppler profile predominated.

The third column of Table 4 converts the Young and Chapman tabulated (S_J/α_L^0) values to line center $\hat{k}_T(\nu_0, \nu_0)$, in units of $(\text{atmos cm-STP})^{-1}$ for (any state) CO_2 molecules at 300°K (and one atmos pressure) merely by dividing through by π . The fourth column of this table converts $\hat{k}(\nu_0, \nu_0)$ to $\hat{\sigma}(\nu_0, \nu_0)$ by multiplying the former quantity by the (p_1/N) ratio of $(1 \text{ atmos-STP})/2.69 \cdot 10^{19}$ molecules cm^{-3} . The 5th and 6th column $k(\nu_0, \nu_0)$ and $\sigma(\nu_0, \nu_0)$ for lower state ($V''J''$) molecules were calculated by multiplying the respective $\hat{k}_T(\nu_0, \nu_0)$ and $\hat{\sigma}_T$ values by $(N/N_{V''J''})$ values which in turn were computed by assuming thermal equilibrium at $T_0 = 300^\circ\text{K}$.

[†] Owing to all odd (or all even) J-levels being missing for CO_2 normal $\text{C}^{12}\text{O}_2^{16}$ isotope, $Q_R(T)$ is reduced by a factor of 1/2 to $\approx (1/2 kT/hcB)$.

Table 4a. $C^{12}O_2^{16}$ Parameters Calculated from Young and Chapman Data for the $\sim 10.4\mu$ $0\ 0^0\ 1 \leftarrow (1\ 0^0\ 0, 0\ 2^0\ 0)_1$ Band; $T_0 = 300^\circ K$.

Line	ν_0 (in cm^{-1})	* $\hat{k}_{T_0}(\nu_0, \nu_0)$ $\cdot 10^{+3}$ (in atm cm) $^{-1}$	* $\hat{\sigma}_{T_0}(\nu_0, \nu_0)$ $\cdot 10^{+23}$ (in cm^2/mol)	$k(\nu_0, \nu_0)$ {in (atm cm) $^{-1}$ for $\nu''J''$ mols.}	$\sigma(\nu_0, \nu_0)$ $\cdot 10^{+18}$ {in cm^2 per $\nu''J''$ mol}
P 8	954.5458	1.17	4.35	19.4	0.720
P 10	952.8816	1.44	5.35		
P 14	949.4800	1.75	6.50		
P 20	944.1948	1.84	6.84	24.4	0.907
P 22	942.3841	1.75	6.50		
P 24	940.5488	1.56	5.80	24.4	0.906
P 28	936.8045	1.29	4.80		
P 32	932.9611	0.875	3.25	24.5	0.908
P 34	931.0022	0.815	3.03		
P 36	929.0182	0.653	2.43	27.4	1.02
P 38	927.0091	0.598	2.22		
P 40	924.9749	0.458	1.70	31.1	1.15
R 28	980.9139	1.33	4.94	26.7	0.992
R 30	982.0962	1.17	4.35		
R 32	983.2530	0.993	3.69		
R 34	984.3840	0.815	3.03		
R 36	985.4891	0.652	2.42		
R 38	986.5682	0.512	1.90	27.1	1.01

* Molecules assumed to be in thermal equilibrium at $300^\circ K$. See text for comparison values.

Note: Only even J'' 's exist (some omitted).

Table 4b. $C^{12}O_2$ 16 Parameters Calculated from Young and Chapman Data for the $\sim 9.4\mu$ $0\ 0\ 1 \leftarrow (1\ 0\ 0, 0\ 2\ 0)_{11}$ Band; $T_0 = 300^\circ K$.

Line	ν_0 (in cm^{-1})	$\hat{k}_T^*(\nu_0, \nu_0)$ $\cdot 10^{+3}$ (in atm cm) $^{-1}$	$\hat{\sigma}_T^*(\nu_0, \nu_0)$ $\cdot 10^{+23}$ (in cm^2/mol)	$k(\nu_0, \nu_0)$ {in (atm cm) $^{-1}$ for $\nu''J''$ mols}	$\sigma(\nu_0, \nu_0)$ $\cdot 10^{+18}$ (in cm^2 per $\nu''J''$ mol)
P 6	1058.9487	1.39	5.15	28.4	1.05
P 8	1057.3002	1.76	6.54		
P 12	1053.9235	2.37	8.81		
P 16	1050.4413	2.58	9.59		
P 20	1046.8542	2.63	9.77	34.9	1.30
P 24	1043.1633	2.33	8.66		
P 28	1039.3693	1.88	6.99		
P 30	1037.4341	1.71	6.36		
P 32	1035.4736	1.45	5.39	40.5	1.51
P 34	1033.4881	1.23	4.57		
P 36	1031.4775	1.02	3.08		
P 38	1029.4423	0.84	3.12	44.5	1.65
R 6	1069.0141	1.63	6.05	33.3	1.24
R 10	1071.8837	2.38	8.84		
R 12	1073.2785	2.66	9.90	34.3	1.28

* Molecules assumed to be internal equilibrium at 300°K. See text for comparison values.

Note: Only even J'' 's exist (some omitted).

For comparison with the Table 4 data, the McClatchey, et al., computed data, when applied to Equation (18) for the P 20 line of the $\sim 10.4 \mu$ $0\ 0^{\circ}\ 1 \leftarrow (10^{\circ}\ 0, 0\ 2^{\circ}\ 0)_1$ band gives a $\hat{S}_{296^{\circ}\text{K}}(\nu_o)$ value of $1.65 \cdot 10^{-23}$ ($\text{cm}^2 \text{cm}^{-1}$) per CO_2 molecule. A P 20 line width of $\sim 0.0768 \text{ cm}^{-1}$ at one atmosphere then would be required to give the $\hat{\sigma}_T$ of $6.84 \cdot 10^{-23}$ ($\text{cm}^2/\text{mol.}$) shown in the 4th column of Table 4a for the P 20 line. The a_o value of $\sim 0.105 \text{ cm}^{-1}$ reported by Young and Chapman for the self-broadening of the P 20 line gives, however, a poorer matching value of $\hat{\sigma}_T = 5.00 \cdot 10^{-23}$ ($\text{cm}^2/\text{mol.}$) for the McClatchey, et al. data. The agreement still is probably within the limits of accuracy of the data upon which the two computations were based, and of the simplifying assumptions made, particularly in the McClatchey, et al., report. An integrated line strength $\hat{S}'_{300^{\circ}\text{K}}(\text{P } 20)$ of $5.48 \cdot 10^{-4}$ ($\text{atmos cm}^{-1} \text{ cm}^{-1}$) has been reported by J. H. McCoy (10 September 1968). When divided by $(\pi \cdot 0.105 \text{ cm}^{-1})$, this gave a P 20 value of $\hat{k}_{300^{\circ}\text{K}}(\nu_o)$ equal to $1.66 \cdot 10^{-3}$ (atmos cm^{-1}), for comparison with the Table 4 value of $1.84 \cdot 10^{-3}$ (atmos cm^{-1}), again probably within the precision of the two determinations.

CO_2 also has several other vibration rotation bands, originating either from isotopes other than $\text{C}^{12}\text{O}_2^{16}$ or from lower state v'' levels that lie higher than $(1\ 0^{\circ}\ 0, 0\ 2^{\circ}\ 0)_1$, that can exhibit absorption lines interleaving with those of either the previously discussed $\sim 10.4 \mu$ or 9.4μ bands. For thermal equilibrium distributions near room temperature, the isotope abundance weighted $\hat{\sigma}$ or \hat{k} absorption coefficients for the lines of these bands are much weaker than those for the latter [see, for example, the S_v^o factors listed in Table 10, page 27 of McClatchey, et al., for their ν_o (our ν_{oo}) between ~ 900 and 1080 cm^{-1}]. At sufficiently high temperatures, however, these "hotter bands" can contribute significantly to the absorption in the spectral regions of interest, and reduce the effective mean line spacing $\bar{\sigma}$ from ~ 1 or 2 cm^{-1} to the order of $\sim 0.1 \text{ cm}^{-1}$ to $\sim 0.3 \text{ cm}^{-1}$. Then, for high pressures, the absorption would appear as a quasi-continuum in the CO_2 laser regions.

Figures 5a, b, c, and d, taken from Young and Chapman, show the variations with the $|m|$ parameter of self-broadened and N_2 broadened CO_2 lines.

$$|m| = \begin{cases} J'' & \text{for P-branch lines.} \\ J'' + 1 & \text{for R-branch lines.} \end{cases}$$

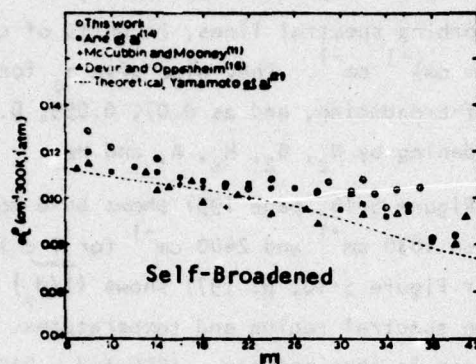


Fig. 5a.

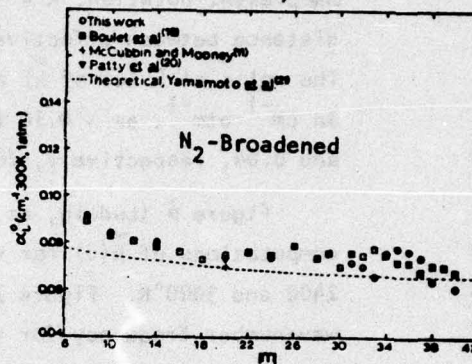


Fig. 5b.

Variation of half-width with rotational quantum number for the 10.4- μm CO_2 band:
 $|m| = J''$ for P-branch lines; $|m| = (J'' + 1)$ for R-branch lines; (a) self-broadening; (b)
 N_2 -broadening.

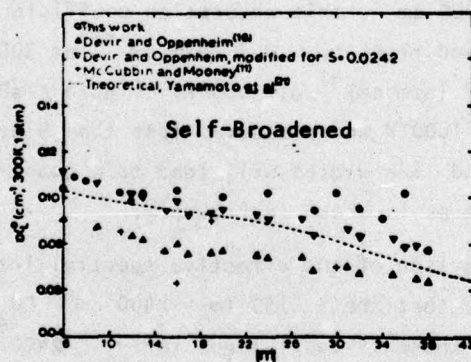


Fig. 5c.

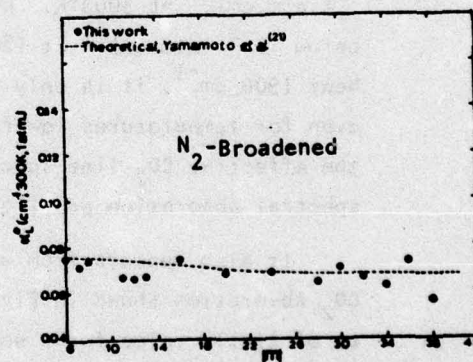


Fig. 5d.

Variation of half-width with rotational quantum number for the 9.4- μm CO_2 band:
 (a) self-broadening; (b) N_2 -broadening.

3.2.2 CO_2 Absorption in the 1830 to 2400 cm^{-1} Spectral Region of CO and DF Laser Radiation

Most of the information presented in this and the next few subsections is taken directly from the band model plots given by Ludwig, et al. [1973]. The quantities they plot are spectrally-dependent mean values $\bar{k} = (\bar{S}/d)$ [in the present notation, $\bar{k} = (\bar{S}/d)$]; where d represents as before, the mean distance between effectively absorbing spectral lines, in units of cm^{-1} . The units of \bar{k} (or of \bar{k}) are $(\text{atm cm})^{-1} \text{cm}^{-1}$. They also give a_0 for CO_2 , in $\text{cm}^{-1} \text{atm}^{-1}$, as ~ 0.10 for self-broadening, and as 0.07, 0.055, 0.08, 0.05, and 0.04, respectively, for broadening by N_2 , O_2 , H_x , A, and He.

Figure 6 (Ludwig, et al.'s Figure 5-16, page 195) shows band model computations of $\bar{k}(\nu)$ for ν between 1830 cm^{-1} and 2400 cm^{-1} for $T = 1800$, 2400 and 3000°K. Figure 7 (their Figure 5-18, p. 197) shows $(1/d_0)$ versus wavenumber frequency for the same spectral region and temperatures. The spectral region of current interest is that between ~ 1900 and $\sim 2100 \text{ cm}^{-1}$ as a possible absorber of CO laser line radiation. Currently CO lasers have been made to emit $\Delta v = 1$ P branch lines extending from the $(1 - 0)$ band in the ~ 2135 to $\sim 2013 \text{ cm}^{-1}$ region to the $(32 \rightarrow 31)$ band P 11 line near 1325 cm^{-1} . It is quite possible that $(1 - 0)$ lines near 2100 cm^{-1} eventually will be made to emit very strong radiation. It can be seen from Figure 17 that near 2100 cm^{-1} \bar{k} for CO_2 rises from $\sim 0.2 (\text{atm cm})^{-1}$ at 1800°K to $\sim 3 (\text{atm cm})^{-1}$ at 3000°K. Near 2000 cm^{-1} , this absorption coefficient drops below $10^{-2} (\text{atm cm})^{-1}$ at 1800°K and rises to $\sim 0.7 (\text{atm cm})^{-1}$ at 3000°K. Near 1900 cm^{-1} , it is only $\sim 0.07 (\text{atm cm})^{-1}$ at 3000°K. Figure 7 shows that even for temperatures lower than 1800°K and pressures less than 5 atmospheres, the effective CO_2 line spacing and line widths will lead to a quasi-continuous spectral absorption profile, such as is shown in Figure 6.

It also appears from a comparison of the effective spectral interval for CO_2 absorption shown in Figure 6, that the ~ 2150 to $\sim 2400 \text{ cm}^{-1}$ CO_2 would be of little value for absorbing those DF laser lines for $\nu_c \gtrsim 2400 \text{ cm}^{-1}$. However, many of the DF $(5 \rightarrow 4)$, $(6 \rightarrow 5)$, $(7 \rightarrow 6)$, $(8 \rightarrow 7)$ and $(9 \rightarrow 8)$ lines fall between 2400 and 2000 cm^{-1} where the CO_2 absorption is strongest [McClatchey and Selby (3 January 1974), pp. 23 and 24]. If sufficient DF laser power could be channeled into some of these lines, then even lower temperature CO_2 (down to $\sim 1200^\circ\text{K}$) might prove to be a very efficient absorber.

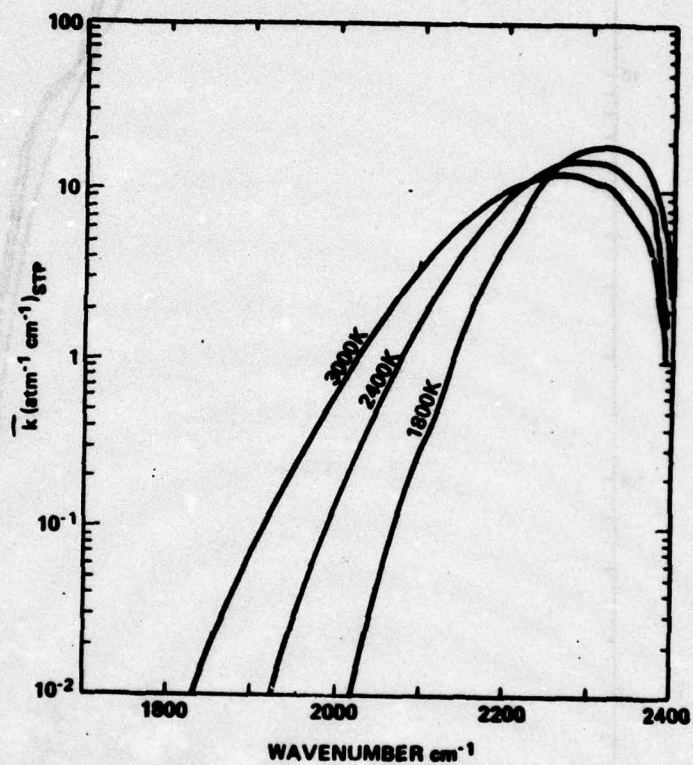


Figure 6. $\bar{k} = \overline{S/d}$ of C^{12}O_2 versus wavenumber for $T = 1800, 2400$, and 3000K .

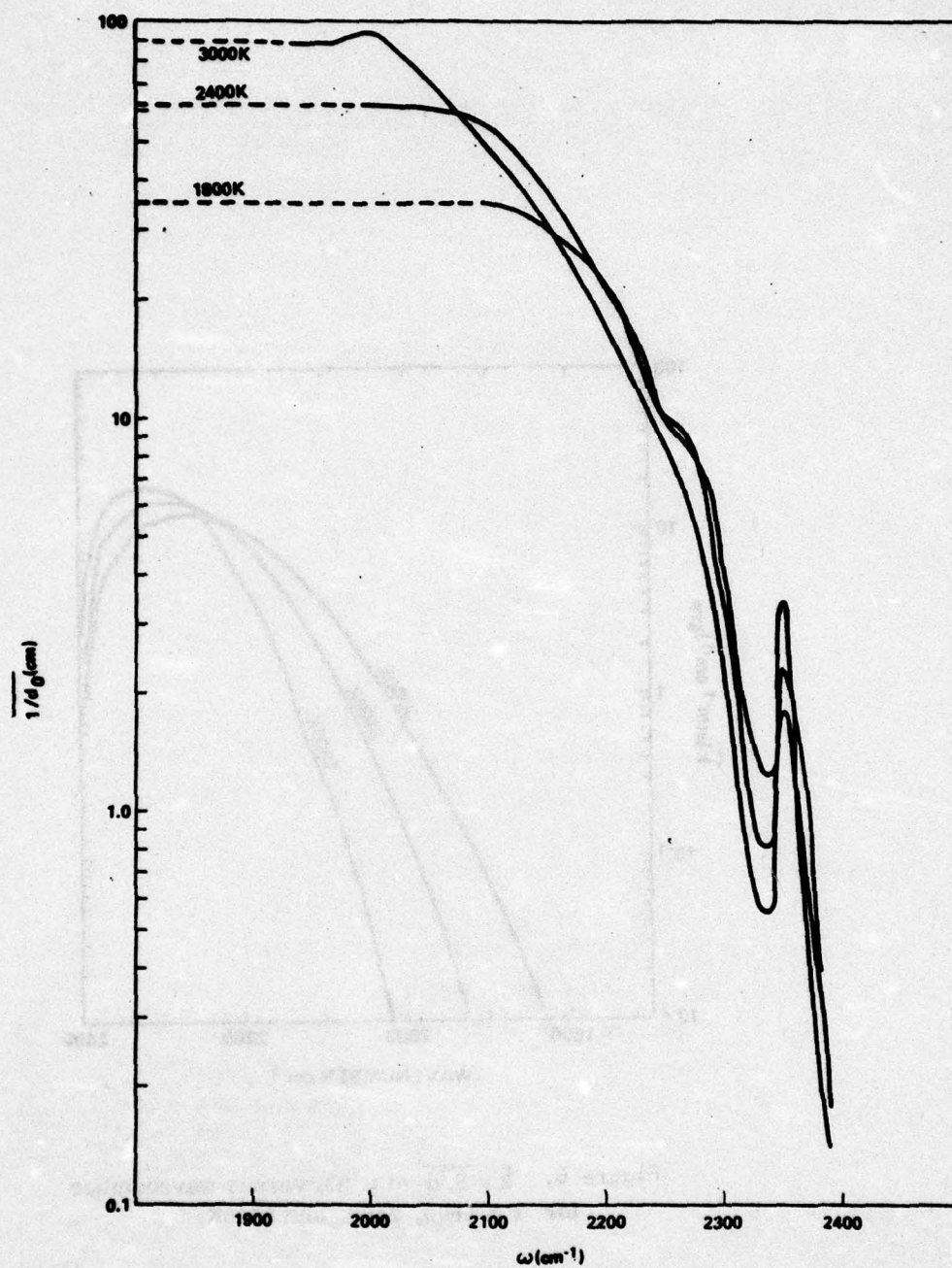


Figure 7. Values of the line density parameter $1/d_0$ for the $4.3\text{-}\mu$ band of C^{12}O_2 . (The dashed portions of the curves are extrapolated values. These data are tabulated in the General Appendix.)

3.2.3 CO₂ Absorption in the ~ 3100 to ~ 3750 cm⁻¹ Spectral Region of HF Laser Radiation

Figures 8, 9, and 10 are copies of Ludwig, et al.'s Figures 5-19, 5-20, and 5-21 (on their pages 198 to 200). A comparison of Figures 8 and 9 with Table 2 here shows that the spectral interval of strongest absorption in this essentially $1\ 0^{\circ}\ 1 \leftarrow 0\ 0^{\circ}\ 0$ band region also includes many of the strongest HF laser emission lines. Figure 10 shows that above 1200°K and at pressures of ~ 4 atmospheres, the CO₂ absorption can be treated as quasi-continuous. It thus appears that 10 or 20 atmos cm of CO₂ might prove a fairly efficient absorber of selected HF lines.

3.3 SELF ABSORPTION OF CO LASER RADIATION

3.3.1 Band Model Studies

3.3.1.1 Inferences from data given by Ludwig, et al. (1973)

Figures 11 and 12 are Ludwig, et al.'s Figures 5-2 and 5-3 for band models of spectrally distributed mean CO absorption and line density in the $\Delta v = 1$ (~ 1500 to ~ 2350 cm⁻¹) region. As would be expected, the figures show that at low temperatures, CO would self-absorb mainly those lines arising from low v'' and low J'' states, but at higher temperatures would begin to absorb in the higher v'' J'' "hot regions." Self-absorption of laser lines corresponding to $v'' \gtrsim 2$ or 3, particularly for higher J'' , thus would be more efficient for CO₂ heated above say 600 or 1000°K. Figure 12 shows that the line density (of effectively absorbing lines) also requires a fairly high temperature in order to produce anything approaching a pseudo continuum. Ludwig, et al, give mean a_0 line width factors for CO as ~ 0.06 for self-broadening and for N₂, H₂, or H₂O broadening, and 0.05 and 0.07, respectively for broadening by O₂ and CO₂, all in units of cm⁻¹ atm⁻¹ at 300°K. At an effective pressure P, in atmospheres, and temperature T, the mean line widths then would be $\sim a_0 \sqrt{300^{\circ}\text{K}/T}$. From this relation, a_0 for CO (P = at 8.5 atmospheres) would be ~ 0.16 cm⁻¹ at 3000°K, 0.18 cm⁻¹ at 2400°K, 0.21 cm⁻¹ at 1800°K, 0.26 cm⁻¹ at 1200°, and 0.51 cm⁻¹ at 300°K. Even at 3000°K, however, it is seen that the mean effective line separation is of the order of ~ 0.5 cm⁻¹ or greater, and approximately 4 or 6 cm⁻¹ near 300°K.

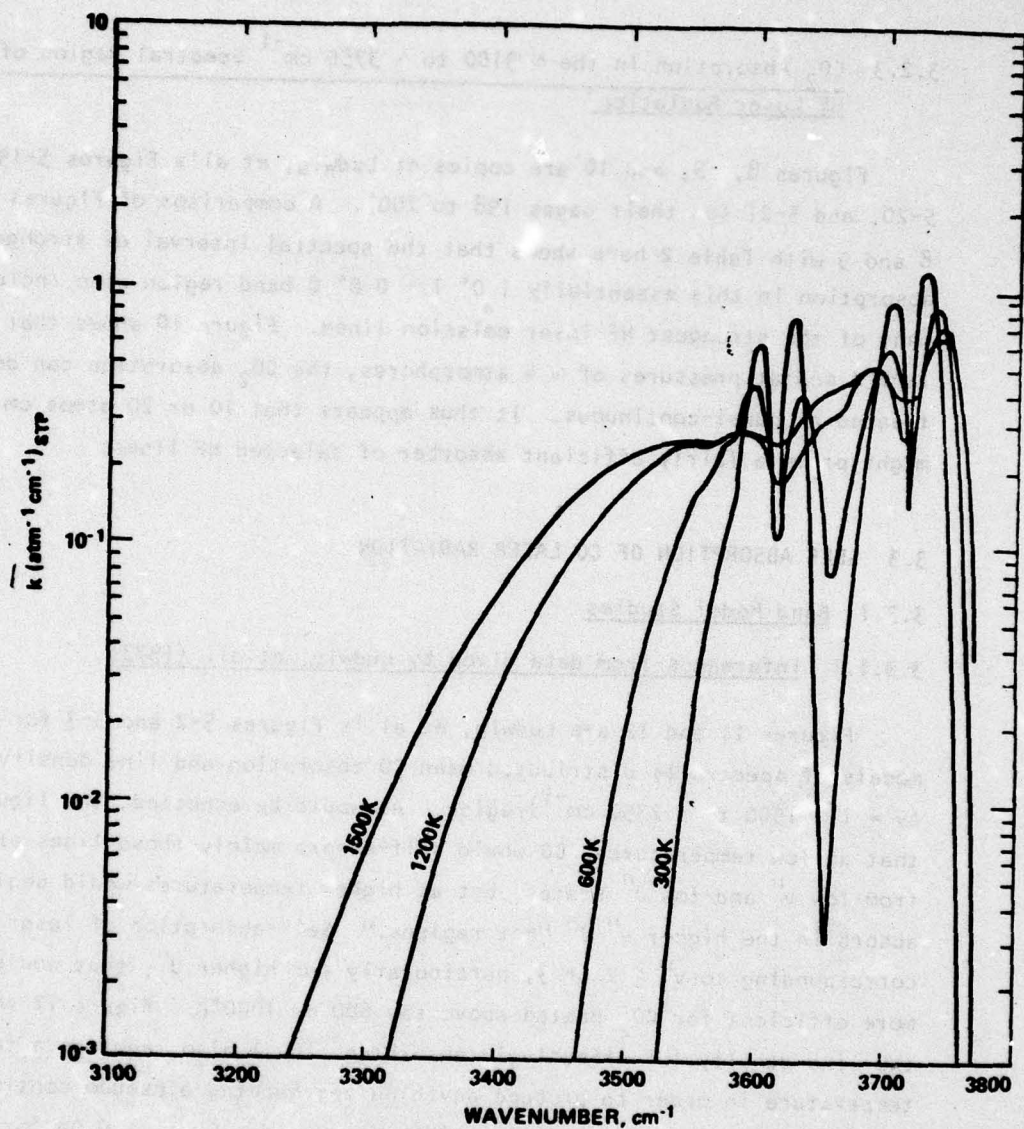


Figure 8. $k = \overline{S/d}$ of C^{12}O_2 versus wavenumber for $T = 300, 600, 1200$, and 1500K .

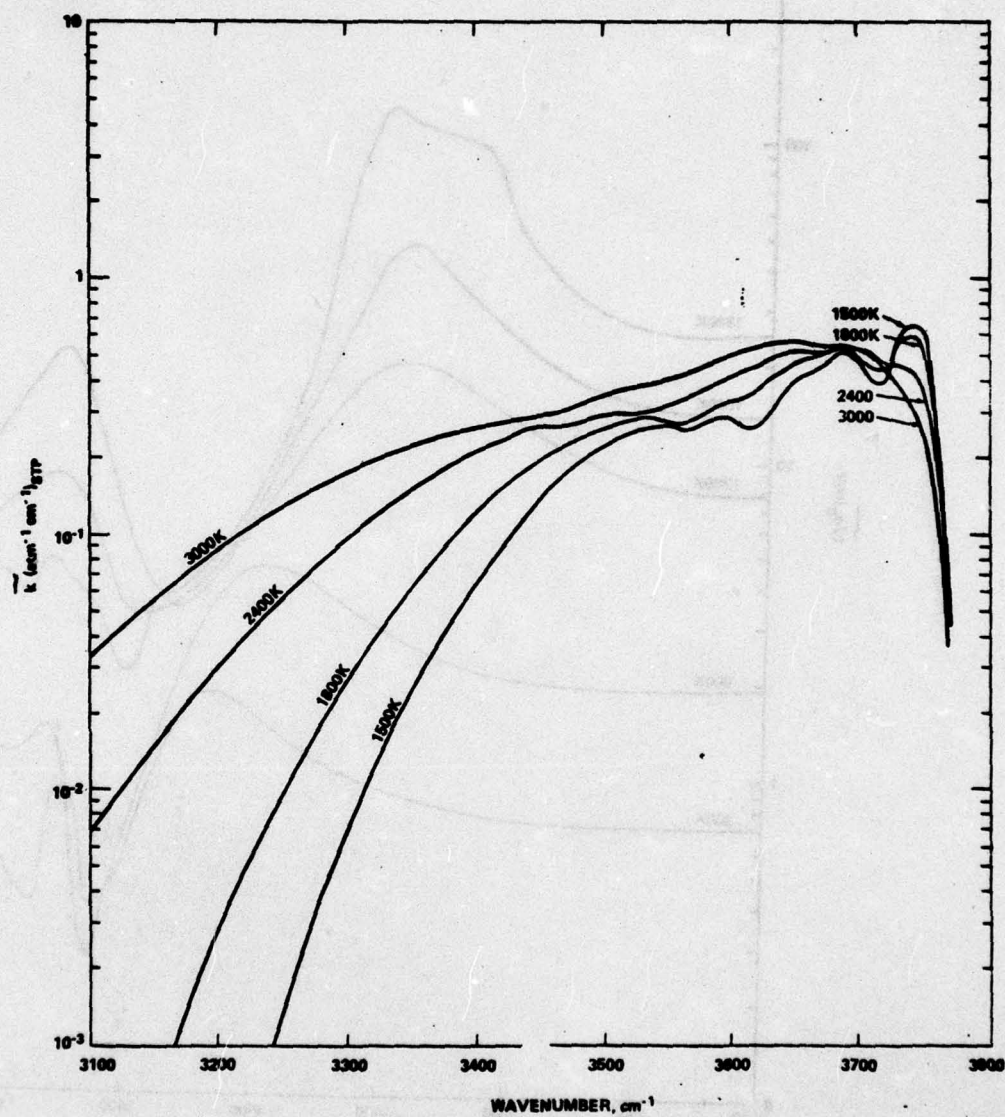


Figure 9. $k = \overline{S/d}$ of C^{12}O_2 versus wavenumber for $T = 1500, 1800, 2400,$ and 3000K .

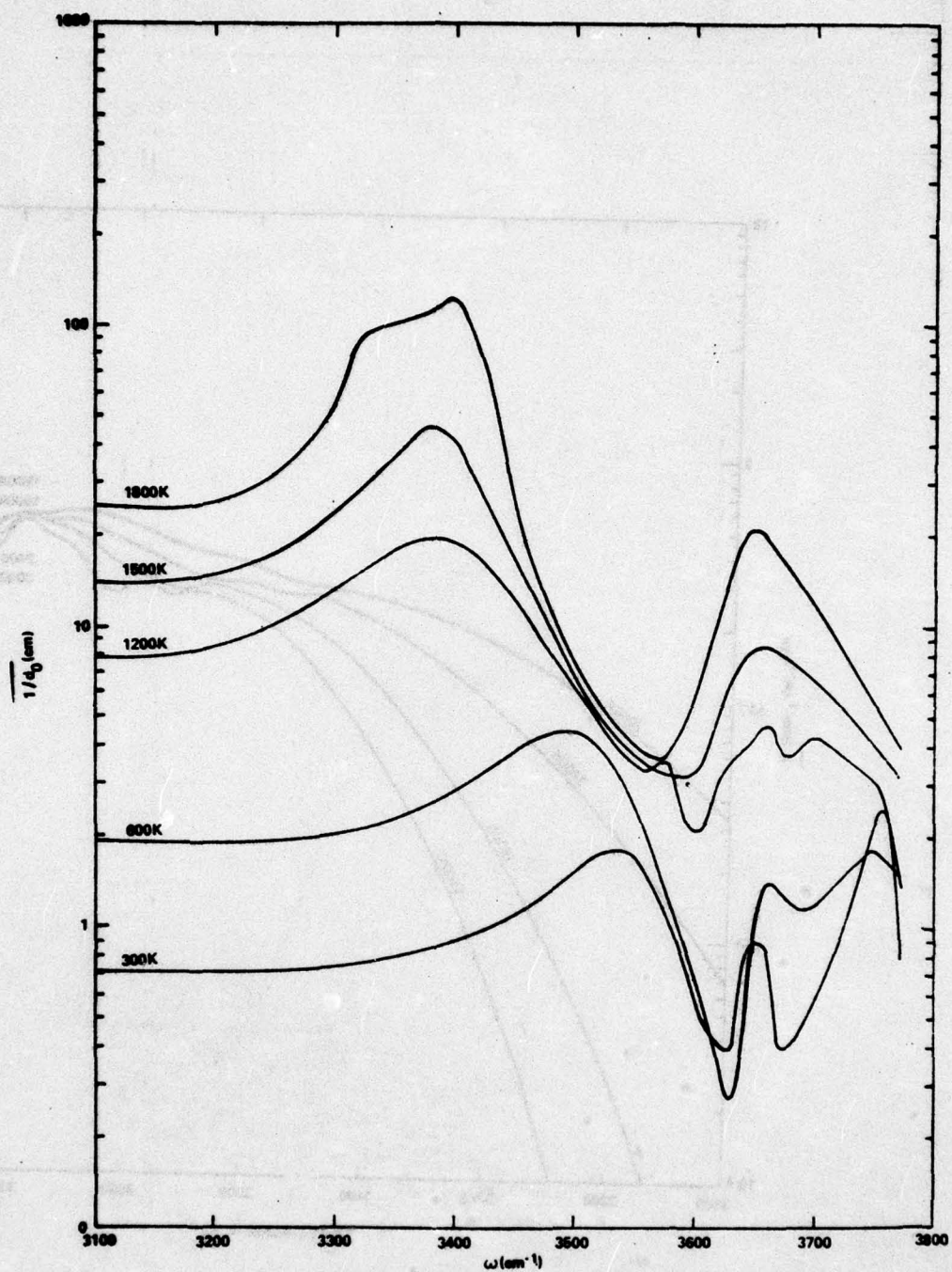


Figure 10. Values of the line density parameter $1/d_0$ for the $2.7\text{-}\mu$ band of C^{12}O_2 .

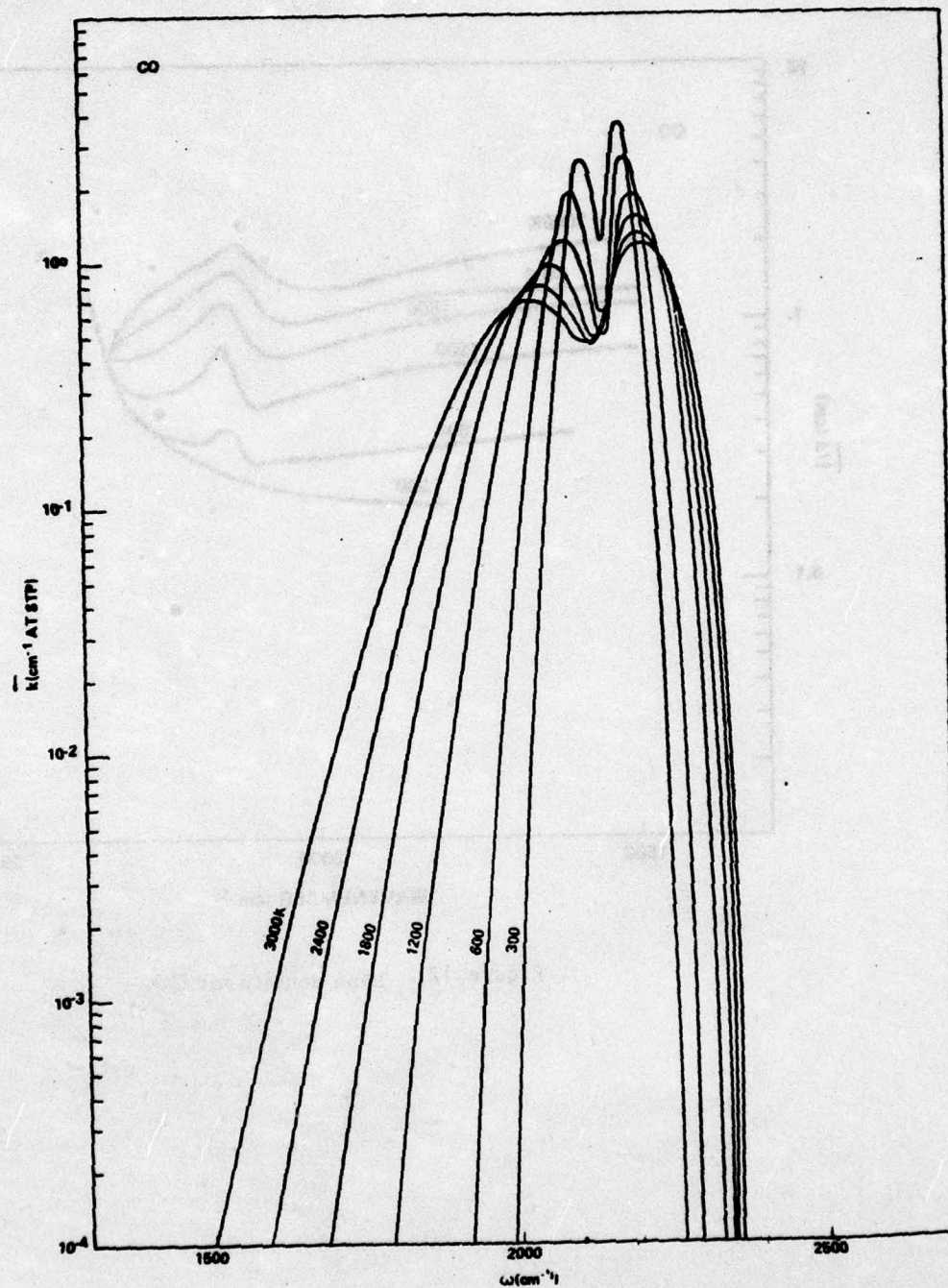


Figure 11. Absorption coefficient for CO at standard temperature and pressure.

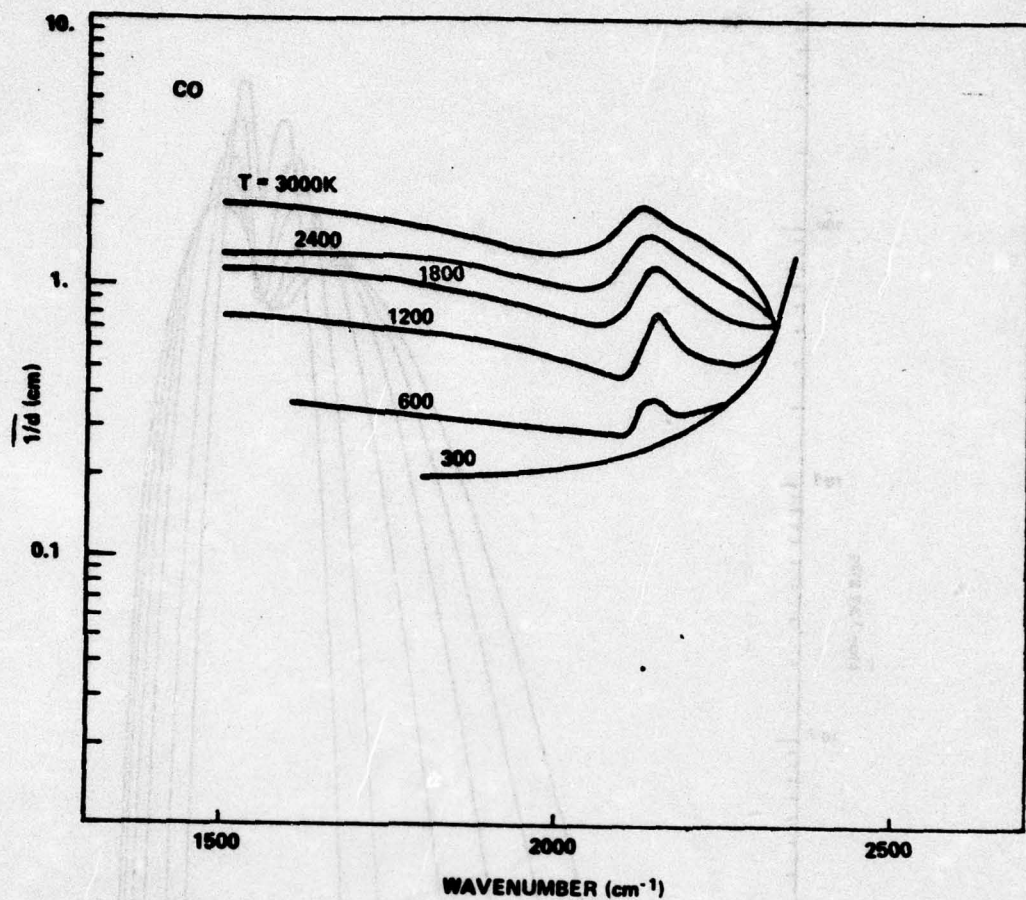


Figure 12. Line density for CO.

There will, therefore, be dips between lines even at 3000°K, and larger fluctuations at lower temperatures. The superposition of line wings, however, appears to be sufficient to keep the $\bar{\kappa}(\nu)$ minima to within at least 10 or 20% of the mean values shown in Figure 11 for the higher temperatures. Then, for selected laser lines occurring within the broad center regions, $\bar{\kappa}(\nu)$ [or my $\bar{\kappa}'(\nu)$] should be of the order of $0.08 \text{ (atm cm)}^{-1}$ or greater. Also, molecules "bleached" out of one ν'' state would then be capable of contributing to absorption in the next $\nu''+1$ state, particularly since rotational relaxation is very rapid.

3.3.1.2 Self-absorption of CO Laser Radiation by a Pressure-Broadened Quasi-Continuum

Caledonia, et al. (1975), have addressed themselves directly to the problem of self-absorption of CO laser radiation for use in rocket propulsion. Their band model assumes pressure broadening sufficient to blend the individual absorption lines into a quasi-continuum. Their assumption is that this condition occurs when the line width, a_L (half-width at half maxima), is broadened to approximately $(\bar{d}/2)$ where \bar{d} is the (spectrally-variable) mean separation, in wave number units, of adjacent effectively absorbing spectral lines. As we have seen from the preceding \bar{d}^{-1} vs. ν figures, taken from Ludwig et al., $\bar{d}_T(\nu)$ tends to decrease with increasing temperatures as "hot bands" make significant contributions to the absorption in the spectral region of interest. For thermal equilibrium near room temperature, where only the $\nu'' = 0$ to $\nu' = 1$ band makes significant contribution, $\bar{d}_{300^\circ\text{K}}(\nu)$ is of the order of 3.9 cm^{-1} near the center of the preceding band, but tends to increase toward $\sim 4.5 \text{ cm}^{-1}$ for the higher intensity $\nu' = 1 \rightarrow \nu'' = 0$ P-branch laser lines. The 30 atmospheres pressure assumed leads to an a_L value of $\sim 1.8 \text{ cm}^{-1}$, and thus to some oscillation in the resulting pressure broadened absorption curve. The oscillations would become more significant at lower pressures and higher temperatures. At $P = 8.5 \text{ atmos}$, and $T = 3000^\circ\text{K}$, for example, the a_L value would be $\sim 0.16 \text{ cm}^{-1}$, while the effective value of $(1/2\bar{d}_{3000^\circ\text{K}})$ near 2100 cm^{-1} would be $\sim 0.25 \text{ cm}^{-1}$. Thus, while there still would be relatively strong absorption in between the ν_0 positions of spectral line centers, the effective absorption coefficients half-way between a pair of equal intensity lines would be only $\sim 58\%$ of the line center values.

Caledonia, et al., present a detailed discussion of "bleaching" by absorption processes, and the consequent transfer of absorption from the $(0 \rightarrow 1)$ vibrational band to the $(1 \rightarrow 2)$ band, to the $(2 \rightarrow 3)$ band, etc. Figures 13 and 14 presented here are their Figures 3.2 and 3.4. Since these figures are quite familiar, further discussion here will be omitted except to denote that the absorption cross sections shown appear to include the effects of rotational, but not vibrational partition. That is, they are referred to the entire rotational level population, assumed to be in rotational thermal equilibrium at each temperature T , of a given v'' state, and not to molecules specifically in the $v'' J''$ state which are candidates for the absorption transitions occurring very near to ν_0 . This is probably reasonably valid, since rotational relaxation is much more rapid than is vibrational relaxation.

3.3.2 Self Absorption by the Inverse of the CO Laser Line Transition

S. H. Chan, et al. (1974), have used a Fourier transform spectrometer coupled with a 303.2 cm gas cell to measure the spectral transmission curves of very low concentrations of CO at room temperature with a resolution of 0.5 cm^{-1} . Their partial pressures of CO ranged from 2.32 to 0.004 torr (i.e., mm of Hg), N_2 being the diluent used to raise the total pressure to 1 atmosphere (i.e., to 760 torr). Their tabulation of apparent absorption coefficients, at 0.2 cm^{-1} intervals about each ($v'' = 0 \rightarrow v' = 1$) absorption line is reproduced here as Table 5. For $\delta\nu$'s not too far removed from the line center, their data is somewhat similar to that which would be observed for much higher resolution, but with a_c equal to about 0.5 cm^{-1} . Line center absorption coefficients for $k_{T_0}(\nu_0, \nu_0)$ at $P = 8.5 \text{ atmos}$ and $T = 300^\circ\text{K}$ and 3000°K , corresponding to a_c 's of $\sim 0.5 \text{ cm}^{-1}$ and $\sim 0.16 \text{ cm}^{-1}$ would be, respectively, about equal to, and about 3 times the peak values they show for each line.

The "apparent absorption" coefficients tabulated by Chan, et al., are related to the true absorption coefficients by convolution with the instrument response function $g(\nu - \nu')$. For a Fourier transform interferometer-spectrometer, with a resolution $\delta\nu$ (here 0.5 cm^{-1}), $g(\nu - \nu')$ is proportional to a truncated $\sin x/x$ function. That is,

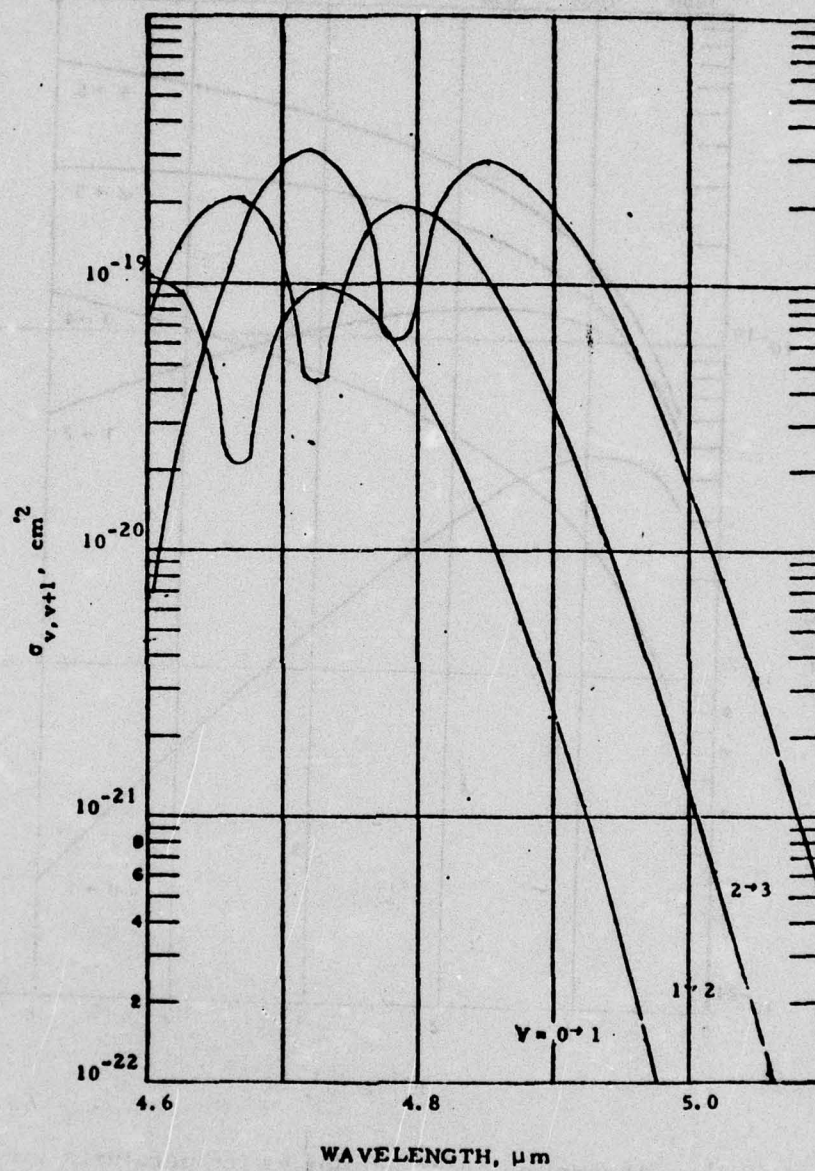


Fig. 13. Room temperature, high pressure absorption spectra of the $V = 0 \rightarrow 1$, $V = 1 \rightarrow 2$ and $V = 2 \rightarrow 3$ bands of CO.

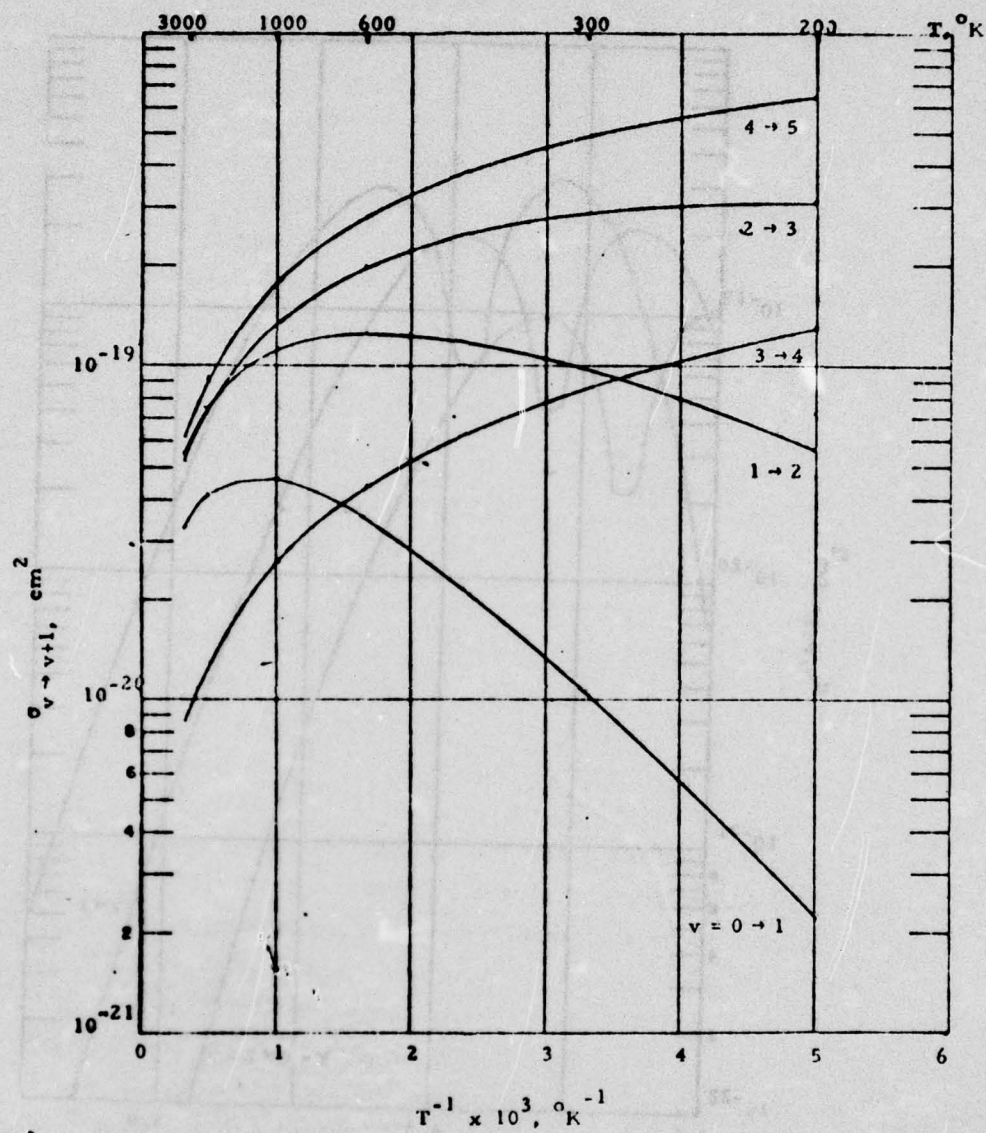


Fig. 14. Absorption cross section vs temperatures for the five lowest vibrational transitions in CO at a wavelength of $4.855 \mu\text{m}$.

Table 5. Apparent Absorption Coefficients of CO

ν (cm ⁻¹)	Apparent absorption coefficients (atm ⁻¹ cm ⁻¹)	ν (cm ⁻¹)	Apparent absorption coefficients (atm ⁻¹ cm ⁻¹)
R(18) 2210-0	0.86	R(10) 2184-2	1.06
2209-8	1.02	2184-0	2.08
2209-6	1.06	2183-8	3.61
2209-4	0.70	2183-6	5.10
R(17) 2207-0	1.00	2183-4	6.90
2206-8	1.72	2183-2	6.02
2206-6	1.88	2183-0	4.42
2206-4	2.04	2182-8	2.13
2206-2	1.48	2182-6	0.88
R(16) 2203-8	1.04	R(9) 2180-6	1.12
2203-6	1.80	2180-4	3.01
2203-4	2.60	2180-2	5.90
2203.2	2.60	2180-0	8.29
2203-0	1.40	2179-8	7.27
R(15) 2200-6	1.12	2179-6	5.46
2200-4	2.37	2179-4	2.85
2200-2	3.75	2179-2	0.96
2200-0	3.53	R(8) 2177-2	1.72
2199-8	2.25	2177-0	3.37
2199-6	1.52	2176-8	5.50
R(14) 2197-4	1.20	2176-6	7.23
2197-2	2.17	2176-4	8.68
2197-0	3.29	2176-2	7.27
2196-8	3.89	2176-0	4.98
2196-6	3.27	2175-8	2.41
2196-4	2.00	2175-6	1.04
2196-2	1.00	R(7) 2173-6	1.44
R(13) 2194-0	2.16	2173-4	3.77
2193-8	4.09	2173-2	5.90
2193-6	4.86	2173-0	8.65
2193-4	5.28	2172-8	7.87
2193-2	3.37	2172-6	5.98
2193-0	1.64	2172-4	3.37
2192-8	0.80	2172-2	1.88
R(12) 2191-0	1.24	2172-0	1.20
2190-8	2.13	R(6) 2170-4	0.92
2190-6	3.49	2170-2	1.28
2190-4	4.98	2170-0	2.45
2190-2	5.42	2169-8	4.70
2190-0	4.58	2169-6	6.79
2189-8	3.01	2169-4	8.45
2189-6	1.60	2169-2	7.99
R(11) 2187-4	1.48	2169-0	4.98
2187-2	3.37	2168-8	2.77
2187-0	5.06	2168-6	1.00
2186-8	6.05	R(5) 2166-6	1.96
2186-6	6.35	2166-4	2.29
2186-4	4.09	2166-2	4.70
2186-2	2.33	2166-0	6.75
2186-0	0.80	2165-8	7.85
		2165-6	6.27

Table 5. Apparent Absorption Coefficients of CO (Continued)

ν (cm ⁻¹)	Apparent absorption coefficients (atm ⁻¹ cm ⁻¹)	ν (cm ⁻¹)	Apparent absorption coefficients (atm ⁻¹ cm ⁻¹)
2165.4	4.22	P(3) 2132.4	0.92
2165.2	2.41	2132.2	2.45
2165.0	0.88	2132.0	3.61
R(4) 2163.0	1.16	2131.8	4.88
2162.8	2.29	2131.6	4.84
2162.6	3.65	2131.4	2.93
2162.4	5.46	2131.2	1.28
2162.2	7.07	P(4) 2128.2	2.00
2162.0	6.87	2128.0	3.60
2161.8	4.74	2127.8	4.94
2161.6	2.77	2127.6	5.48
2161.4	1.16	2127.4	4.09
R(3) 2159.2	1.04	2127.2	2.49
2159.0	2.81	2127.0	1.08
2158.8	4.78	P(5) 2124.4	1.36
2158.6	6.06	2124.2	2.65
2158.4	6.71	2124.0	4.62
2158.2	4.86	2123.8	8.37
2158.0	2.65	2123.6	6.18
2157.8	1.32	2123.4	4.74
R(2) 2155.4	1.92	2123.2	2.73
2155.2	3.81	2123.0	1.08
2155.0	5.22	P(6) 2120.4	1.16
2154.8	5.18	2120.2	2.89
2154.6	3.93	2120.0	5.06
2154.4	2.37	2119.8	6.70
2154.2	1.24	2119.6	6.85
R(1) 2151.6	2.13	2119.4	5.02
2151.4	2.33	2119.2	2.29
2151.2	3.17	2119.0	1.08
2151.0	3.43	P(7) 2116.4	1.20
2150.8	2.20	2116.2	2.25
2150.6	1.16	2116.0	4.30
R(0) 2147.6	0.96	2115.8	5.94
2147.4	1.64	2115.6	7.25
2147.2	1.80	2115.4	6.14
2147.0	1.56	2115.2	3.45
2146.8	1.08	2115.0	1.32
P(1) 2140.0	0.84	P(8) 2112.2	1.76
2139.8	1.20	2112.0	3.77
2139.6	1.56	2111.8	6.31
2139.4	1.48	2111.6	6.81
2139.2	0.76	2111.4	6.10
P(2) 2136.2	1.12	2111.2	4.50
2136.0	1.84	2111.0	2.13
2135.8	2.69	P(9) 2108.0	2.17
2135.6	3.05	2107.8	3.93
2135.4	2.73	2107.6	5.42
2135.2	1.56	2107.4	6.87

Table 5. Apparent Absorption Coefficients
of CO (Continued)

$\nu(\text{cm}^{-1})$	Apparent absorption coefficients ($\text{atm}^{-1} \text{cm}^{-1}$)	$\nu(\text{cm}^{-1})$	Apparent absorption coefficients ($\text{atm}^{-1} \text{cm}^{-1}$)
2107.2	6.74	2086.2	4.29
2107.0	3.89	2086.0	3.37
2106.8	1.80	2085.8	1.76
2106.6	1.28	2085.6	0.92
P(10) 2103.8	1.52	P(15) 2082.4	1.36
2103.6	3.13	2082.2	2.16
2103.4	5.14	2082.0	2.81
2103.2	6.08	2081.8	3.01
2103.0	5.26	2081.6	1.92
2102.8	3.33	2081.4	1.08
2102.6	2.00	P(16) 2078.0	1.56
2102.4	0.96	2077.8	2.74
P(11) 2099.6	1.60	2077.6	2.41
2099.4	3.37	2077.4	2.41
2099.2	5.54	2077.2	1.60
2099.0	6.22	2077.0	1.00
2098.8	5.30	P(17) 2073.6	0.92
2098.6	3.49	2073.4	1.60
2098.4	1.16	2073.2	2.00
P(12) 2095.4	1.56	2073.0	1.80
2095.2	2.81	2072.8	1.20
2095.0	4.13	P(18) 2069.4	0.88
2094.8	4.79	2069.2	1.01
2094.6	4.01	2069.0	1.22
2094.4	2.64	2068.8	1.51
2094.2	1.04	2068.6	1.32
P(13) 2091.0	1.60	2068.4	0.92
2090.8	3.09	P(19) 2064.6	1.04
2090.6	4.13	2064.4	1.36
2090.4	4.44	2064.2	1.36
2090.2	3.29	2064.0	1.08
2090.0	1.60	P(20) 2060.2	0.72
2089.8	0.84	2060.0	1.00
P(14) 2086.8	1.12	2059.8	1.04
2086.6	2.29	2059.6	1.10
2086.4	3.69	2059.4	0.68

$$g(v - v') = \begin{cases} \frac{\pi}{3.704 \delta v} \frac{\sin x}{x} & \text{for } |x| \leq \pi \\ 0 & \text{for } |x| > \pi \end{cases}, \quad (19)$$

where

$$x = \frac{\pi}{\delta v} (v - v') \quad (20)$$

Then, their absorption coefficient, which shall be labeled as $\hat{k}(v)$, is given by the relation,

$$\bar{k}_{T_0}(v) = \int_{-\infty}^{\infty} \hat{k}_{T_0}(v) g(v - v') dv' \quad (21)$$

For a conceptual isolated line at v_0 , Eq. (21) becomes

$$\bar{k}_{T_0}(v) = \hat{S}_{T_0}^i(v_0) \int_{-\infty}^{\infty} f(v_0, v) g(v - v') dv' \quad (21a)$$

3.4 NO AS AN ABSORBER FOR CO LASER RADIATION

It is evident from band model absorption data presented both by Caledonia, et al. (1975), and by Ludwig, et al. (1973) that NO might prove to be a fairly effective absorber, particularly when heated and at high pressures, of selected CO laser line radiation. Figure 15 is Caledonia, et al.'s Figure 3-6. It is a band model representation of smoothed-out NO absorption by the $v'' = 0 \rightarrow v' = 1$ and $v'' = 1 \rightarrow v' = 2$ bands, with superimposed positions of three selected CO laser lines. Again, the σ cross-sections shown for the smeared out NO absorption, like those for their CO absorption is not per $v''J''$ molecule, but for all v'' molecules assuming rotational relaxation at $T_R = 300^\circ\text{K}$. The mean line separation \bar{d} is of the order of $\sim 3.5 \text{ cm}^{-1}$ near the center of the $0 \rightarrow 1$ band at low temperatures, as compared to $\sim 3.9 \text{ cm}^{-1}$ for CO. The peak absorption coefficients for NO are approximately 40 to 70% of those for CO, and shifted to lower wavenumber positions so, as is evident from Figure 15, the fundamental $v'' = 0 \rightarrow v' = 1$ NO band will tend to absorb spectral lines radiated by CO $\Delta v = 1$ spectral lines with $v' = 8, 9$ and 10 . Near 3000°K , however, NO will exhibit a \bar{k} absorption coefficient of $\sim 10^{-1} (\text{atm-cm})^{-1}$ for $1950 \sim 1600 \text{ cm}^{-1}$, which includes many of the strongest CO laser lines. This can be seen from Figure 16, which is reproduced from Ludwig, et al.'s Figure 5-4. Also, from Figure 17 (Ludwig, et al.'s Figure 5-5), it can be seen that at high temperatures, the effective number of NO lines contributing to absorption is approximately 2 or 3 times that of corresponding CO lines, thus improving the quasi-continuum absorption approximation.

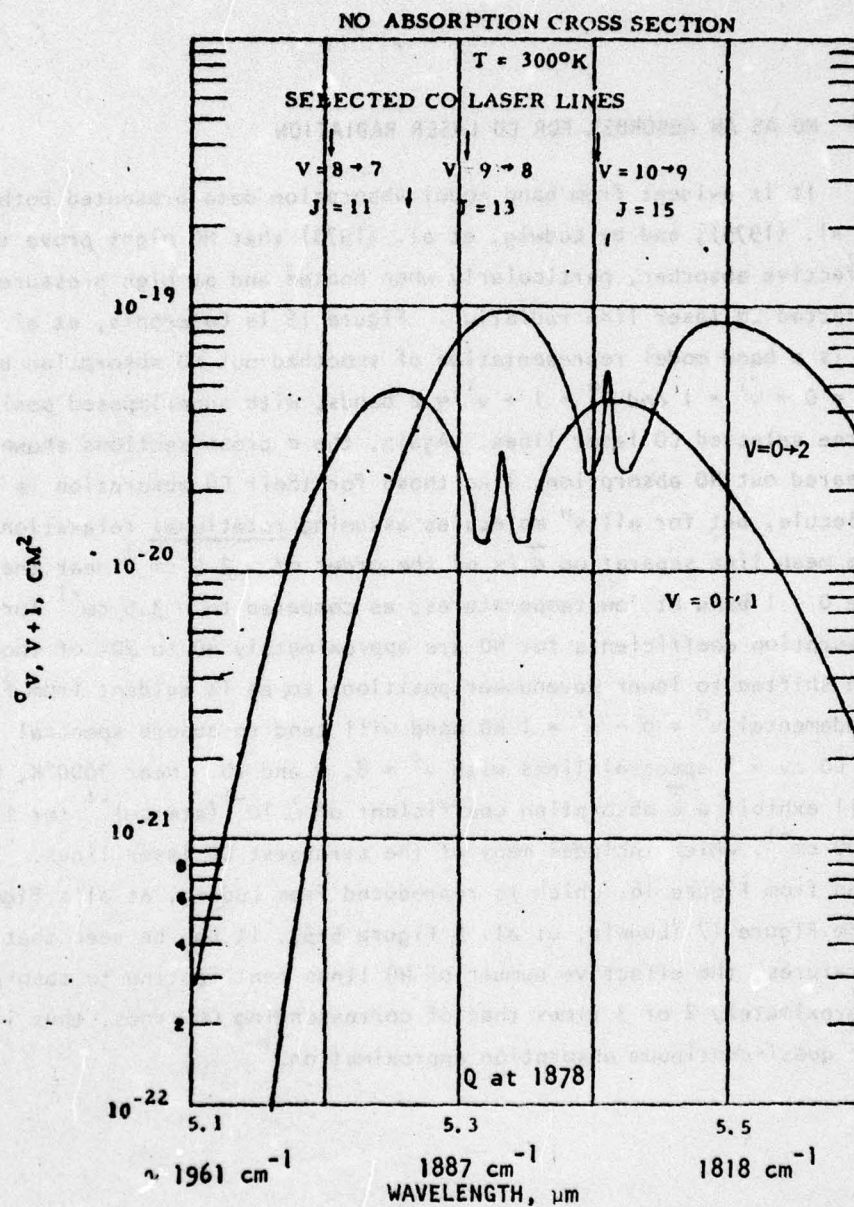


Fig. 15. Room temperature high pressure absorption spectra of the $V = 0 \rightarrow 1$, $V = 1 \rightarrow 2$ bands of NO.

AD-A035 061

TRW DEFENSE AND SPACE SYSTEMS GROUP REDONDO BEACH CALIF F/G 21/8.1
INVESTIGATION OF BEAMED ENERGY CONCEPTS FOR PROPULSION. LASER/P--ETC(U)
OCT 76 M HUBERMAN, J M SELLEN, R BENSON F04611-76-C-0003

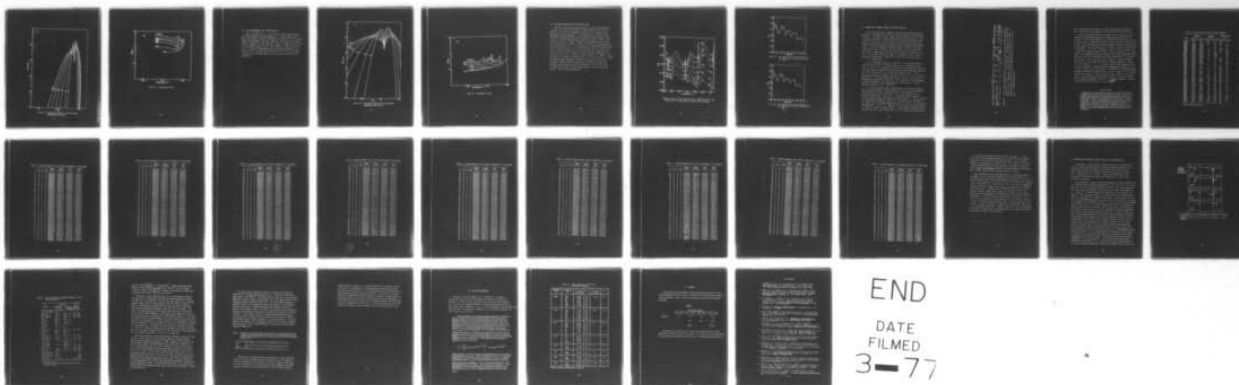
UNCLASSIFIED

AFRPL-TR-76-66-VOL-2

NL

2 OF 2

AD
A035061



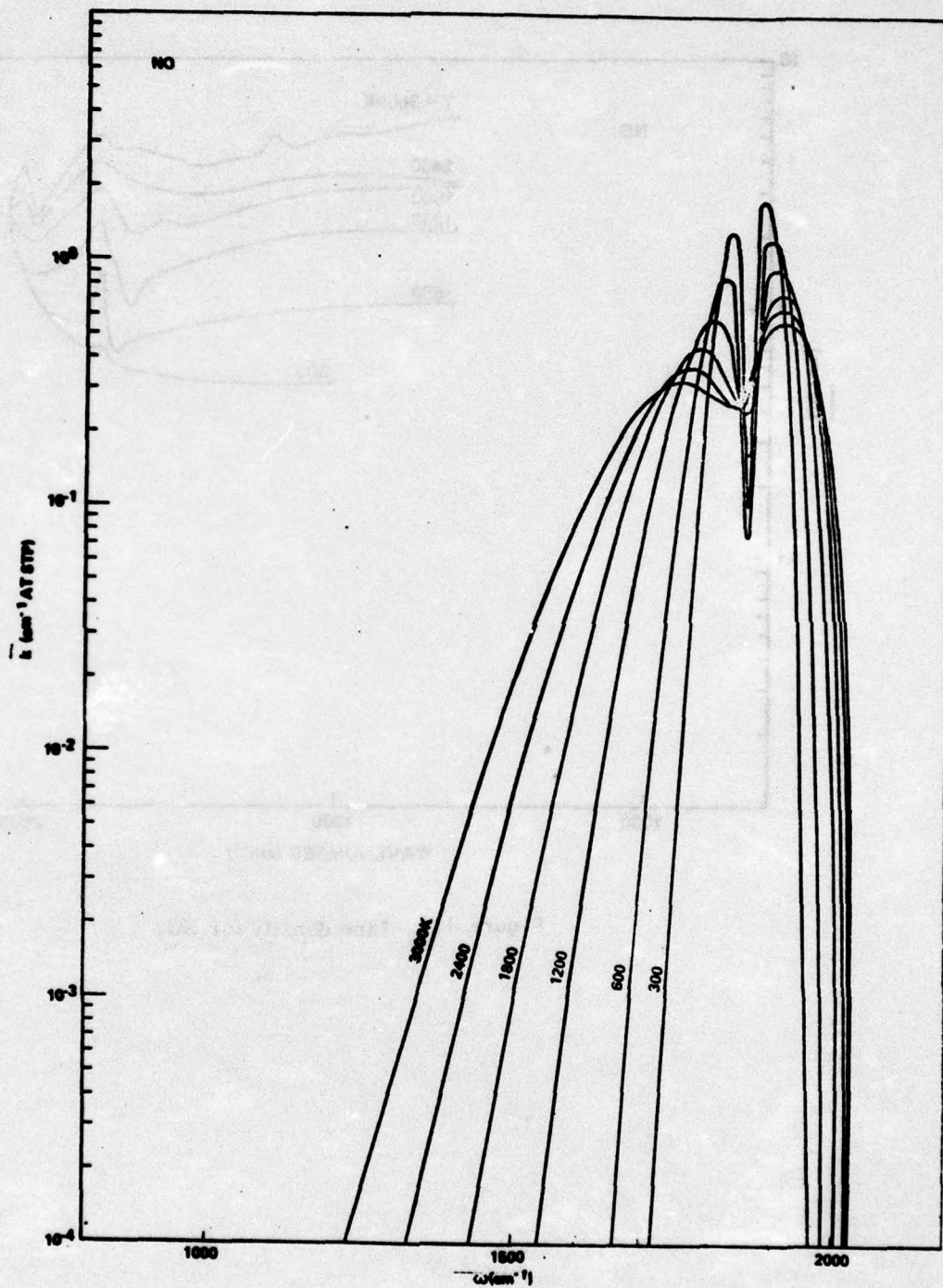


Figure 16. Absorption coefficient for NO at standard temperature and pressure.

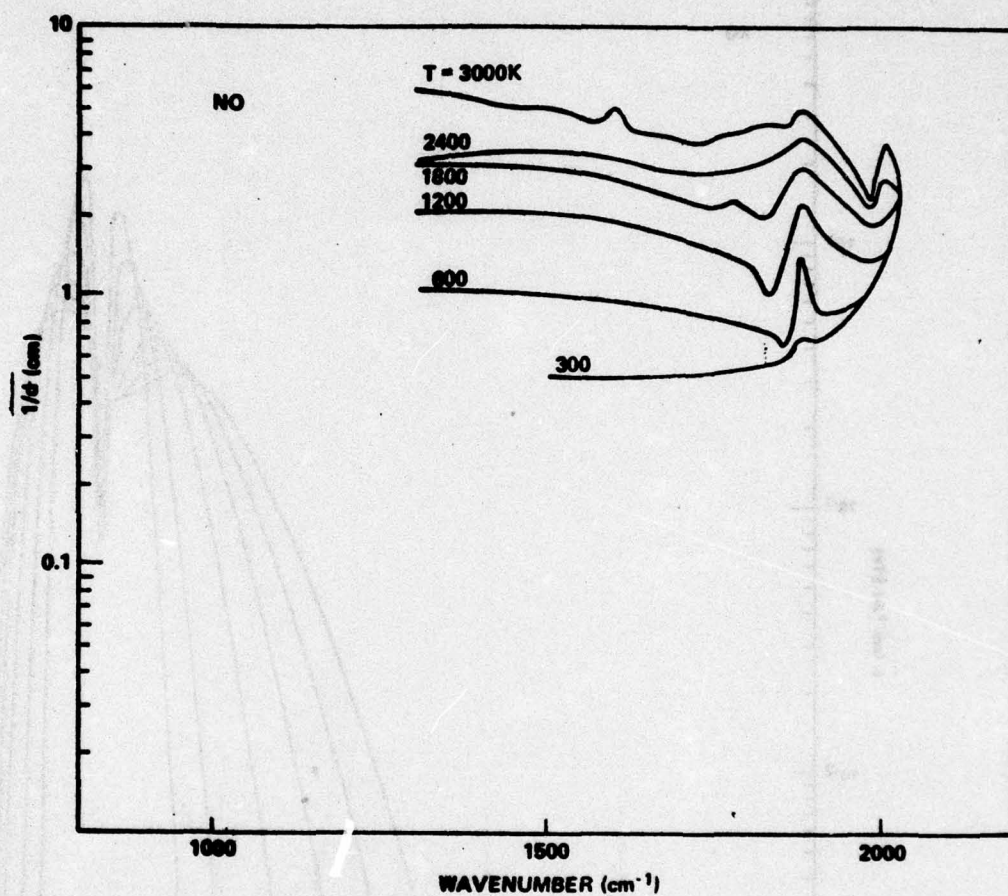


Figure 17. Line density for NO.

3.5 OH AS AN ABSORBER FOR HF LASER RADIATION

Figure 18 (Ludwig, et al.'s Figure 5-8) gives band model absorption for the OH radical at selected temperatures. It might appear at first glance that with \bar{k}_{T_0} values of the order of $10^{-1}(\text{atmos cm})^{-1}$ over a broad spectral range between ~ 3200 and $\sim 3800 \text{ cm}^{-1}$, that OH possibly might be a useful absorber of HF laser radiation. However, the mole fraction of the OH radical would probably be low in most reactions. Figure 19 (Ludwig, et al.'s Figure 5-9) shows effective line separation distance \bar{d}_v of the order of 10 cm^{-1} near 600°K but reducing to ~ 2.5 to $\sim 1 \text{ cm}^{-1}$ at 3000°K . It appears the OH would be useful, if at all, only at relatively high temperatures.

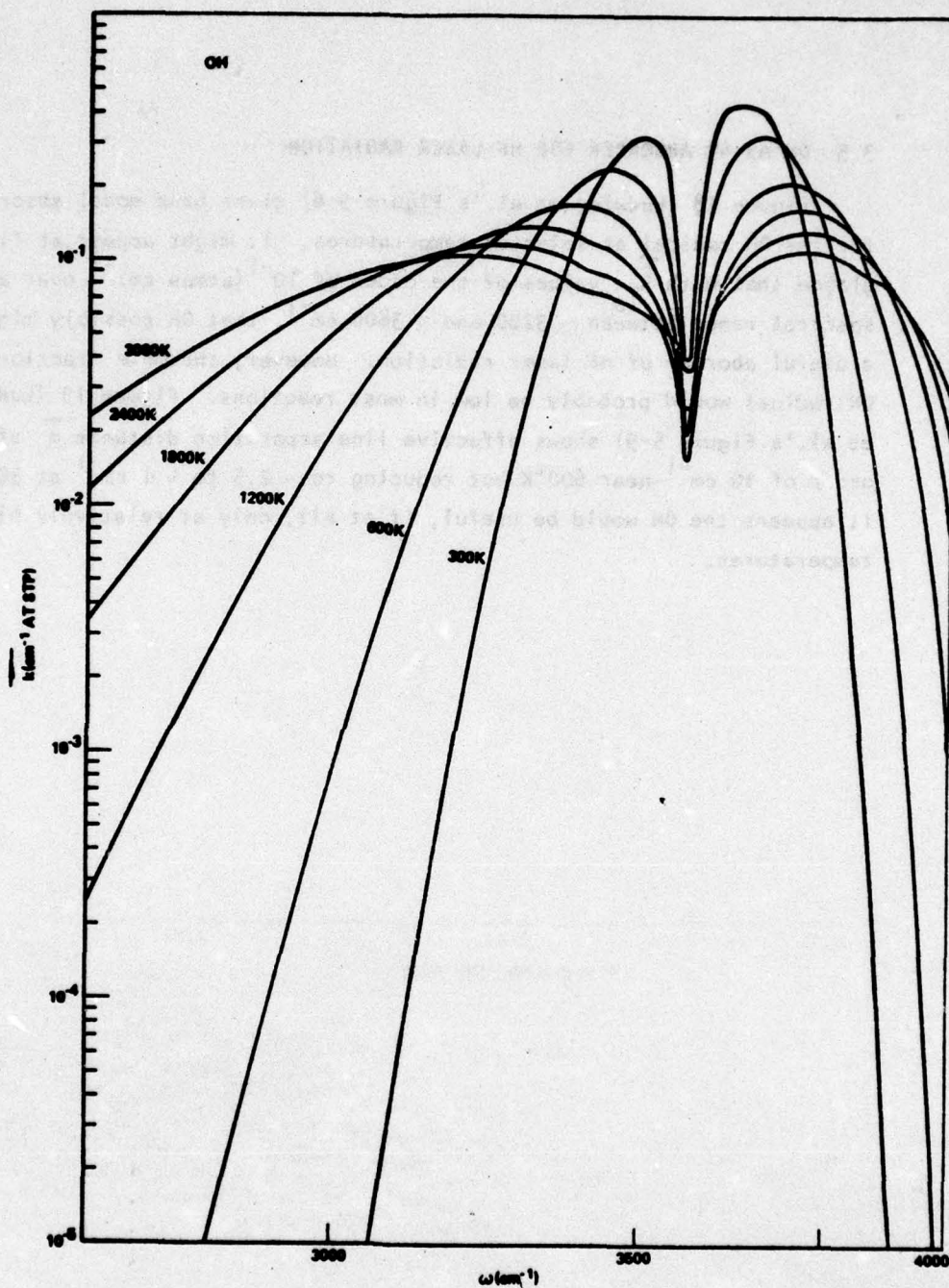


Figure 18. Absorption coefficient for OH at standard temperature and pressure.

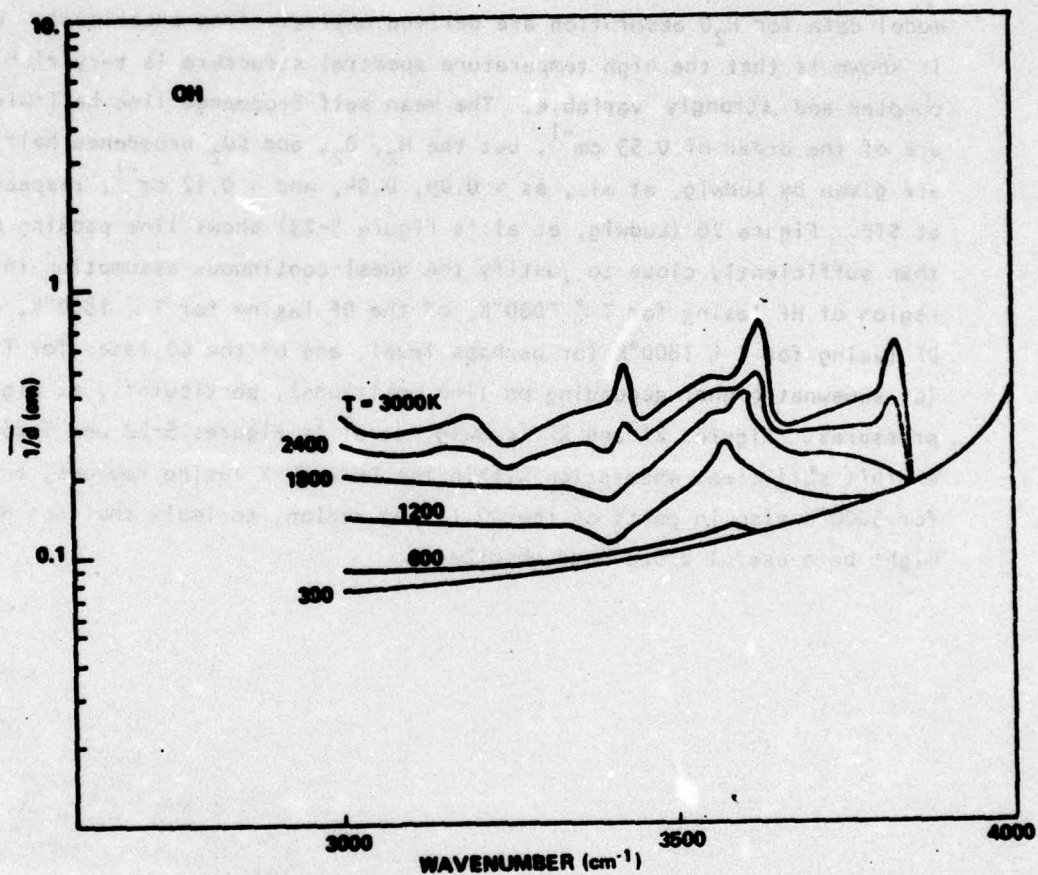


Figure 19. Line density for OH.

3.6 BAND MODEL ABSORPTION FOR WATER VAPOR (H_2O)

Line-by-line calculations have been made for H_2O at low temperatures ($\sim 300^\circ K$), but an accurate extension of these calculations to higher temperatures of the order of thousands of degrees Kelvin is beyond current knowledge of the H_2O parameters. At the present time, all existing band model data for H_2O absorption are derived entirely from experiment. What is known is that the high temperature spectral structure is very rich and complex and strongly variable. The mean self-broadened line half-widths are of the order of 0.53 cm^{-1} , but the N_2 , O_2 , and CO_2 broadened half-widths are given by Ludwig, et al., as ~ 0.09 , 0.04 , and $\sim 0.12 \text{ cm}^{-1}$, respectively, at STP. Figure 20 (Ludwig, et al.'s Figure 5-23) shows line packing more than sufficiently close to justify the quasi-continuous assumption in the region of HF lasing for $T \gtrsim 2000^\circ K$, of the DF lasing for $T \gtrsim 1800^\circ K$, of the DF lasing for $T \gtrsim 1800^\circ K$ (or perhaps less), and of the CO laser for $T \gtrsim 2000^\circ K$ (or somewhat higher depending on line positions), particularly at high pressures. Figures 21 and 22 (Ludwig, et al.'s Figures 5-22 and 5-23) exhibit sufficient absorption within the DF and HF lasing regions, and for $3000^\circ K$ also in parts of the CO lasing region, to imply that hot H_2O might be a useful broad band absorber.

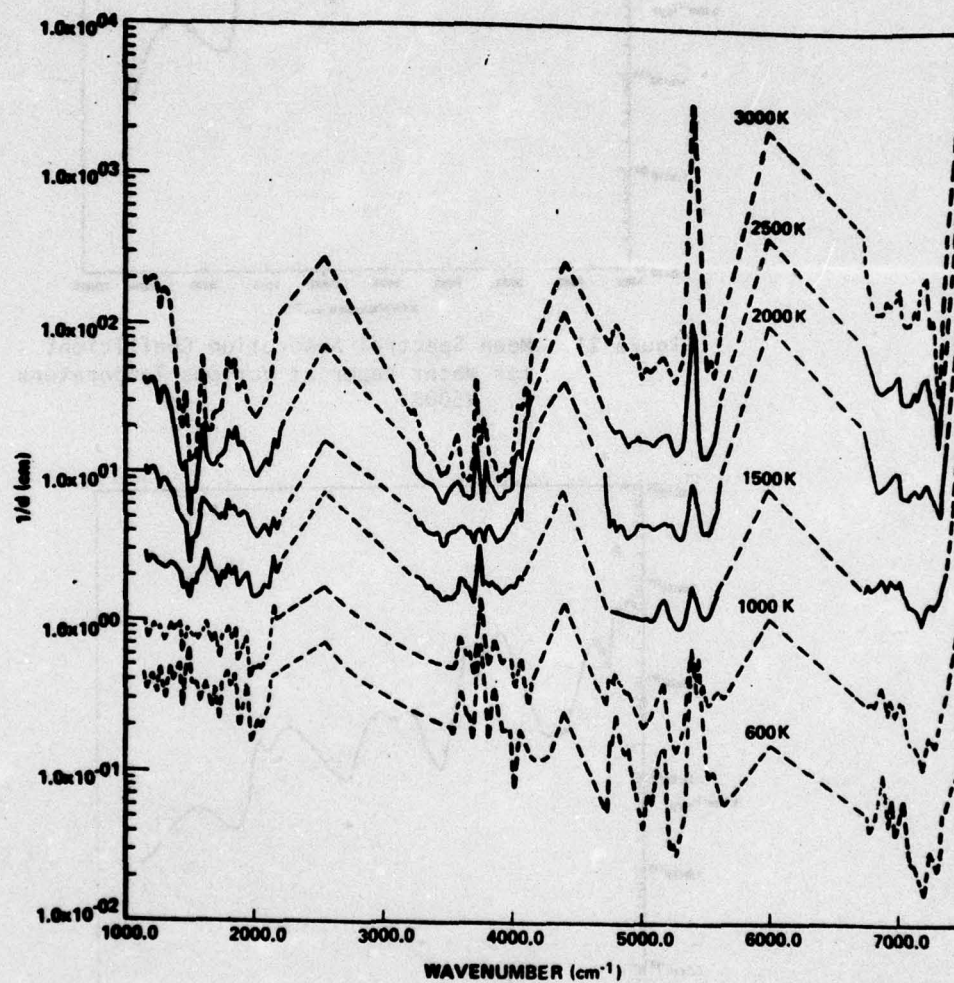


Figure 20. Plot of $(1/d)$ for H_2O versus ω between 1150 cm^{-1} and 7500 cm^{-1} for $T = 600, 1000, 1500, 2000, 2500, \text{ and } 3000 \text{ K}$.

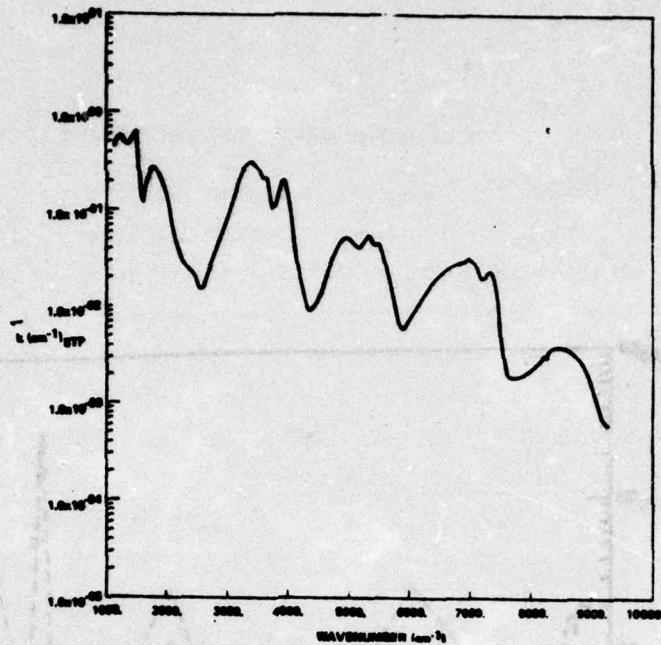


Figure 21. Mean Spectral Absorption Coefficient
for Water Vapor at Various Temperature
f. 2500K.

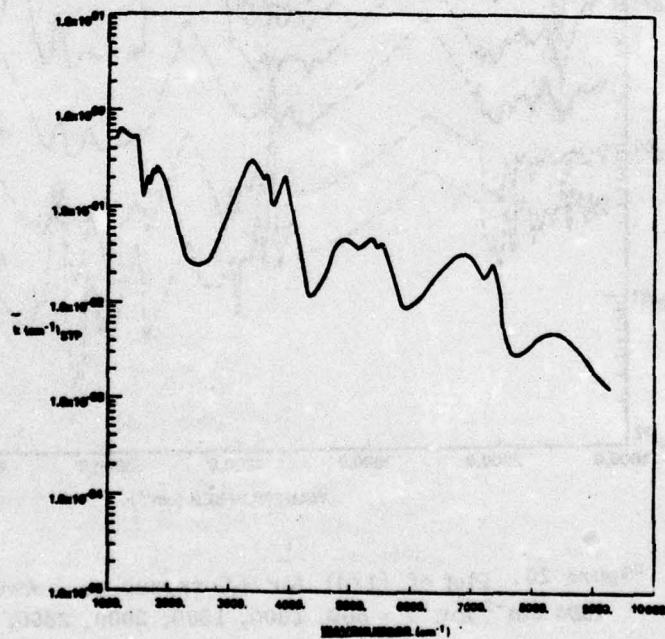


Figure 22. Mean Spectral Absorption Coefficient
for Water Vapor at Various Temperatures
g. 3000K

3.7 ABSORPTION BY AMMONIA (NH_3) OF CO_2 LASER RADIATION

The spectral absorption of ammonia, NH_3 , has been studied extensively owing to its importance as the principal infrared absorber in the atmosphere of Jupiter. The spectra of NH_3 is complicated by inversion doubling. That is, every energy level is split because the molecule has two stable configurations of the N-atom, one on either side of the H_3 -plane, and these have slightly different energies which depend upon the rotational quantum numbers J and K . While the fundamental inversion frequency (measured in the microwave region) is only $\sim 0.8 \text{ cm}^{-1}$, the energy levels for the configurations tend to split increasingly further apart with increasing vibrational excitation. The two levels labeled as s and a (or sometimes as $+$ and $-$) have ν_{00} band centers separated by $\sim 35.6 \text{ cm}^{-1}$ for the s and a sub-levels of the ν_2 or $(0\ 1\ 0\ 0)$ energy level.

The ν_2 band complex centered on $\sim 950 \text{ cm}^{-1}$ or $\sim 10.5\mu$ and originating in transitions from the $(0\ 0\ 0\ 0)$ ground states to the corresponding s and a levels of the $(0\ 1\ 0\ 0)$ vibrational state exhibits the strongest NH_3 absorption. The integrated band strength for this band complex has been variously measured as $\sim (560 \pm 30) (\text{atm cm})^{-1} \text{ cm}^{-1}$ to $(790 \pm 30) (\text{atm cm})^{-1} \text{ cm}^{-1}$. This is appreciably stronger, for example, than the $\sim 260 (\text{atm cm}^{-1}) \text{ cm}^{-1}$ for the CO fundamental $(0 \rightarrow 1)$ band centered near 2143 cm^{-1} , or the $\sim 132 (\text{atm cm}^{-1}) \text{ cm}^{-1}$ NO fundamental centered near 1876 cm^{-1} , or the $\sim 450 (\text{atm cm})^{-1}$ HF fundamental centered near 3962 cm^{-1} , but weaker than the $\sim 2700 (\text{atm cm})^{-1} \text{ cm}^{-1}$ CO_2 absorption region near 4.3μ ($\sim 2350 \text{ cm}^{-1}$).

It will be seen that the $\text{NH}_3 \nu_2$ band complex is excellently situated to absorb CO_2 laser radiation. Figure 23 [Figure 127 from G. Herzberg (1945)] shows a small part of the structure of the $\text{NH}_3 \nu_2$ band complex with an estimated resolution of ~ 1 or 2 cm^{-1} . It can be seen that the spectral interval covered overlaps that of both the strong $\text{CO}_2 (0\ 0^0\ 1) \rightarrow (0\ 0^0\ 1, 0\ 2^0\ 0)_1$ lines [extending from 1000 to $\sim 962 \text{ cm}^{-1}$ for the R-branch, and from $\sim 956 \text{ cm}^{-1}$ to $\sim 900 \text{ cm}^{-1}$ for the stronger P-branch] and $(0\ 0^0\ 1) \rightarrow (0\ 0^0\ 1, 0\ 2^0\ 0)_{11}$ lines [extending from $\sim 1100 \text{ cm}^{-1}$ to $\sim 1066 \text{ cm}^{-1}$ for the R branch, and from $\sim 1060 \text{ cm}^{-1}$ to $\sim 1000 \text{ cm}^{-1}$ for the stronger P branch]. In particular, the strong P-branch lines of the former l-type, transitions will fall on the very closely packed

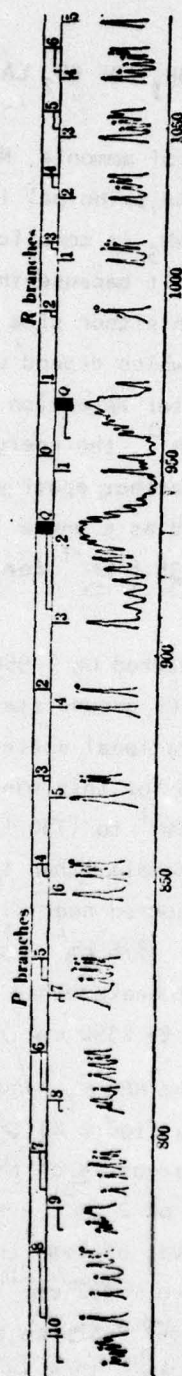


Figure 23. Fine Structure of the fundamental ν_2 of NH_3 at 10.5μ . At the top the two component bands $\nu_2 (1^+ - 0^-)$ and $\nu_2 (1^- - 0^+)$ are indicated. The numbers on the leading lines are the J values. The numbers directly above some of the maxima are K values. It should be noted that the lines P(1) and R(0) are missing in the $\nu_2 (1^+ - 0^-)$ and $\nu_2 (1^- - 0^+)$ bands respectively.

lower frequency Q-branch of NH_3 . The total integrated line strength for each of the two NH_3 ν_2 Q-branches is of the order of $120 \text{ (atm cm)}^{-1} \text{ cm}^{-1}$.

The old spectrogram reproduced in Figure 23 fails to give more than a vague hint of the actual complexity of the NH_3 spectral activity in its ν_2 region. A more recent report by F. W. Taylor [March 1973] presents data on the positions, integrated line intensities [\hat{S}_T' in units of $(\text{atm cm})^{-1} \text{ cm}^{-1}$ at 300°K , referred to total NH_3 population rather than lower state population] self-broadened line width factors a_0 in $\text{cm}^{-1} \text{ atm}^{-1}$, and lower state energies in wavenumbers. This data is tabulated, in Taylor's Table 2 and Table 3 for ~ 1700 of the strongest spectral lines in the ν_2 and overlapping $2\nu_2$ region. Table 6 is a reproduction of Taylor's Table 2, while Table 7 reproduces that portion of his Table 4 extending from 1140.76 to 888.108 cm^{-1} . A paragraph listing Taylor's key to his Table 4 (i.e., Table 7) is reproduced below. Note, however, that although his wording is somewhat ambiguous, he intends his ΔJ to symbolize $\{2 + J' - J''\}$, and that he really means lower state when he says ground state. Although he fails to explicitly so state anywhere in his text, it appears from the context that he intends his "Strength" parameter to represent what we have labeled as \hat{S}_T' , in units of $(\text{atm cm})^{-1} \text{ cm}^{-1}$ for NH_3 molecules distributed in thermal equilibrium at $T_0 = 300^\circ\text{K}$ in all possible states. Also presumably, although again not explicitly stated, it appears that his $(\text{NH}_3\text{-NH}_3 \text{ broadened})$ width in cm^{-1} is really intended to represent the parameter I have called a_0 , with $a_c \approx a_0 P \sqrt{\frac{300^\circ\text{K}}{T}}$.

Key to Table 7.

Table 7 lists the ν_2 band parameters. All lines with J -values up to 23 were included in the computation, but those with intensities less than $10^{-5} \text{ cm}^{-2} \text{ atm}^{-1}$ do not appear in the table. The headings to the columns have the following meanings: J and K are the rotational quantum numbers in the conventional notation; ΔJ is equal to the change in $J+2$, so that $\Delta J = 1$ refers to the P -branch and so on; SYM is 1 for an $s \rightarrow a$ transition and 0 for an $a \rightarrow s$ transition in the fundamental band, and 2 and 3 respectively for these transitions in the overtone band; FREQUENCY is the frequency in wavenumbers (cm^{-1}) at the line center; STRENGTH is the strength or intensity of the line in $\text{cm}^{-2} \text{ atm}^{-1}$; WIDTH is the half width at half-maximum in cm^{-1} ; ENERGY is the energy of the ground state in cm^{-1} for use in computing the Boltzmann term in the dependence of the line strength on temperature.

Table 6. Spectral Data for the ν_2 Bands of Ammonia

Transition	Wavenumber cm^{-1}		Intensity $\text{cm}^{-2} \text{atm}^{-1}$		Width* ($\text{NH}_3\text{-NH}_3$) cm^{-1}	
	Measured	Calculated	Measured	Calculated	Measured	Calculated
$aQ(J,K)$	935	935	120	118	0.40	—
$sQ(J,K)$	965	965	120	117	0.40	—
$aR(2,2)$	991.68	991.69	2.7	2.6	0.51	0.52
$aR(2,1)$	992.70	992.46	13	8.6	—	0.27
$aR(2,0)$	992.70	992.71		3.9	—	0.27
$sR(1,K)$	1007.55	1007.53	10.3	10.8	0.40	—
$aR(3,3)$	1011.20	1011.20	4.8	4.5	0.54	0.56
$aR(3,2)$	1012.44	1012.46	4.0	3.5	0.47	0.45
$aR(3,1)$	1013.17	1013.21	4.0	4.2	0.35	0.35
$2sR(3,0)$	1022.80	1022.79	0.15	0.093	—	0.25
$2sR(3,1)$	1023.2	1023.23		0.044	—	0.35
$2sR(3,2)$	1024.57	1024.56	0.06	0.04	—	0.45
$2sR(3,3)$	1026.84	1026.83	6.7	0.05	—	0.55
$sR(2,K)$	1027.04	1027.04		6.69	0.40	—
$aR(4,4)$	1030.43	1030.41	2.0	1.8	0.55	0.57
$aR(4,3)$	1032.13	1032.15	6.0	5.7	0.50	0.49
$aR(4,2)$	1033.32	1033.36	3.5	3.4	0.40	0.40
$aR(4,1)$	1034.03	1034.07	12	3.7	—	0.32
$aR(4,0)$	1034.23	1034.31		7.6	—	0.23
$sR(3,K)$	1046.40	—	22	22.1	0.40	—
$aR(5,5)$	1049.34	1049.33	1.4	1.4	0.54	0.58
$aR(5,4)$	1051.51	1051.54	2.1	2.2	0.50	0.51
$aR(5,3)$	1053.13	1053.19	5.0	5.1	0.43	0.44
$sR(4,K)$	1065.57	—	14.8	15.3	0.40	—
$aR(6,6)$	1067.96	1067.94	2.0	1.9	0.55	0.58
$aR(6,5)$	1070.59	1070.61	1.4	1.5	0.50	0.52
$aR(6,4)$	1072.64	1072.69	1.6	1.7	0.45	0.46
$aR(6,3)$	1074.14	1074.25	3.8	3.7	0.40	0.40
$sR(5,K)$	1084.62	—	20.0	20.0	0.40	—
$aR(7,7)$	1086.31	1086.25	0.57	0.63	0.55	0.56
$aR(7,6)$	1089.42	1089.38	1.84	1.89	0.50	0.52
$aR(7,5)$	1091.87	1091.88	1.04	1.08	0.44	0.47
$aR(7,4)$	1093.76	1093.82	1.1	1.1	0.40	0.42
$aR(7,3)$	1095.15	1095.27	2.3	2.3	0.35	0.37
$sR(6,K)$	1103.46	—	12.4	13.0	0.40	—
$aR(8,8)$	1104.33	1104.24	0.33	0.40	—	0.57
$aR(8,7)$	1107.85	1107.84	0.57	0.57	0.50	0.52
$aR(8,6)$	1110.69	1110.75	1.19	1.27	0.45	0.48
$aR(8,5)$	1112.96	1113.07	0.69	0.65	0.41	0.43
$aR(8,4)$	1114.71	1114.85	0.62	0.64	0.36	0.39
$aR(8,3)$	1116.03	1116.19	1.14	1.26	0.31	0.34
$sR(7,K)$	1122.14	—	11.5	11.7	0.4	—
$aR(9,8)$	1126.02	1126.00	0.32	0.33	0.54	0.52
$aR(9,7)$	1129.25	1129.32	0.37	0.35	0.49	0.48
$aR(9,6)$	1131.86	1131.99	0.61	0.71	0.45	0.44
$aR(9,5)$	1133.94	1134.09	0.39	0.34	0.42	0.39
$aR(9,4)$	1135.53	1135.72	0.39	0.32	0.36	0.36
$aR(9,3)$	1136.76	1136.92	0.62	0.62	0.29	0.31
$aR(10,10)$	1139.45	1139.28	0.13	0.13	—	0.53
$sR(8,K)$	1140.65	—	6.2	6.2	0.40	—

* "Width" means half width at half intensity.

Table 7. V_2 Band Parameters from 1140.76 to 88.108 cm^{-1}

J	ΔJ	K	I Sym	Frequency (cm^{-1})	Strength ($\text{cm}^{-2} \text{atm}^{-1}$)	Width (cm^{-1})	Energy (cm^{-1})
8	3	3	1	.114076+04	.129051+01	.347828+00	.678938+03
8	3	4	1	.114072+04	.660172+00	.391784+00	.643291+03
8	3	8	1	.114071+04	.411626+00	.567607+00	.675275+03
8	3	5	1	.114068+04	.668432+00	.435739+00	.670198+03
8	3	7	1	.114066+04	.589413+00	.523651+00	.631308+03
8	3	6	1	.114066+04	.130981+01	.479695+00	.679573+03
10	3	6	3	.113966+04	.337975+02	.387326+00	.188976+04
10	3	10	0	.113928+04	.127124+00	.532516+00	.718073+03
9	3	8	3	.113854+04	.355949+02	.515267+00	.158040+04
9	3	1	0	.113822+04	.291153+00	.278979+00	.885270+03
9	3	2	0	.113774+04	.297561+00	.278449+00	.874418+03
9	3	3	0	.113692+04	.615836+00	.317918+00	.856299+03
10	3	5	3	.113585+04	.154659+02	.351028+00	.103215+04
9	3	4	0	.113572+04	.321455+00	.357388+00	.870866+03
9	3	5	0	.113409+04	.336381+00	.396858+00	.708052+03
10	3	4	3	.113293+04	.142614+02	.314731+00	.106658+04
9	3	6	0	.113199+04	.697506+00	.436328+00	.757772+03
9	3	7	3	.113196+04	.374903+02	.475707+00	.163093+04
10	3	3	3	.113079+04	.266644+02	.275433+00	.109322+04
10	3	2	3	.112933+04	.126808+02	.242135+00	.201216+04
9	3	7	0	.112932+04	.350191+00	.475797+00	.770021+03
10	3	1	3	.112849+04	.122967+02	.205838+00	.202349+04
9	3	6	3	.112666+04	.729765+02	.436328+00	.169102+04
8	3	8	3	.112619+04	.446122+02	.567607+00	.129070+04
9	3	8	0	.112600+04	.323209+00	.515267+00	.654379+03
9	3	5	3	.112248+04	.345540+02	.396858+00	.173380+04
7	3	0	1	.112232+04	.233137+01	.223074+00	.654344+03
7	3	1	1	.112231+04	.116818+01	.273362+00	.650676+03
7	3	2	1	.112229+04	.117396+01	.323649+00	.630663+03
7	3	3	1	.112226+04	.235426+01	.373936+00	.621276+03
7	3	4	1	.112222+04	.116518+01	.424274+00	.605466+03
7	3	5	1	.112218+04	.111375+01	.474511+00	.662165+03
7	3	7	1	.112217+04	.662328+00	.575086+00	.372715+03
7	3	6	1	.112216+04	.195232+01	.524798+00	.621283+03
9	3	9	0	.112192+04	.463143+00	.554737+00	.691005+03
9	3	4	3	.111927+04	.325552+02	.357388+00	.176873+04
8	3	7	3	.111915+04	.622222+02	.523651+00	.145082+04
8	3	0	0	.111781+04	.120887+01	.215261+00	.712300+03
8	3	1	0	.111764+04	.607574+00	.259916+00	.708660+03
8	3	2	0	.111710+04	.616534+00	.303872+00	.697730+03
9	3	3	3	.111689+04	.617113+02	.317018+00	.179567+04
8	3	3	0	.111619+04	.125935+01	.347828+00	.679683+03
9	3	2	3	.111527+04	.296706+02	.278449+00	.181483+04
8	3	4	0	.111486+04	.643381+00	.391784+00	.653870+03
9	3	1	3	.111432+04	.288394+02	.238979+00	.182610+04
9	3	0	3	.111401+04	.571699+02	.199509+00	.183011+04
8	3	6	3	.111346+04	.135328+01	.479695+00	.151143+04
8	3	5	0	.111307+04	.650256+00	.435739+00	.620826+03
8	3	6	0	.111075+04	.127118+01	.479695+00	.680264+03
8	3	5	3	.110895+04	.678779+02	.435739+00	.155474+04
8	3	7	0	.110784+04	.570223+00	.523651+00	.632082+03
7	3	7	3	.110595+04	.710095+02	.575086+00	.120015+04
8	3	4	3	.110547+04	.661398+02	.391784+00	.158003+04
8	3	8	0	.110424+04	.396748+00	.567607+00	.676160+03
6	3	1	1	.110362+04	.196204+01	.284078+00	.612566+03
6	3	2	1	.110359+04	.194152+01	.343024+00	.601472+03
6	3	3	1	.110356+04	.377740+01	.402070+00	.382083+03
6	3	4	1	.110352+04	.176851+01	.461016+00	.367030+03
6	3	5	1	.110348+04	.151448+01	.520011+00	.323545+03

Table 7. V_2 Band Parameters from 1140.76 to 88.108 cm^{-1} (Continued)

J	ΔJ	K	I Sym	Frequency (cm^{-1})	Strength ($\text{cm}^{-2} \text{atm}^{-1}$)	Width (cm^{-1})	Energy (cm^{-1})
6	3	6	1	.110346+04	.200512+01	.579007+00	.282440+03
8	3	3	3	.110289+04	.127991-01	.367828+00	.161715+04
8	3	2	3	.110111+04	.621658-02	.303872+00	.163651+04
8	3	1	3	.110007+04	.609787-02	.259916+00	.164810+04
7	3	6	3	.109992+04	.204465-01	.524708+00	.135121+04
7	3	1	0	.109686+04	.113856+01	.273162+00	.551238+03
7	3	2	0	.109627+04	.114352+01	.323649+00	.540240+03
7	3	3	0	.109527+04	.229090+01	.373036+00	.521879+03
7	3	5	3	.109512+04	.114537-01	.674511+00	.139491+04
7	3	4	0	.109382+04	.113215+01	.424224+00	.696107+03
7	3	5	0	.109188+04	.108001+01	.474511+00	.462859+03
7	3	4	3	.109140+04	.118119-01	.424224+00	.143042+04
7	3	6	0	.108938+04	.188823+01	.524798+00	.422748+03
7	3	3	3	.108863+04	.236115-01	.373036+00	.145789+04
7	3	2	3	.108672+04	.116866-01	.323649+00	.147743+04
7	3	7	0	.108625+04	.638929+00	.575086+00	.373573+03
6	3	6	3	.108591+04	.212697-01	.579007+00	.121058+04
7	3	1	3	.108560+04	.115782-01	.273162+00	.148012+04
7	3	0	3	.108523+04	.230735-01	.223074+00	.149301+04
5	3	0	1	.108474+04	.591143+01	.226013+00	.297601+03
5	3	1	1	.108474+04	.292603+01	.296626+00	.293895+03
5	3	2	1	.108471+04	.282444+01	.367239+00	.282769+03
5	3	3	1	.108467+04	.521835+01	.437852+00	.264193+03
5	3	4	1	.108463+04	.219492+01	.508466+00	.238118+03
5	3	5	1	.108459+04	.142256+01	.579079+00	.274476+03
6	3	5	3	.108086+04	.157607-01	.520011+00	.125462+04
6	3	4	3	.107693+04	.181301-01	.461016+00	.129041+04
6	3	0	0	.107617+04	.382515+01	.225032+00	.416842+03
6	3	1	0	.107596+04	.190715+01	.284029+00	.413150+03
6	3	2	0	.107533+04	.188599+01	.363024+00	.402102+03
6	3	3	0	.107425+04	.366527+01	.402020+00	.383641+03
6	3	3	3	.107400+04	.382700-01	.402020+00	.131809+04
6	3	4	0	.107269+04	.171325+01	.461016+00	.357730+03
6	3	2	3	.107197+04	.195266-01	.363024+00	.133778+04
6	3	1	3	.107079+04	.196421-01	.284028+00	.134957+04
6	3	5	0	.107061+04	.146394+01	.520011+00	.324303+03
5	3	6	0	.106794+04	.193268+01	.579007+00	.283276+03
5	3	5	3	.106606+04	.149666-01	.579079+00	.113404+04
4	3	1	1	.106568+04	.383387+01	.315869+00	.194842+03
4	3	2	1	.106565+04	.354249+01	.401540+00	.183673+03
4	3	3	1	.106561+04	.491219+01	.487211+00	.165024+03
4	3	4	1	.106556+04	.188931+01	.572881+00	.132847+03
5	3	4	3	.106195+04	.227241-01	.508466+00	.117007+04
5	3	3	3	.105888+04	.534172-01	.437852+00	.119703+04
5	3	2	3	.105676+04	.286762-01	.367239+00	.121776+04
5	3	1	3	.105551+04	.295644-01	.296626+00	.122962+04
5	3	0	3	.105510+04	.596335-01	.226013+00	.123357+04
5	3	1	0	.105501+04	.283667+01	.296626+00	.294557+03
5	3	2	0	.105434+04	.273626+01	.367239+00	.283449+03
5	3	3	0	.105319+04	.504935+01	.437852+00	.264003+03
5	3	4	0	.105154+04	.212012+01	.508466+00	.238874+03
5	3	5	0	.104933+04	.137083+01	.579079+00	.275294+03
3	3	0	1	.104646+04	.907069+01	.241769+00	.119215+03
3	3	1	1	.104644+04	.432998+01	.366469+00	.115482+03
3	3	2	1	.104641+04	.365857+01	.451169+00	.104279+03
3	3	3	1	.104637+04	.467615+01	.555869+00	.955716+02
4	3	4	3	.104636+04	.197475-01	.572881+00	.106955+04
4	3	3	3	.104318+04	.610465-01	.487211+00	.109757+04
4	3	2	3	.104098+04	.362686-01	.401540+00	.111751+04

Table 7. V_2 Band Parameters from 1140.76 to 88.108 cm^{-1} (Continued)

J	ΔJ	K	I Sym	Frequency (cm^{-1})	Strength ($\text{cm}^{-2}\text{atm}^{-1}$)	Width (cm^{-1})	Energy (cm^{-1})
4	3	1	3	.103968+04	.390555-01	.315869+00	.112043+04
4	3	0	0	.103431+04	.758674+01	.230198+00	.109261+03
4	3	1	0	.103407+04	.377740+01	.315869+00	.105547+03
4	3	2	0	.103336+04	.347305+01	.401540+00	.104397+03
4	3	3	0	.103215+04	.570549+01	.487211+00	.104570+03
4	3	4	0	.103041+04	.181984+01	.572881+00	.103652+03
14	3	0	3	.102836+04	.245936-04	.857400-01	.301351+04
2	3	1	1	.102705+04	.403958+01	.393178+00	.588963+02
2	3	2	1	.102702+04	.266689+01	.521371+00	.446654+02
14	3	1	2	.102694+04	.124358-04	.112176+00	.301001+04
3	3	3	3	.102683+04	.486373-01	.555869+00	.101713+04
3	3	2	3	.102456+04	.377217-01	.451169+00	.100715+04
3	3	1	3	.102323+04	.444142-01	.346469+00	.1004913+04
3	3	0	3	.102279+04	.928825-01	.241749+00	.100312+04
14	3	2	2	.102271+04	.128616-04	.138602+00	.299951+04
15	3	6	2	.101591+04	.101313-04	.229173+00	.317404+04
14	3	3	2	.101581+04	.272030-04	.165029+00	.298197+04
3	3	1	0	.101321+04	.417731+01	.346465+00	.116225+03
3	3	2	0	.101246+04	.352674+01	.451169+00	.105040+03
3	3	3	0	.101120+04	.450148+01	.555869+00	.863679+02
0	3	0	1	.100753+04	.708154+01	.303789+00	.108844+02
1	3	1	1	.100752+04	.270454+01	.460589+00	.161392+02
2	3	2	3	.100745+04	.276487-01	.521371+00	.974793+02
14	3	4	2	.100644+04	.147036-04	.191455+00	.205726+04
2	3	1	3	.100609+04	.416588-01	.393178+00	.988814+03
14	3	5	2	.094894+03	.162402-04	.217881+00	.292562+04
2	3	0	0	.092718+03	.859414+01	.264906+00	.604074+02
2	3	1	0	.092463+03	.388887+01	.393178+00	.546668+02
2	3	2	0	.091692+03	.256523+01	.521371+00	.445467+02
13	3	1	2	.090570+03	.415771-04	.119036+00	.274100+04
1	3	1	3	.088223+03	.279944-01	.460589+00	.048561+03
1	3	0	3	.087768+03	.731599-01	.303789+00	.082571+03
13	3	2	2	.086697+03	.420454-04	.147417+00	.273038+04
14	3	6	2	.081558+03	.366245-04	.244307+00	.288666+04
13	3	3	2	.080382+03	.906264-04	.175801+00	.271267+04
17	2	17	3	.075257+03	.606815-04	.456680+00	.283633+04
1	3	1	0	.071884+03	.259884+01	.460589+00	.162296+02
13	3	4	2	.071836+03	.488156-04	.204185+00	.268780+04
16	2	16	3	.071013+03	.155234-03	.461580+00	.243017+04
1	2	1	1	.067957+03	.259427+01	.503580+00	.161392+02
2	2	1	1	.067759+03	.118681+01	.423072+00	.588063+02
2	2	2	1	.067700+03	.501440+01	.565825+00	.446654+02
3	2	1	1	.067467+03	.620935+00	.367501+00	.115683+03
3	2	2	1	.067405+03	.262317+01	.483371+00	.104279+03
3	2	3	1	.067306+03	.129313+02	.599241+00	.855716+02
15	2	15	3	.067284+03	.748302-03	.466480+00	.243548+04
4	2	1	1	.067085+03	.325056+00	.329455+00	.194842+03
4	2	2	1	.067019+03	.137297+01	.424111+00	.183673+03
4	2	3	1	.066913+03	.676632+01	.518766+00	.165024+03
14	3	7	2	.066896+03	.210534-04	.270733+00	.284040+04
4	2	4	1	.066774+03	.683310+01	.613422+00	.138847+03
5	2	1	1	.066622+03	.163250+00	.305122+00	.203805+03
5	2	2	1	.066551+03	.680386+00	.382801+00	.282769+03
5	2	3	1	.066436+03	.339621+01	.460480+00	.264103+03
5	2	4	1	.066284+03	.342797+01	.538159+00	.238118+03
5	2	5	1	.066104+03	.631072+01	.615837+00	.204476+03
6	2	1	1	.066086+03	.771863-01	.290701+00	.412546+03
6	2	2	1	.066008+03	.325863+00	.354108+00	.447147+03
6	2	3	1	.065883+03	.160464+01	.418606+00	.382983+03

Table 7. V_2 Band Parameters from 1140.76 to 88.108 cm^{-1} (Continued)

J	ΔJ	K	I Sym	Frequency (cm^{-1})	Strength ($\text{cm}^{-2} \text{atm}^{-1}$)	Width (cm^{-1})	Energy (cm^{-1})
6	2	4	1	.965717+03	.161866+01	.483014+00	.357030+03
6	2	5	1	.965518+03	.297752+01	.547422+00	.323545+03
7	2	1	1	.965487+03	.340169+01	.278748+00	.550676+03
7	2	2	1	.965402+03	.143568+00	.333049+00	.539663+03
6	2	6	1	.965298+03	.104778+02	.611830+00	.282440+03
7	2	3	1	.965265+03	.706606+00	.387370+00	.521276+03
7	2	4	1	.965082+03	.712770+00	.441682+00	.405466+03
7	2	5	1	.964862+03	.130902+01	.495993+00	.462165+03
8	2	1	1	.964839+03	.138940+01	.267281+00	.708151+03
8	2	2	1	.964745+03	.586190+01	.314139+00	.697700+03
7	2	6	1	.964615+03	.460121+01	.550304+00	.421283+03
8	2	3	1	.964595+03	.288340+00	.360996+00	.678938+03
15	3	9	2	.964555+03	.166608+04	.303342+00	.301555+04
8	2	4	1	.964392+03	.290415+00	.407854+00	.643291+03
7	2	7	1	.964356+02	.396786+01	.604615+00	.372715+03
9	2	1	1	.964155+03	.524148+02	.250679+00	.884816+03
8	2	5	1	.964147+03	.533167+00	.454712+00	.620198+03
9	2	2	1	.964052+03	.221051+01	.292194+00	.873052+03
14	2	14	3	.964023+03	.848788+03	.471380+00	.225236+04
9	2	3	1	.963886+03	.108661+00	.333709+00	.855812+03
8	2	6	1	.963870+03	.187168+01	.501549+00	.579573+03
9	2	4	1	.963662+03	.109342+00	.375274+00	.830348+03
8	2	7	1	.963575+03	.161160+01	.548427+00	.531308+03
10	2	1	1	.963452+03	.182259+02	.224228+00	.108050+04
9	2	5	1	.963389+03	.200503+00	.416740+00	.797402+03
10	2	2	1	.963339+03	.768312+02	.261981+00	.106972+04
8	2	8	1	.963279+03	.276610+01	.595284+00	.475275+03
10	2	3	1	.963155+03	.377401+01	.299744+00	.105172+04
9	2	6	1	.963078+03	.702852+00	.458755+00	.757155+03
10	2	4	1	.962907+03	.379380+01	.337406+00	.102646+04
11	2	1	1	.962747+03	.583503+03	.183218+00	.129499+04
9	2	7	1	.962743+03	.604156+00	.499770+00	.709230+03
11	2	2	1	.962623+03	.245858+02	.218256+00	.128431+04
10	2	5	1	.962603+03	.694761+01	.375239+00	.003860+04
11	2	3	1	.962421+03	.125670+01	.253204+00	.126648+04
9	2	8	1	.962400+02	.103491+01	.541285+00	.653590+03
10	2	6	1	.962254+03	.243155+00	.412902+00	.953852+03
11	2	4	1	.962146+03	.121167+01	.288332+00	.124144+04
9	2	9	1	.962068+03	.357006+01	.582801+00	.590088+03
12	2	1	1	.962061+03	.171911+03	.129932+00	.152810+04
12	2	2	1	.961925+03	.722961+03	.161863+00	.151752+04
10	2	7	1	.961874+03	.208614+00	.450744+00	.906305+03
11	2	5	1	.961807+03	.221575+01	.323371+00	.120014+04
12	2	3	1	.961701+03	.355020+02	.193705+00	.149987+04
10	2	8	1	.961479+03	.356573+00	.488407+00	.851102+03
11	2	6	1	.961417+03	.774105+01	.358409+00	.116947+04
13	2	1	1	.961415+03	.466071+04	.122575+00	.177958+04
12	2	4	1	.961398+03	.356044+02	.225727+00	.147507+04
13	3	5	2	.961354+03	.536481+04	.232569+00	.265574+04
13	2	2	1	.961265+03	.196163+03	.152051+00	.176912+04
13	2	13	3	.961190+03	.181034+02	.476290+00	.208081+04
10	2	9	1	.961089+03	.122700+01	.526249+00	.788095+03
12	2	5	1	.961022+03	.650064+02	.257658+00	.144308+04
13	2	3	1	.961019+03	.961044+03	.181526+00	.175165+04
11	2	7	1	.960957+03	.662760+01	.393447+00	.112234+04
14	2	1	1	.960832+03	.116314+04	.115570+00	.204918+04
10	2	10	1	.960723+03	.107052+01	.564002+00	.717110+03
13	2	4	1	.960684+03	.967540+03	.211002+00	.172712+04
14	2	2	1	.960667+03	.489250+04	.142940+00	.203884+04

Table 7. V_2 Band Parameters from 1140.76 to 88.108 cm^{-1} (Continued)

J	ΔJ	K	I Sym	Frequency (cm^{-1})	Strength ($\text{cm}^{-2} \text{atm}^{-1}$)	Width (cm^{-1})	Energy (cm^{-1})
12	2	6	1	.960586+03	.226673-01	.289590+00	.140380+04
11	2	8	1	.960536+03	.113010+00	.428485+00	.106762+04
14	2	3	1	.960397+03	.239449-03	.170310+00	.202158+04
13	2	5	1	.960268+03	.175440-02	.240477+00	.169547+04
15	2	2	1	.960157+03	.112388-04	.134371+00	.232642+04
12	2	7	1	.960103+03	.193628-01	.321522+00	.145712+04
11	2	9	1	.960081+03	.307818+00	.463524+00	.100516+04
14	2	4	1	.960028+03	.239479-03	.197680+00	.199733+04
15	2	3	1	.959861+03	.549448-04	.159936+00	.230938+04
13	2	6	1	.959782+03	.610475-02	.269952+00	.165660+04
11	2	10	1	.959643+03	.337329+00	.498562+00	.934788+03
12	2	8	1	.959589+03	.329297-01	.353453+00	.130292+04
14	2	5	1	.959569+03	.435694-03	.225050+00	.196605+04
15	2	4	1	.959456+03	.548676-04	.185481+00	.228544+04
16	2	3	1	.959437+03	.116217-04	.150246+00	.261476+04
11	2	11	1	.959247+03	.598347+00	.533600+00	.886329+03
13	2	7	1	.959241+03	.520196-02	.299428+00	.161042+04
12	2	9	1	.959063+03	.117670+00	.285385+00	.124106+04
14	2	6	1	.959030+03	.151267-02	.252420+00	.192763+04
16	2	4	1	.958993+03	.115859-04	.174195+00	.259115+04
15	2	5	1	.958949+03	.996265-04	.211027+00	.225454+04
12	2	12	3	.958746+03	.725127-02	.481180+00	.102008+04
13	2	8	1	.958660+03	.882168-02	.328903+00	.155679+04
12	2	10	1	.958547+03	.976769-01	.417317+00	.117135+04
16	2	5	1	.958437+03	.203931-04	.198144+00	.256067+04
14	2	7	1	.958426+03	.120555-02	.279790+00	.180198+04
15	2	6	1	.958354+03	.345059-03	.216572+00	.221661+04
12	2	11	1	.958064+03	.172620+00	.449248+00	.109363+04
13	2	9	1	.958058+03	.300864-01	.258378+00	.149554+04
16	2	6	1	.957781+03	.725239-04	.222007+00	.252325+04
14	2	8	1	.957772+03	.217343-02	.207140+00	.182896+04
15	2	7	1	.957682+03	.292418-03	.262117+00	.217152+04
12	2	12	1	.957640+03	.624706+00	.481180+00	.100767+04
12	3	0	3	.957551+03	.250714-03	.955500-01	.249373+04
13	2	10	1	.957457+03	.259891-01	.387854+00	.142658+04
17	2	6	1	.957339+03	.140594-04	.208740+00	.284724+04
17	2	16	3	.957105+03	.273312-04	.434140+00	.207090+04
14	2	9	1	.957089+03	.738685-02	.334530+00	.176842+04
16	2	7	1	.957037+03	.612730-04	.246041+00	.267877+04
15	2	8	1	.956951+03	.492759-03	.287663+00	.211916+04
13	2	11	1	.956879+03	.457469-01	.417329+00	.134965+04
11	2	11	3	.956654+03	.680805-02	.533600+00	.177299+04
17	2	7	1	.956519+03	.118402-04	.231280+00	.280340+04
14	2	10	1	.956395+03	.635614-02	.361000+00	.170021+04
12	3	1	2	.956356+03	.126646-03	.126274+00	.249016+04
13	2	12	1	.956353+03	.164936+00	.446805+00	.126456+04
16	2	8	1	.956223+03	.102893-03	.269900+00	.242710+04
15	2	9	1	.956179+03	.166853-02	.313208+00	.205937+04
13	2	13	1	.955905+03	.152553+00	.476280+00	.117111+04
14	2	11	1	.955717+03	.111404-01	.389270+00	.162414+04
17	2	8	1	.955618+03	.198087-04	.253820+00	.275247+04
15	2	10	1	.955388+03	.142976-02	.378753+00	.199198+04
16	2	9	1	.955358+03	.347024-03	.293939+00	.236810+04
14	2	12	1	.955179+03	.399535-01	.416640+00	.153099+04
10	2	10	3	.954883+03	.119650-01	.564002+00	.163662+04
17	2	9	1	.954652+03	.665277-04	.276360+00	.249432+04
15	2	11	1	.954601+03	.249446-02	.364299+00	.191682+04
14	2	13	1	.954510+03	.367890-01	.444010+00	.144755+04
16	2	10	1	.954461+03	.296051-03	.317887+00	.230160+04

Table 7. V_2 Band Parameters from 1140.76 to 88.108 cm^{-1} (continued)

J	ΔJ	K	I Sym	Frequency (cm^{-1})	Strength ($\text{cm}^{-2} \text{atm}^{-1}$)	Width (cm^{-1})	Energy (cm^{-1})
16	2	15	3	.954409+03	.144870-03	.437631+00	.275622+04
18	2	9	1	.954093+03	.117703-04	.260190+00	.303768+04
14	2	14	1	.954042+03	.698033-01	.471380+00	.134658+04
15	2	12	1	.953844+03	.890110-02	.389844+00	.183368+04
17	2	10	1	.953644+03	.564886-04	.298900+00	.262876+04
16	2	11	1	.953558+03	.513987-03	.341836+00	.222742+04
9	2	9	3	.953403+03	.392742-01	.582801+00	.161270+04
15	2	13	1	.953146+03	.815117-02	.415389+00	.174234+04
18	2	10	1	.952967+03	.994444-04	.281478+00	.293137+04
12	3	2	2	.952812+03	.130577-03	.156859+00	.267945+04
16	2	12	1	.952674+03	.182427-02	.365785+00	.214535+04
17	2	11	1	.952618+03	.975630-04	.321440+00	.255562+04
14	2	14	1	.952538+03	.153754-01	.440935+00	.144254+04
9	2	8	3	.952187+03	.300094-01	.595284+00	.139070+04
15	2	14	3	.952135+03	.180593-03	.440935+00	.255308+04
14	2	15	1	.952055+03	.590146-01	.466480+00	.153403+04
16	2	13	1	.951838+03	.166085-02	.389734+00	.205517+04
19	2	11	1	.951810+03	.170809-04	.302746+00	.290108+04
0	3	0	0	.951778+03	.366875+01	.362600+00	.793444+00
17	2	12	1	.951599+03	.344307-03	.343980+00	.267468+04
14	3	8	2	.951454+03	.246281-04	.297140+00	.278673+04
7	2	7	3	.951211+03	.425325-01	.404615+00	.129915+04
16	2	14	1	.951082+03	.311316-02	.413682+00	.195667+04
18	2	12	1	.950649+03	.592159-04	.324053+00	.282135+04
17	2	13	1	.950616+03	.311527-03	.366570+00	.238574+04
6	2	6	3	.950453+03	.111174+00	.611830+00	.121058+04
16	2	15	1	.950438+03	.120497-01	.437631+00	.186947+04
14	2	13	3	.950250+03	.421050-03	.444010+00	.236156+04
16	2	16	1	.949944+03	.122721-01	.461580+00	.173340+04
5	2	5	3	.949902+03	.563083-01	.615837+00	.113406+04
19	2	12	1	.949855+03	.962730-05	.305708+00	.218500+04
17	2	14	1	.949701+03	.580041-03	.389040+00	.228853+04
4	2	4	3	.949536+03	.714145-01	.613422+00	.106955+04
18	2	13	1	.949511+03	.538570-04	.345341+00	.273371+04
1	2	1	3	.949461+03	.268509-01	.503590+00	.948561+03
3	2	3	3	.949345+03	.136485+00	.599261+00	.101713+04
2	2	2	3	.949322+03	.510806-01	.565825+00	.976793+03
13	3	6	2	.949317+03	.120132-03	.260952+00	.261639+04
17	2	15	1	.948888+03	.222905-02	.411600+00	.218280+04
13	2	12	3	.948714+03	.185960-02	.446805+00	.218173+04
18	2	14	1	.948428+03	.995711-04	.366629+00	.263792+04
17	2	16	1	.948212+03	.221605-02	.434140+00	.206827+04
1	1	0	1	.948191+03	.332398+01	.362600+00	.108854+02
2	2	1	3	.947970+03	.122364-01	.423972+00	.988814+03
17	2	17	1	.947712+03	.457152-02	.456880+00	.104643+04
15	2	2	0	.947504+03	.110805-04	.134391+00	.232561+04
12	2	11	3	.947497+03	.191444-02	.449248+00	.201364+04
18	2	15	1	.947434+03	.379741-03	.387917+00	.253371+04
14	2	1	0	.947345+03	.114557-04	.115570+00	.204940+04
19	2	14	1	.947294+03	.157700-04	.346043+00	.300445+04
16	2	3	0	.947180+03	.114637-04	.150246+00	.261492+04
15	3	10	2	.947144+03	.101711-04	.328063+00	.204737+04
3	2	2	3	.947097+03	.270362-01	.483371+00	.103715+04
12	3	3	2	.947046+03	.274668-03	.187513+00	.266157+04
15	2	3	0	.947036+03	.541590-04	.159076+00	.230957+04
14	2	2	0	.947009+03	.481747-04	.142940+00	.203007+04
16	2	4	0	.946649+03	.114272-04	.174195+00	.259132+04
11	2	10	3	.946569+03	.368469-02	.498562+00	.185736+04
18	2	16	1	.946566+03	.374467-03	.409204+00	.262080+04

Table 7. V_2 Band Parameters from 1140.76 to 88.108 cm^{-1} (continued)

J	ΔJ	K	$I \text{ Sym}$	Frequency (cm^{-1})	Strength ($\text{cm}^{-2} \text{ atm}^{-1}$)	Width (cm^{-1})	Energy (cm^{-1})
13	2	1	0	.946533+03	.458278-04	.122575+00	.177986+04
14	2	3	0	.946427+03	.235697-03	.170310+00	.202181+04
4	2	3	3	.946388+03	.698311-01	.518766+00	.109757+04
15	2	4	0	.946335+03	.540626-04	.185481+00	.228565+04
13	2	2	0	.946132+03	.192826-03	.152041+00	.176938+04
19	2	15	1	.946110+03	.596615-04	.366211+00	.200186+04
10	2	9	3	.945906+03	.132244-01	.526249+00	.171299+04
16	2	4	0	.945887+03	.206996-04	.198144+00	.256086+04
18	2	17	1	.945861+03	.765829-03	.430492+00	.279889+04
5	2	4	3	.945846+03	.354847-01	.538159+00	.117007+04
3	2	1	3	.945775+03	.636586-02	.367501+00	.104013+04
14	2	4	0	.945565+03	.235586-03	.197680+00	.199758+04
9	2	8	3	.945483+03	.110265-01	.441285+00	.148040+04
6	2	5	3	.945475+03	.309657-01	.547422+00	.125462+04
15	2	3	0	.945443+03	.944192-03	.181526+00	.175192+04
12	2	1	0	.945419+03	.168688-03	.129932+00	.152840+04
18	2	18	1	.945361+03	.325638-02	.451790+00	.216765+04
15	2	4	0	.945354+03	.981069-04	.211027+00	.225477+04
7	2	6	3	.945283+03	.481568-01	.550304+00	.135121+04
8	2	7	3	.945281+03	.170037-01	.548477+00	.145982+04
17	2	6	0	.945115+03	.138646-04	.208740+00	.284740+04
19	2	16	1	.945038+03	.587296-04	.396378+00	.279065+04
12	2	2	0	.944959+03	.710115-03	.161863+00	.151784+04
16	2	6	0	.944836+03	.714730-04	.222092+00	.252345+04
13	2	4	0	.944432+03	.944900-03	.211002+00	.172741+04
14	2	5	0	.944379+03	.428236-03	.225050+00	.196632+04
4	2	2	3	.944209+03	.140655-01	.424111+00	.111751+04
12	2	3	0	.944170+03	.347097-02	.193795+00	.150019+04
19	2	17	1	.944117+03	.118205-03	.405445+00	.267056+04
11	2	1	0	.944082+03	.571213-03	.183218+00	.129434+04
17	2	7	0	.944037+03	.116752-04	.231280+00	.280358+04
15	2	6	0	.944034+03	.330496-03	.236572+00	.221686+04
11	2	2	0	.943566+03	.240568-02	.218256+00	.128467+04
16	2	7	0	.943421+03	.603355-04	.246041+00	.267890+04
19	2	18	1	.943388+03	.497766-03	.426713+00	.254125+04
13	2	5	0	.943052+03	.172028-02	.240477+00	.169579+04
12	2	4	0	.943019+03	.348651-02	.225727+00	.147542+04
4	2	1	3	.942928+03	.330809-02	.329455+00	.112943+04
19	2	19	1	.942894+03	.545809-03	.446880+00	.240239+04
5	2	3	3	.942819+03	.347267-01	.460480+00	.119793+04
14	2	6	0	.942806+03	.148495-02	.252420+00	.192793+04
11	2	3	0	.942685+03	.117980-01	.253294+00	.126686+04
10	2	1	0	.942595+03	.177964-02	.224228+00	.108090+04
17	2	8	0	.942562+03	.195181-04	.253820+00	.275268+04
20	2	17	1	.942514+03	.168361-04	.384503+00	.204026+04
17	2	15	3	.942311+03	.253416-04	.411400+00	.209462+04
15	2	7	0	.942302+03	.287337-03	.262117+00	.217180+04
10	2	2	0	.942029+03	.749807-02	.261981+00	.107011+04
6	2	4	3	.941605+03	.165708-01	.483014+00	.129041+04
16	2	8	0	.941557+03	.101188-03	.269090+00	.242736+04
20	2	18	1	.941543+03	.701774-04	.403662+00	.203200+04
18	2	9	0	.941478+03	.116036-04	.260190+00	.203788+04
12	2	5	0	.941459+03	.635675-02	.257658+00	.144345+04
11	2	4	0	.941404+03	.118324-01	.288332+00	.124184+04
13	2	6	0	.941243+03	.497645-02	.269052+00	.163605+04
10	2	3	0	.941063+03	.367971-01	.299734+00	.105215+04
9	2	1	0	.941026+03	.510441-02	.250679+00	.085270+03
16	2	14	3	.940856+03	.353671-04	.413482+00	.287177+04
20	2	19	1	.940794+03	.761245-04	.422821+00	.279529+04

Table 7. V_2 Band Parameters from 1140.76 to 88.108 cm^{-1} (Continued)

J	ΔJ	K	I Sym	Frequency (cm^{-1})	Strength ($\text{cm}^{-2} \text{atm}^{-1}$)	Width (cm^{-1})	Energy (cm^{-1})
14	2	7	0	.940775+03	.125986-02	.279790+00	.188231+04
5	2	2	3	.940726+03	.698911-02	.382801+00	.121776+04
17	2	9	0	.940591+03	.654705-04	.276260+00	.769456+04
7	2	5	3	.940567+03	.134391-01	.495593+00	.179491+04
9	2	2	0	.940413+03	.215141-01	.292194+00	.874418+03
20	2	20	1	.940313+03	.172237-03	.441080+00	.764878+04
15	2	2	0	.940071+03	.483331-03	.287463+00	.711947+04
21	2	18	1	.939864+03	.914074-05	.382740+00	.373949+04
15	2	13	3	.939755+03	.909201-04	.415389+00	.766052+04
8	2	6	3	.939710+03	.193021-01	.501569+00	.141143+04
11	2	5	0	.939678+03	.216021-01	.323271+00	.120957+04
10	2	4	0	.939663+03	.369396-01	.337486+00	.102692+04
5	2	1	3	.939497+03	.164674-02	.305122+00	.172962+04
8	2	1	0	.939436+03	.134947-01	.267281+00	.708660+03
12	2	6	0	.939430+03	.221238-01	.289090+00	.140421+04
18	2	10	0	.939419+03	.979212-05	.281478+00	.707335+04
9	2	3	0	.939369+03	.105646+00	.333709+00	.866299+03
12	3	4	2	.939269+03	.147221-03	.218168+00	.743647+04
16	2	9	0	.939144+03	.340643-03	.293939+00	.746840+04
9	2	7	3	.939041+03	.626877-02	.499770+00	.163093+04
14	2	12	3	.938977+03	.438379-03	.416640+00	.746094+04
13	2	7	0	.938933+03	.508213-02	.299428+00	.161081+04
21	2	19	1	.938847+03	.980359-05	.400587+00	.320504+04
8	2	2	0	.938781+03	.568963-01	.314139+00	.697730+03
6	2	3	3	.938723+03	.162241-01	.418606+00	.121809+04
10	2	8	3	.938570+03	.372872-02	.488497+00	.178038+04
13	2	11	3	.938493+03	.494654-03	.417329+00	.227307+04
11	2	9	3	.938310+03	.409395-02	.463524+00	.103275+04
12	2	10	3	.938278+03	.104266-02	.417317+00	.209699+04
14	2	8	0	.938199+03	.212512-02	.307160+00	.182933+04
21	2	20	1	.938083+03	.219306-04	.418833+00	.306001+04
17	2	10	0	.938010+03	.554854-04	.298000+00	.762004+04
7	2	1	0	.937880+03	.329538-01	.278748+00	.441238+03
9	2	4	0	.937861+03	.106144+00	.175224+00	.830866+03
10	2	5	0	.937783+03	.675217-01	.175239+00	.924364+03
8	2	3	0	.937667+03	.279546+00	.360396+00	.679483+03
21	2	21	1	.937622+03	.107575-03	.437780+00	.200673+04
11	2	6	0	.937445+03	.753056-01	.358409+00	.116095+04
15	2	9	0	.937241+03	.163261-02	.313208+00	.205973+04
7	2	2	0	.937187+03	.138980+00	.333059+00	.440240+03
7	2	4	3	.936914+03	.720304-02	.441682+00	.143042+04
12	2	7	0	.936858+03	.188518-01	.321522+00	.145758+04
6	2	2	3	.936732+03	.326977-02	.154198+00	.133778+04
18	2	11	0	.936681+03	.167870-04	.302766+00	.700135+04
6	2	1	0	.936428+03	.745915-01	.289791+00	.413150+03
13	3	7	2	.936188+03	.683654-04	.289336+00	.246066+04
16	2	10	0	.936069+03	.289852-03	.317887+00	.230105+04
8	2	4	0	.936060+03	.281096+00	.407854+00	.653870+03
13	2	8	0	.936032+03	.850480-02	.328003+00	.145723+04
7	2	3	0	.936011+03	.683179+00	.387370+00	.521870+03
14	1	9	2	.935867+03	.584257-04	.323586+00	.272551+04
9	2	5	0	.935841+03	.194238+00	.416740+00	.708052+03
6	2	2	0	.935683+03	.314665+00	.354108+00	.402102+03
6	2	1	3	.935565+03	.770744-03	.289791+00	.140057+04
10	2	6	0	.935361+03	.235732+00	.412992+00	.044307+03
8	2	4	3	.935297+03	.539848-02	.445471+00	.145474+04
22	2	21	1	.935257+03	.119101-04	.414763+00	.133805+04
19	2	17	0	.935168+03	.946625-05	.305708+00	.118476+04

Table 7. V_2 Band Parameters from 1140.76 to 88.108 cm^{-1} (Continued)

J	ΔJ	K	J Sym	Frequency (cm^{-1})	Strength ($\text{cm}^{-2} \text{atm}^{-1}$)	Width (cm^{-1})	Energy (cm^{-1})
5	2	1	0	.935064+03	.157411+00	.305122+00	.294557+03
14	2	9	0	.934975+03	.720096-02	.334530+00	.176886+04
22	2	22	1	.934823+03	.143955-04	.432180+00	.317616+04
17	2	11	0	.934693+03	.955690-04	.321440+00	.255595+04
11	2	7	0	.934630+03	.647912-01	.373447+00	.112287+04
6	2	3	0	.934451+03	.154744+01	.418606+00	.383641+03
7	2	4	0	.934316+03	.687410+00	.441682+00	.446107+03
5	2	2	0	.934310+03	.664194+00	.382801+00	.283440+03
7	2	3	3	.934200+03	.706531-02	.387370+00	.145780+04
8	2	5	0	.933913+03	.514869+00	.454712+00	.620826+03
4	2	1	0	.933886+03	.312819+00	.329455+00	.195547+03
9	2	6	3	.933872+03	.713697-02	.458255+00	.169102+04
15	2	10	0	.933697+03	.139441-02	.338753+00	.109241+04
12	2	8	0	.933654+03	.319583-01	.353453+00	.130345+04
9	2	6	0	.933247+03	.679033+00	.458255+00	.747772+03
18	2	12	0	.933122+03	.587172-04	.324093+00	.282168+04
4	2	2	0	.933109+03	.132016+01	.424111+00	.184397+03
5	2	3	0	.933032+03	.326747+01	.460480+00	.244903+03
3	2	1	0	.932905+03	.596589+00	.367501+00	.116225+03
6	2	4	0	.932679+03	.155795+01	.483014+00	.357730+03
10	2	7	3	.932643+03	.212782-02	.450764+00	.183024+04
13	2	9	0	.932439+03	.292056-01	.358378+00	.149608+04
7	2	3	3	.932330+03	.142428-02	.333059+00	.147743+04
10	2	7	0	.932323+03	.201604+00	.450764+00	.906915+03
16	2	11	0	.932202+03	.501455-03	.341396+00	.222784+04
2	2	1	0	.932147+03	.113885+01	.423972+00	.566668+02
3	2	2	0	.932109+03	.251808+01	.483371+00	.105060+03
7	2	5	0	.932055+03	.126024+01	.495003+00	.462859+03
8	2	4	3	.931891+03	.289868-02	.407954+00	.158993+04
4	2	3	0	.931790+03	.649649+01	.518766+00	.163780+03
1	2	1	0	.931631+03	.248729+01	.503580+00	.149296+02
11	2	8	3	.931617+03	.115968-02	.428485+00	.109037+04
2	2	2	0	.931336+03	.480737+01	.565825+00	.454567+02
7	2	1	3	.931235+03	.335910-03	.278748+00	.148912+04
5	2	4	0	.931193+03	.329132+01	.538159+00	.238874+03
8	2	6	0	.931163+03	.180208+01	.501569+00	.580264+03
11	2	8	0	.931146+03	.109228+00	.428485+00	.106872+04
14	2	10	0	.930990+03	.617193-02	.361900+00	.170072+04
15	3	11	2	.930855+03	.125328-04	.352784+00	.287143+04
12	2	9	3	.930802+03	.116509-02	.385385+00	.217138+04
3	2	3	0	.930758+03	.123945+02	.509241+00	.843679+02
17	2	12	0	.930498+03	.335996-03	.363980+00	.247510+04
6	2	4	0	.930319+03	.285837+01	.547422+00	.324303+03
13	2	10	3	.930212+03	.271247-03	.337954+00	.235522+04
9	2	7	0	.930004+03	.581644+00	.400770+00	.709921+03
16	2	13	3	.929960+03	.179298-04	.389734+00	.297731+04
4	2	4	0	.929896+03	.654567+01	.613422+00	.139652+03
14	2	11	3	.929862+03	.117545-03	.389270+00	.255086+04
9	2	5	3	.929799+03	.200105-02	.416740+00	.173389+04
12	3	5	2	.929777+03	.160539-03	.248822+00	.240410+04
15	2	12	3	.929771+03	.951012-04	.389844+00	.275824+04
12	2	9	0	.929718+03	.108901+00	.385385+00	.124166+04
1	1	0	3	.929623+03	.343395+01	.362400+00	.952571+03
8	2	3	3	.929369+03	.284725-02	.360906+00	.141715+04
15	2	11	0	.929310+03	.242737-02	.364209+00	.191733+04
7	2	6	0	.929167+03	.441561+01	.540306+00	.422048+03
5	2	5	0	.928747+03	.604252+01	.615837+00	.205204+03
18	2	13	0	.928588+03	.925441-04	.345341+00	.273412+04
10	2	8	0	.928580+03	.343205+00	.488497+00	.841798+03

Table 7. V_2 Band Parameters from 1140.76 to 88.108 cm^{-1} (Continued)

J	ΔJ	K	I Sym	Frequency (cm^{-1})	Strength ($\text{cm}^{-2} \text{atm}^{-1}$)	Width (cm^{-1})	Energy (cm^{-1})
2	1	1	1	.928200+03	.204503+01	.460589+00	.558963+02
13	2	10	0	.928040+03	.251161-01	.387854+00	.142719+04
10	2	6	3	.927921+03	.243042-02	.412992+00	.188976+04
8	2	7	0	.927736+03	.154580+01	.548427+00	.512783+03
8	2	2	3	.927637+03	.574547-03	.314139+00	.167651+04
16	2	12	0	.927403+03	.177148-02	.365785+00	.214586+04
6	2	6	0	.927308+03	.100244+02	.611430+00	.282276+03
11	2	9	0	.926889+03	.374128+00	.463524+00	.100586+04
9	2	4	3	.926672+03	.107663-02	.375224+00	.176874+04
8	2	1	3	.926624+03	.135586-03	.267281+00	.144810+04
19	2	14	0	.926476+03	.153927-04	.346043+00	.300488+04
11	2	7	3	.926257+03	.664522-03	.393447+00	.205750+04
14	2	11	0	.926113+03	.107632-01	.389270+00	.162475+04
9	2	8	0	.926024+03	.991966+00	.541285+00	.644379+03
7	2	7	0	.925574+03	.379238+01	.604615+00	.375573+03
17	2	13	0	.925268+03	.302467-03	.356520+00	.238626+04
12	2	10	0	.924930+03	.939235-01	.417317+00	.117206+04
12	2	8	3	.924810+03	.331725-03	.353443+00	.223710+04
9	2	3	3	.924367+03	.105921-02	.333709+00	.179467+04
10	2	5	3	.924227+03	.683320-03	.375299+00	.193215+04
11	3	1	2	.924071+03	.350735-03	.155780+00	.225774+04
10	2	9	0	.924027+03	.117505+01	.526249+00	.788903+03
15	2	12	0	.923938+03	.859505-02	.389844+00	.184430+04
13	2	9	3	.923586+03	.304981-03	.358378+00	.242852+04
8	2	8	0	.923540+03	.264056+01	.595284+00	.475160+03
18	2	14	0	.922908+03	.966490-04	.366429+00	.263844+04
9	2	2	3	.922789+03	.213980-03	.292194+00	.181483+04
13	2	11	0	.922701+03	.439565-01	.417329+00	.175037+04
14	2	10	3	.922593+03	.649339-04	.361900+00	.243171+04
13	3	8	2	.922516+03	.788205-04	.317720+00	.251545+04
11	2	6	3	.922027+03	.761759-03	.358409+00	.210739+04
9	2	1	3	.921869+03	.505310-04	.250679+00	.182630+04
15	2	11	3	.921843+03	.257218-04	.364299+00	.284644+04
11	2	10	0	.921741+03	.322696+00	.498562+00	.935618+03
16	2	13	0	.921511+03	.160301-02	.389734+00	.205590+04
10	2	4	3	.921408+03	.368484-03	.337486+00	.106652+04
16	2	12	3	.921351+03	.190165-04	.365785+00	.307326+04
9	2	9	0	.921200+03	.340315+01	.582801+00	.501005+03
14	3	10	2	.920850+03	.349283-04	.350012+00	.265661+04
11	3	2	2	.920832+03	.360707-03	.189688+00	.224694+04
19	2	15	0	.920321+03	.578878-04	.366211+00	.292236+04
14	2	12	0	.920199+03	.383545-01	.416640+00	.154074+04
12	2	7	3	.920070+03	.190949-03	.321572+00	.229444+04
10	2	3	3	.919344+03	.363161-03	.299734+00	.109322+04
12	2	11	0	.919159+03	.164919+00	.449248+00	.109448+04
12	3	6	2	.918949+03	.356030-03	.279476+00	.236430+04
17	2	14	0	.918831+03	.553431-03	.389060+00	.228017+04
11	2	5	3	.918748+03	.214826-03	.323371+00	.214925+04
10	2	10	0	.918545+03	.101877+01	.564002+00	.718073+03
13	2	8	3	.918353+03	.873191-04	.328903+00	.249326+04
10	2	2	3	.917938+03	.734580-04	.261941+00	.201216+04
15	2	13	0	.917418+03	.781631-02	.415389+00	.174310+04
10	2	1	3	.917122+03	.173601-04	.224228+00	.202349+04
14	2	9	3	.916880+03	.735006-04	.334530+00	.270383+04
15	3	12	2	.916572+03	.308400-04	.377505+00	.278753+04
12	2	6	3	.916376+03	.219753-03	.289490+00	.234364+04
13	2	12	0	.916276+03	.157245+00	.446805+00	.176545+04
11	2	4	3	.916271+03	.116136-03	.288372+00	.218325+04
18	2	15	0	.915894+03	.365922-03	.387917+00	.254437+04

Table 7. V_2 Band Parameters from 1140.76 to 88.108 cm^{-1} (Continued)

J	ΔJ	K	I Sym	Frequency (cm^{-1})	Strength ($\text{cm}^{-2} \text{atm}^{-1}$)	Width (cm^{-1})	Energy (cm^{-1})
15	2	10	3	.915656+03	.143225-04	.338753+00	.292610+04
11	3	3	2	.915576+03	.755343-03	.223596+00	.227890+04
11	2	11	0	.915567+03	.568321+00	.533600+00	.857127+03
11	2	3	3	.914471+03	.114681-03	.253796+00	.220954+04
16	2	14	0	.914352+03	.298137-02	.413682+00	.195742+04
13	2	7	3	.914283+03	.505111-04	.299478+00	.254074+04
12	2	5	3	.913551+03	.621802-04	.257658+00	.238491+04
11	2	7	3	.913254+03	.732293-04	.218756+00	.227874+04
14	2	13	0	.913084+03	.350326-01	.444010+00	.144848+04
19	2	16	0	.912695+03	.561474-04	.386178+00	.279132+04
14	2	8	3	.912466+03	.211710-04	.307160+00	.276753+04
12	2	12	0	.912236+03	.592063+00	.481180+00	.100872+04
12	2	4	3	.911444+03	.337070-04	.225727+00	.241844+04
13	2	6	3	.911170+03	.583798-04	.269952+00	.259820+04
17	2	15	0	.910996+03	.213146-02	.411600+00	.218363+04
15	2	9	3	.910923+03	.163294-04	.313208+00	.299697+04
12	2	3	3	.909933+03	.333558-04	.193795+00	.244436+04
15	2	14	0	.909579+03	.146126-01	.440935+00	.164451+04
20	2	17	0	.909229+03	.161861-04	.384503+00	.305996+04
2	1	1	3	.909207+03	.210815-01	.460589+00	.998814+03
14	2	7	3	.909118+03	.123120-04	.279790+00	.282308+04
13	3	9	2	.908933+03	.182992-03	.346103+00	.245362+04
13	2	5	3	.908837+03	.165789-04	.240477+00	.263884+04
13	2	13	0	.908600+03	.144223+00	.476280+00	.117221+04
11	3	4	2	.908513+03	.402059-03	.257504+00	.220359+04
3	1	0	1	.908201+03	.586958+01	.244906+00	.119215+03
3	1	1	1	.908172+03	.265656+01	.393138+00	.115483+03
3	1	2	1	.908087+03	.175350+01	.521371+00	.104279+03
18	2	16	0	.907341+03	.357451-03	.409204+00	.242166+04
16	3	15	2	.907292+03	.154632-04	.424295+00	.279990+04
12	3	7	2	.907249+03	.190621-03	.310131+00	.231773+04
14	3	11	2	.907206+03	.416433-04	.376438+00	.257985+04
13	2	4	3	.907132+03	.901394-05	.211002+00	.267185+04
14	2	6	3	.906630+03	.142960-04	.252420+00	.287073+04
16	2	15	0	.905733+03	.114262-01	.437631+00	.185048+04
15	3	13	2	.905266+03	.185413-04	.402227+00	.269548+04
14	2	14	0	.904587+03	.658074-01	.471380+00	.134775+04
19	2	17	0	.903378+03	.112610-03	.406545+00	.267145+04
17	2	16	0	.901553+03	.209599-02	.434140+00	.206035+04
15	2	15	0	.900204+03	.563098-01	.466480+00	.153527+04
11	3	5	2	.899937+03	.434230-03	.291412+00	.217094+04
20	2	18	0	.899097+03	.667065-04	.403662+00	.293294+04
15	3	14	2	.897992+03	.207082-04	.426948+00	.249408+04
18	2	17	0	.897021+03	.722265-03	.430492+00	.230003+04
13	3	10	2	.896158+03	.105770-03	.374487+00	.238403+04
15	3	15	2	.894888+03	.363457-04	.451669+00	.248608+04
14	3	12	2	.895821+03	.968934-04	.402864+00	.249507+04
16	2	16	0	.895436+03	.113057-01	.461580+00	.173473+04
12	3	8	2	.895225+03	.225174-03	.340785+00	.226251+04
10	3	0	3	.894507+03	.174769-02	.169540+00	.204757+04
21	2	19	0	.894487+03	.929527-05	.400587+00	.320603+04
10	3	1	2	.893507+03	.881121-03	.205838+00	.204395+04
2	1	0	0	.892171+03	.512776+01	.303799+00	.000000+02
19	2	18	0	.892124+03	.467949-03	.426713+00	.294246+04
2	1	1	0	.891894+03	.195756+01	.460589+00	.566668+02
10	3	2	2	.891551+03	.903003-03	.262135+00	.203306+04
17	2	17	0	.890267+03	.426460-02	.456680+00	.104606+04
11	3	6	2	.890230+03	.948075-03	.325120+00	.213089+04
3	1	2	3	.888966+03	.180672-01	.521371+00	.103715+04
4	1	1	1	.888108+03	.247706+01	.346469+00	.194842+03

At pressures of appreciably less than 8.5 atmospheres, it is quite clear that the already densely packed NH_3 lines must blend into a pseudo-continuum for even relatively short absorption paths. Also, at higher temperatures, hot bands of the type $(0\ 1\ 0\ 0) \rightarrow (0\ 2\ 0\ 0)$, etc. will enter to make the absorption pattern even more dense, and greatly increase the overall integrated band region intensity and average absorption coefficient: $\bar{k}(\nu) = (\hat{S}'/d)_\nu$ over much of the spectral interval of interest.

NH_3 also exhibits strong and broad absorption centered near $1630\ \text{cm}^{-1}$, and weaker but still significant absorption centered near $3400\ \text{cm}^{-1}$. At room temperature, these two absorption regions arise primarily from rotational lines of the so-called ν_4 [or $(0\ 0\ 0\ 0) \rightarrow (0\ 0\ 0\ 1)$], and the closely adjacent ν_1 and ν_3 pair [$(0\ 0\ 0\ 0) \rightarrow (1\ 0\ 0\ 0)$, $(0\ 0\ 0\ 0) \rightarrow (0\ 0\ 1\ 0)$] of fundamental vibration transitions, respectively. The ν_4 band complex has an integrated band intensity of $\sim 110\ (\text{atm cm})^{-1}\ \text{cm}^{-1}$, which while only $\sim 18\%$ of the extremely intense ν_2 band structure previously discussed, is still quite respectable and is comparable to the band intensities of the NO , CN and OH fundamentals. Since the rotational line spacings will be quite similar to those of the ν_2 structure, it would probably be a fairly efficient absorber for many of the lower frequency CO laser lines. At higher temperatures and pressures, it might absorb the full range of CO laser emission. The weaker ν_1 and ν_3 absorption centered on $\sim 3400\ \text{cm}^{-1}$ would be a less likely candidate for HF laser line absorption at room temperature, but at higher temperatures and pressures, it might prove effective.

3.8 ABSORPTION BY METHANOL (CH_3OH) OF CO_2 AND HF LASER RADIATION

The methanol, or methyl alcohol, molecule possesses an intense and very complex rotation vibration spectrum which extends almost continuously from the microwave region to the edge of the visible spectrum. The two most useful references found for methanol spectral absorption were Serrallach, et al. (1974) and Lee, et al. (1975). Figure 24 and Tables 8 and 9 were extracted from the former reference, while Figures 25a, b, and c were extracted from the latter.

The top quarter of Figure 24 shows room temperature infrared gas spectra of pure CH_3OH taken with resolution between 0.5 cm^{-1} and 2 cm^{-1} with $p = P = 3\text{ Torr}$, and $x = 70\text{ cm}$. This corresponds to 0.276 atm cm-STP . Under these conditions, the line contours will be Doppler profiles with half-widths at half-maxima of $a_D = 0.0041\text{ cm}^{-1}$. The Beer equation for transmission of a pure spectral frequency is definitely not applicable to the spectra made under these conditions, since only line center $\delta\nu$ increments of the order of $\sim 2a_D$ to $4a_D$ per line will suffer any appreciable absorption, and there are only of the order of ~ 30 lines per wavenumber (see Figures 25a, b, and c). If the lines were pressure-broadened to half-widths of say $\sim 0.1\text{ cm}^{-1}$, then the absorption spectra would become quite smooth and show a multifold increase (owing to significant contributions from the line wing regions, which are virtually transparent and make no appreciable contributions to the absorption shown in Figure 24. It is worth noting, however, that the pseudo-continuum portions of the spectrum (apparent discontinuities probably due to changes in slit-function resolution) seldom rise above a transmission of $\sim 80\%$. The absorption detected in these relatively weak continuous portions are probably due to the packing together of a very large number of relatively weak lines from numerous overlapping (fundamental and multiply-excited) vibrational transitions [Table 8 shows only a few of the possible bands, and only those originating from the ν_0 or (000000000000) ground vibrational level]. If it is assumed that the line packing is close enough so that Beers Law were applicable to the pseudo-continua structure, then an 80% transmission for an optical thickness of 0.276 atm cm-STP would correspond to a $k_{300^\circ\text{K}}(\nu)$ of $\sim 0.81\text{ (atm cm-STP)}^{-1}$. In the spectral band regions where the measured transmittance is ~ 0.7 (and would be reduced to some fraction of this value by pressure broadening), the Beers Law prediction gives a certainly

Optical
Thickness
= 0.276
(atm cm-STP)

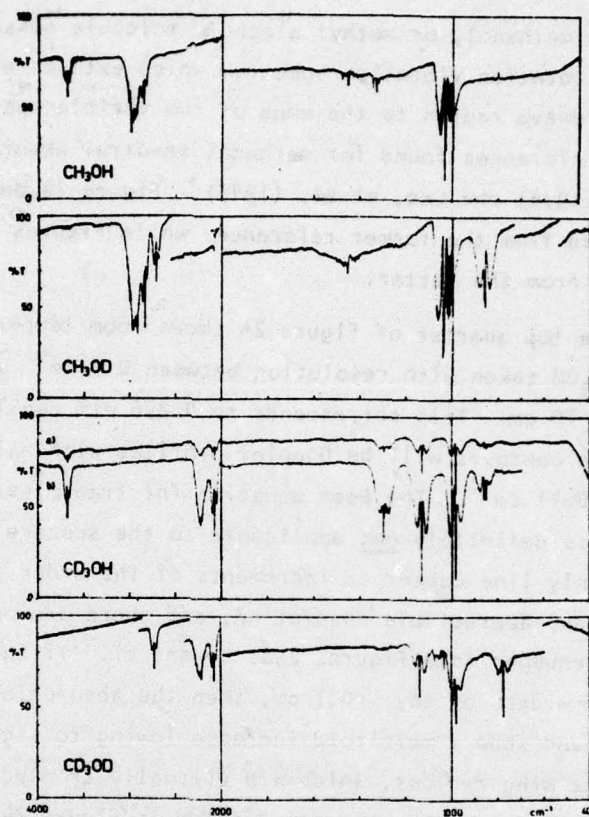


Fig. 24. Infrared gas spectra of species with symmetric methyl groups, taken at resolutions between 0.5 2 cm^{-1} . CH_3OH : $p = 3 \text{ Torr}$, $l = 70 \text{ cm}$. CH_3OD : $p = 4 \text{ Torr}$, $l = 70 \text{ cm}$ (25% CH_3OH impurity compensated). CD_3OH : (a) $p = 4 \text{ Torr}$, $l = 10 \text{ cm}$, (b) $p = 3 \text{ Torr}$, $l = 70 \text{ cm}$ (1% CD_3OD , 1% CHD_2OH impurities). CD_3OD : $p = 5 \text{ Torr}$, $l = 70 \text{ cm}$ (25% CD_3OH impurity compensated, 1% CHD_2OD).

OH-Stretch Fundamental of Methanol

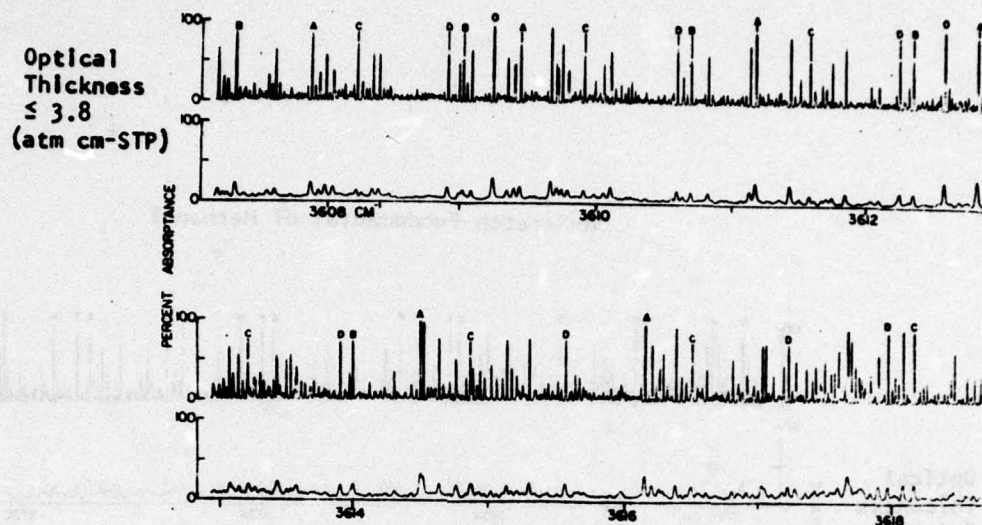


Fig. 25a. Observed and deconvoluted spectra on the *P*-branch side of the OH-stretching band of CH₃OH showing some of the identified series in this region. Lines labeled A, B, C are members of the series $(037J - 1)^* \leftarrow (028J)$, $(018J - 1)^* \leftarrow (039J)$, and $(017J - 1)^* \leftarrow (038J)$, respectively. The lines labeled D are part of a series as yet not identified. Strong water lines are indicated by circles.

OH-Stretch Fundamental of Methanol

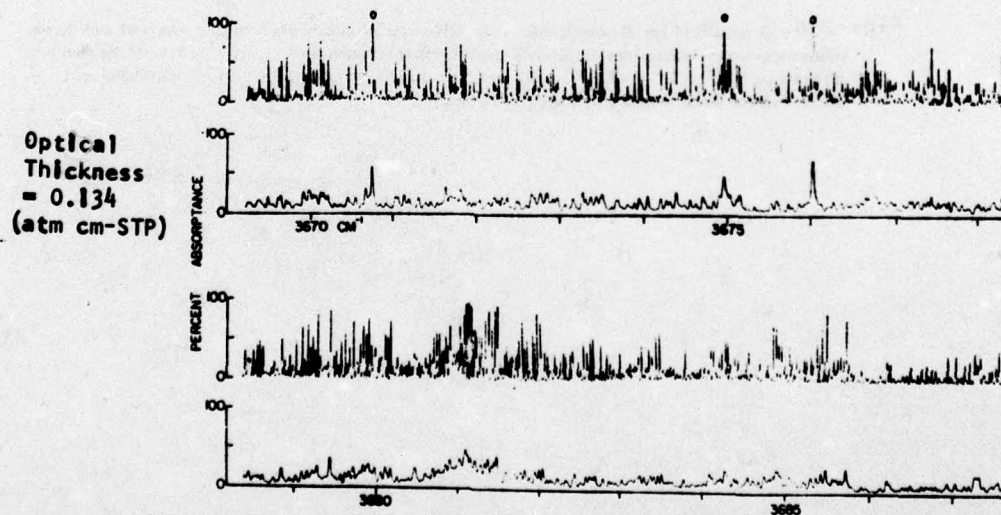


Fig. 25b. Observed and deconvoluted spectra in the region of the band center. The pressure was approximately 30 microns with a path of 34 m. Strong water lines are indicated by circles.

OH-Stretch Fundamental of Methanol

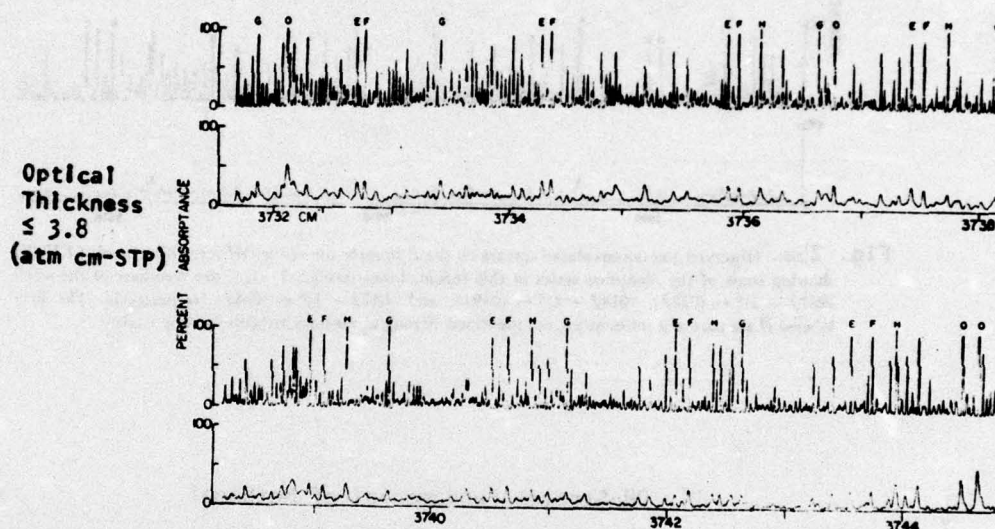


Fig. 25c. A section of the *R*-branch side of the OH-stretch fundamental showing observed and deconvoluted spectra as well as some of the lines identified in this region. Lines labeled *E*, *F*, *G*, *H* are members of the series $(025J + 1)^* \rightarrow (034J)$, $(016J + 1)^* \rightarrow (025J)$, $(037J + 1)^* \rightarrow (010J)$, and $(026J + 1)^* \rightarrow (035J)$. Strong water lines are indicated by circles.

Table 8. Infrared Spectrum of CH₃OH (Frequency in cm⁻¹, Accuracy ± 0.5 cm⁻¹).

Assignment	observed data				calculated	
	Ar-matrix(15K)		vapour		frequency	
	$\tilde{\nu}$	rel. int.	$\tilde{\nu}$	rel. band int. shape	force constant set I	set II
$\nu_1(a')$, $\nu(\text{OH})$, second site or dimer	3672 \pm 2	vw sh				
$\nu_1(a')$, $\nu(\text{OH})$	3667.0 ^a	m	3681.5	m AB	3682.3	3682.4
$\nu_2(a')$, $\nu(\text{CH}_3)$ asym	3005.5 ^a	m	2999.0	w B	3006.5	3004.3
$\nu_3(a'')$, $\nu(\text{CH}_3)$ asym	2961.5 ^a	m	2970 \pm 4	m C	2959.8	2960.8
$2\nu_6(A')$	2956.0	m	2956 \pm 4	m AB,A		
$\nu_4 + \nu_{10}(A'')$	2930.0	m	2929.5	w C		
$2\nu_{10}(A')$	2921.0	w	2920 \pm 2	w AB		
$\nu_4 + \nu_5(A')$	2915.0	w	2912 \pm 2	vw B		
$\nu_5 + \nu_{10}(A'')$	2908.0	vw sh				
$2\nu_5(A')$			2893.2	w A		
$\nu_3(a')$, $\nu(\text{CH}_3)$ sym	2847.5 ^a	m	2844.2	m A	2961.5	2961.9
$\nu_7 + \nu_8(A')$	2103.0	vw	2102 \pm 2	vw B		
$2\nu_8(A')$	2053.5	w	2054.5	w A		
$\nu_4(a')$, $\delta(\text{CH}_3)$ asym	1473.0 ^a	w	1479.5 1477.2	w AB	1473.5	1474.6
$\nu_{10}(a'')$, $\delta(\text{CH}_3)$ asym	1466.0 ^a	w	1465 \pm 3	w C	1471.4	1473.4
$\nu_5(a')$, $\delta(\text{CH}_3)$ sym	1451.5 ^a	vw	1454.5	m A	1456.2	1457.7
$\nu_{11} + \nu_{12}(A')$			1414.0	w AB		
$\nu_7 + \nu_{12}(A'')$			1345.0	m		
$\nu_6(a')$, $\delta(\text{COH})$ } ^b	1334.0 ^a		1339.5 1332.0	m AB	1341.3	1343.9
$\nu_{11}(a'')$, $\nu_4(\text{CH}_3)$			1145 \pm 4	vw C	1155.1	1159.3
$\nu_7(a')$, $\nu_{11}(\text{CH}_3)$	1076.5 ^a	w	1074.5	vw B	1080.7	1079.3
$\nu_8(a')$, $\nu(\text{CO})$	1033.5 ^a	vs	1033.5	vs A	1039.1	1035.5
$\nu_9(a')$, $\nu(\text{CO})$ second site	1027.5	s				
$\nu_8(a')$, $\nu(\text{CO})$ C ¹³ H ₃ OH	1018.5	w				1020.8
$\nu_8(a')$, $\nu(\text{CO})$ CH ₃ O ¹⁸ H	1008.2	w				1009.9
$\nu_{12}(a'')$, $\nu(\text{OH})$	271.5 ^a	m			272.2	272.4

^a used for least squares fit.

^b very complicated structure in the vapour phase. Three dominant Q-branches at 1345, 1339.5 and 1332.0 cm⁻¹.

too low value of $\overline{k_{300^\circ K}(v)} > 1.3 \text{ (atm cm-STP)}^{-1}$. Where the measured transmission is less than 50%, as in the strong $\sim 3000 \text{ cm}^{-1}$ and the strongest $\sim 1033 \text{ cm}^{-1}$ regions, then $\overline{k_{300^\circ K}(v)}$ is greater, and probably for higher pressures appreciably greater, than $2.5 \text{ (atm cm-STP)}^{-1}$.

Figure 25a, b, and c (taken from Lee, et al.) show the high resolution fine structure of the $\text{CH}_3\text{OH } \nu_1(a'')$ OH bond stretching fundamental centered near 3681.5 cm^{-1} (see Table 8). The "raw" scans were made with an instrument response function width at half-maximum varying from 0.020 to 0.028 cm^{-1} . A numerical "deconvolution" procedure then was used to produce the extremely high resolution "deconvoluted spectra" shown above the "raw spectra". The three figures show sections of the P-branch side, band center, and R-branch side of this OH-stretch fundamental. The pressures used ranged from 0.03 Torr (or 30 microns of Hg) at the band center (Figure 25b) to 0.85 Torr in the wings. The pressures used for the measurements resulting in Figures 25a and 25c are not specified, but are $\leq 0.85 \text{ Torr}$. The optical path for all measurements was 34.2 m , thus corresponding to $0.135 \text{ (atm cm-STP)}$ for Figure 25b, and $\leq 3.83 \text{ (atm cm-STP)}^{-1}$ for Figures 25a and c. The Doppler line half-widths at half-maxima are again, $a_D \approx 0.0041 \text{ cm}^{-1}$, and the transmission again must depart considerably from Beer's Law since only spectral regions very near to the line centers will be absorbed and the (raw) spectral resolution is $\sim 2 \frac{1}{2}$ to $3 \frac{1}{2}$ times $2a_D$.

Restricting attention to Figure 25b where the information supplied is more specific, it can be seen that the raw spectra exhibit instrument response function modified apparent transmission ($= 100\% - \text{apparent \% absorption}$) ranging from $\sim 90\%$ to $\sim 50\%$. The deconvoluted spectra, which are an appreciably more reliable indicator (but still do not account for absorption which would occur in pressure broadened line wings) show regions of apparent transmission as low as 10 or 20% . For an optical thickness of $0.135 \text{ (atm cm-STP)}^{-1}$, the higher lower bound predicted by the (poor fit) Beer's Law expression would be $\overline{k_{300^\circ K}(v)}$ greater than $0.78, 5.1, 11.9, \text{ and } 17.1 \text{ (atm cm-STP)}^{-1}$, respectively, for apparent transmissions of $90\%, 50\%, 20\%, \text{ and } 10\%$. Pressure broadening to force absorption contributions from line wings should appreciably increase the preceding $\overline{k_{300^\circ K}(v)}$ figures. The strong CH OH absorption in this region would overlap some of the strongest HF laser lines, particularly when heater to induce hot band absorption.

It is seen from a correlation of Table 9 with Table 8, and also from Figure 24 that the CH_3OH room temperature spectral absorption is both wider and stronger in the $\sim 3000 \text{ cm}^{-1}$ centered ν_9 and $2\nu_4$ region than in the preceding $\sim 3680 \text{ cm}^{-1}$ centered ν_1 region, and stronger still in the $\nu_8(a'')$ CO bond stretching spectral region centered on 1033.5 cm^{-1} . The former region centered on $\sim 3000 \text{ cm}^{-1}$ tends to fall between the regions of HF and of DF line absorption, but might prove useful for absorbing selected low frequency lines of the former or high frequency lines of the latter, particularly when the absorption patterns are intensified and spread out by heating to bring about hot band contributions. The strongest, 1033.5 cm^{-1} centered CH_3OH absorption region is virtually certain to prove an effective absorber for the CO_2 laser radiation from selected lines of either the $\sim 10.4\mu$ or $\sim 9.4\mu$ centered bands. It would be expected, from Table 9, that the $k_{300^\circ\text{K}}(\nu)$ values for this CO bond stretching region would be ~ 4 times as large as those for the OH bond stretching region centered on 3683.5 cm^{-1} .

Table 9. Estimates for relative band intensities from IR spectra (from a calculation using the modified derivatives of the dipole moment and the relative rotamer populations for the species with partially deuterated methyl group.)

CH_3OH	$\nu(\text{OH})$	$\nu_{\text{as}}(\text{CH}_3)$		$\nu_{\text{s}}(\text{CH}_3)$		$\nu_{\text{as}}(\text{CH}_3)$		$\nu_{\text{s}}(\text{CH}_3)$		$\nu(\text{CO})$	
	ν_1	ν_2	ν_9	ν_3	ν_4	ν_{10}	ν_5	ν_6	ν_{11}	ν_7	ν_8
obs. (gas)	0.62 ^a			0.77			0.21	0.31	<0.05	<0.05	2.4
calc.	0.62	0.85	2.0	1.1	0.02	0.04	0.18	0.35	.01	.03	2.0

Unfortunately, the CH_3OH energy level expressions for both vibrational and particularly the rotational energy contributions, are very complex, as also are the expressions for the partition function. However, since there are twelve fundamental vibrational modes (and three fundamental rotational constants varying for each vibrational mode, as well as three rotational

quantum numbers n , K and J), the number of "hot band" lines must increase very rapidly with temperature. At high pressures and temperatures, each contributing hot band should in itself provide effectively continuous absorption. Then, assuming as before rotational relaxation, it is difficult to see how bleaching by radiation absorption would pose any problem. While the effective absorption coefficient at any given frequency would vary with temperature, it would appear fairly safe to assume that at temperatures below 70 or 80% dissociation, that CH_3OH would continue to be a very effective absorber for a wide selection of CO_2 laser lines and probably also for selected HF laser lines.

4. LINE WIDTH PARAMETERS

Table 10 is a copy of Ludwid, et al.'s Table 5-19. It presents a useful compilation of line width parameters for computing the collision-broadened line widths for H_2O , CO_2 , NO , CN , OH , HCl and HF (and presumably DF), including self-broadening from both resonant and nonresonant collisions and foreign species broadening. Their γ_{ci} is the same quantity that has been called a [or $a(p,P,T)$]. The equation for computing γ_{ci} is given below, together with their explanation of its use.

"The specification of the collision broadened half-width as a function of pressure and temperature is more complex than the method used for the absorption coefficient. The line width is expected to be proportional to the number of collisions experienced by a molecule per unit time. Since self broadening collisions are more effective than those with other species, it has been found [5-15] that good agreement with experimental data at room temperature has been obtained by assuming the line width is proportional to $(\gamma_a p_a + \gamma_b p_b)$, where the subscripts a and b designate self broadening and foreign gas broadening. In extending this proportionality to higher temperatures it is necessary to take into account the effect of variation in temperature dependency [5-16, 5-17] between resonating and nonresonating self-broadening collisions described in Section 2.4.3. This results in the formulation of equation (5-34) (see Table 5-18)

$$\gamma_{ci} = \left[\sum_j (\gamma_{i,j})_{273} p_j (273/T)^{\eta_{i,j}} \right] + (\gamma_{i,i})_{273} p_i (273/T)^{\eta_{i,i}} .$$

In this expression, the self-broadening of the radiating species under consideration is included in two ways. First it is included as one of the j foreign gas broadeners to account for nonresonant collisions and, second, it is included in the separate term $(\gamma_{i,i})$ to account for resonant collisions which have a different temperature dependency. The use of this formulation depends upon the assumption that the line widths, which are functions of frequency, can be approximated by a band averaged value so all frequency dependence in the fine structure parameter (a_c) will appear through the mean line density $(1/d)$."

Table 10. Model Values for the Collision Line Width Parameters

Molecule (i)	Broadener (j)	$(\gamma_{i,j})_{273}$ cm ⁻¹ atm ⁻¹	$\eta_{i,j}$	$(\gamma_{i,i})_{273}$ cm ⁻¹ atm ⁻¹	$\eta_{i,i}$
H ₂ O	H ₂ O	(0.09)	0.5	0.44	1.0
	N ₂	0.09	0.5		
	O ₂	0.04	0.5		
	H ₂	(0.05)	0.5		
	CO ₂	0.12	0.5		
	CO	(0.10)	0.5		
CO ₂	CO ₂	0.09	0.5	0.01	1.0
	H ₂ O	(0.07)	0.5		
	N ₂	0.07	0.5		
	O ₂	0.055	0.5		
	H ₂	0.08	0.5		
	CO	(0.06)	0.5		
CO	CO	0.06	0.5	0.0	1.0
	H ₂ O	(0.06)	0.5		
	CO ₂	(0.07)	0.5		
	H ₂	0.06	0.5		
	N ₂	0.06	0.5		
	O ₂	0.05	0.5		
NO	NO	0.05	0.5	0.0	1.0
	N ₂	(0.05)	0.5		
	O ₂	(0.04)	0.5		
	Other	(0.05)	0.5		
CN	CN	(0.05)	0.5	0.0	1.0
	Other	(0.05)	0.5		
OH	OH	(0.05)	0.5	0.45	1.0
	Other	(0.05)	0.5		
HCl	HCl	(0.05)	0.5	0.15	1.0
	Other	(0.05)	0.5		
HF	HF	(0.05)	0.5	0.45	1.0
	Other	(0.05)	0.5		

NOTE: Values in parenthesis are estimated.

5. SUMMARY

A compilation has been made of absorption characteristics of various possible gaseous dopants for selective absorption of some currently popular laser wavelengths. Table I shows the wavelength regimes and the dopants discussed.

Table I

	Wavelength Region			
	3.6 - 3.9 μ	2.6 - 2.9 μ	4.9 - 5.7 μ	9.4 - 10.4 μ
Dopants:	DF	HF	CO	CO ₂
		OH	NO	NH ₃
		CH ₃ OH		CH ₃ OH

The absorption characteristics listed are absorption cross-section, vibrational-rotational level distributions, line densities versus temperature and wave number and absorption coefficients vs. temperature and wave number.

Bibliography

1. Caledonia, G. E., P. K. S. Wu and A. N. Pirri, "Radiant Energy Absorption Studies for Laser Propulsion," Report on Contract NAS 3-18528, Prepared by Physical Sciences, Inc., March, 1975.
2. Chan, S. H., D. Nelson, et al., "High-Resolution Infrared Spectra of Air Pollutants with Fourier Transform Spectroscopy," J. Quant. Spectrosc. Radiat. Transfer, Vol. 14, Pergamon Press, 1974, pp. 287-298.
3. A. Goldman, S. C. Schmidt, et al., "Infrared Spectral Radiance of Hot HF and DF in the $\Delta v = 1$ Bands Region as Seen Through an Atmospheric Path," J. Quant. Spectrosc. Radiat. Transfer, Vol. 14, Pergamon Press, 1974, pp. 299-307.
4. Herzberg, G., Infrared and Raman Spectra, D. Van Nostrand Co., Inc. Princeton, N. J., 1966.
5. Lee, R. Gary, Robert H. Hunt, and Earle K. Plyler, "A High-Resolution Study of the OH-Stretch Fundamental of Methanol," J. of Molec. Spectroscopy, 57, 1975, 138-154.
6. Ludwig, C. B., W. Malkmus, et al., Handbook of Infrared Radiation from Combustion Gases, Report No. NASA SP-3080, MSFC, 1973.
7. McClatchey, R. A., W. S. Benedict, et al., "AFCRL Atmospheric Absorption Line Parameters Compilation," Report No. AFCRL-TR-73-0096 (for AFSC, USAF, Environmental Research Papers No. 434), 26 January 1973.
8. McClatchey, R. A., and J. E. A. Selby, "Atmospheric Attenuation of Laser Radiation from 0.76 to 31.25 μ m," Report No. AFCRL-TR-74-0003 (for AFSC, USAF, Environmental Research Papers No. 460), 3 January 1974.
9. McCoy, J. H., "Atmospheric Absorption of Carbon Dioxide Laser Radiation near Ten Microns," Technical Report 2476-2 (Ohio State University), Prepared for AFAL, AFSC, 10 September 1968.
10. Meridith, R. E., and F. G. Smith, "Investigation of Fundamental Laser Processes; Vol. II, Computation of Electric Dipole Matrix Elements for Hydrogen Fluoride and Deuterium Fluoride," Prepared by Univ. of Michigan for ARPA, Report No. 84130-39-T (II), November 1971.
11. Randall, C. M., "Line-by-Line Calculations of Hot-Gas Spectra Including HF and HCl," Report SAMS0-TR-75-288, Prepared by Aerospace Corp. for DARPA, Interim Report, 4 December 1975.
12. Serrallach, A., R. Meyer, and Hs.H. Gunthard, "Methanol and Deuterated Species: Infrared Data, Valence Force Field, Rotamers, and Conformation," J. of Molec. Spectroscopy, 52, 1974, pp. 94-129.
13. Taylor, F. W., "Spectral Data for the ν_2 Bands of Ammonia with Applications to Radiative Transfer in the Atmosphere of Jupiter," J. Quant. Spectros. Radiat. Transfer, Vol. 13, 1973, pp. 1181-1217.
14. Young, Charles, and R. E. Chapman, "Line-Widths and Band Strengths for the 9.4- and 10.4- μ m CO₂ Bands," J. Quant. Spectrosc. Radiat. Transfer, Vol. 14, 1974, pp. 679-690.